Primary Productivity and its variability in the Atlantic Southern Ocean

Warren R. Joubert

Thesis presented for the Degree of

Doctor of Philosophy

December 2014

UNIVERSITY OF CAPE TOWN

IYUNIVESITHI YASEKAPA • UNIVERSITEIT VAN KAAPSTAD

University of Cape Town

Department of Oceanography

South Africa

Declaration

I declare that this is my own work. I have done all analyses of the data, creating of the figures, and writing the discussions of the results. Work not completed by myself is acknowledged and cited accordingly. All contributions from co-authors (advisory and editorial) are acknowledged and included in the published and material under peer review.

Not by might,

Not by power,

But by My Spirit…

Zechariah 4.6

ABSTRACT

The two principal bottom-up drivers of the High Nutrient Low Chlorophyll (HNLC) characteristics of the Southern Ocean are light and nutrient (mainly dissolved iron) limitation (*Boyd*, 2002; *Mitchell et al*., 1991), which have varying limiting roles over the growing season (*Boyd,* 2002; *Swart et al.*, 2014). This research commenced with an investigation of the meridional characteristics of primary productivity in the Atlantic Southern Ocean during austral summer 2008. It showed meridionally distinct regions of new and regenerated uptake, with low *f*-ratios ($f = 0.2$) in the Sub-Tropical Zone (STZ) dominated by picophytoplankton (< 0.2 μm). New production which contributed up to 50% of productivity in the Sub-Antarctic Zone (SAZ) region, were ascribed to increased input of iron associated with an anticyclonic eddy observed in this region. This highlighted the role of synoptic scale events in supplying nutrients, particularly iron, to the euphotic zone in the Sub Antarctic Zone (SAZ), where phytoplankton blooms occur throughout summer (*Swart et al.*, 2014).

The changing balance between mixing and buoyancy forcing expressed in the mixed layer depth (MLD), which modulates iron supply and light availability were then investigated through high resolution measurements of net community production (NCP) constrained by $\Delta O_2/Ar$ ratios, and MLD. In this study, a quasi-non-linear relationship between NCP and MLD were observed, with the highest and most variable NCP observed in shallow MLDs (< 45 m). It was proposed that NCP variability in the SAZ which showed the highest and most variable NCP rates, may be driven by alternating states of synoptic-scale deepening of the mixed layer, leading to the entrainment of iron (dFe), followed by restratification, allowing rapid growth in an iron replete, high light environment. Synoptic iron fluxes into the euphotic zone based on water column dFe profiles and high resolution glider MLD data,

reveal a potentially significant contribution of 'new iron' which could sustain NCP throughout summer.

Finally, when comparing chl normalized NCP (NCP*) with the average irradiance in the mixed layer ($\bar{I}_{MLD}$), a positive relationship (r^2 = 0.3, p<0.001) is observed. It might be somewhat surprising that $\bar{I}_{MLD}$ alone can explain so much (30%) of the variability in NCP* given the attention that is usually placed on Fe-mediated regulation of productivity in the Southern Ocean (*Boyd* 2002; *Boyd et al.*, 2007). NCP* lies in the 'light-dependent' part of the NCP*- $\bar{I}_{MLD}$ curve, where the slope of the *PvsE* curve is highly dependent on iron availability (*Hiscock et al.* 2008; *MacIntyre et al.,* 2002). Therefore, one might argue that the role of iron is embedded in the NCP*-$\bar{I}_{MLD}$ relationship and the combination of light and iron limitation synergistically control the variability NCP in this region. This result supports the understanding of the role of iron in affecting light dependent productivity, in showing that NCP* responds in a positive way to mean water column irradiance, while variable iron concentrations explains the variability observed in this relationship.

Acknowledgements

I extend my gratitude to several people who were instrumental in the successful completion of this thesis.

My mentor and supervisor Dr Pedro Monteiro for creating the space and opportunities to do this Ph.D research, and guidance, advice and support throughout. My supervisor Dr Howard Waldron for useful discussions and rigourously ensuring that I've dotted my T's and crossed my I's. To my co-supervisor Dr Sandy Thomalla, I am immensely grateful for your encouragement and the countless iterations you endured to ensure that I raise the standard.

I appreciate my colleagues who helped with understanding and interpretation during various sections of this work. Particularly Dr Alessandro Tagliabue for countless discussions, advice, ideas and insightful comments throughout this work. Professor Michael Bender, for the opportunity to spend time at Princeton University during this research, use of research equipment and interpretation of results. Dr Sebastiaan Swart, Prof Mike Lucas, Dr Nicolas Cassar, and Dr Bror Jonsson, all contributed invaluable input and assistance in ensuring the quality of data and results. Dr Frank Dehairs and Dr Anne-Julie Cavagna for providing the unpublished ^{234}Th data collected during the cruise. Annick Masson, Audrey Guenneugues for providing the macronutrient, chl-a and POC data presented in Chapter 3.

The captains, officers and the crews of the *R.V. Marion Dufresne* and *M.V. SA Agulhas* for their invaluable assistance in completing the scientific research campaigns that is the basis for the work presented here. This work was supported by the Institut National des Sciences de L'Univers of the Centre National de la Recherche Scientifique, the French Polar Institute (Institut Polaire Emile Victor), the French Research Institute for Exploitation of the Sea, the National Agency for Research Funding (ANR), the National Science Fund (NSF), and the South African National Antarctic Programme (SANAP). Financial support for this work was

provided through the Southern Ocean Carbon – Climate Observatory (SOCCO) programme and the CSIR Parliamentary Grant.

My colleagues at CSIR and co-students in SOCCO (past and present), Thato (Dr T), Nicolette, Marjo, Nicolas, Natasha, Nomkwe, Precious, Sarah, Marcel, Luke, Emma, Ceinwyn and Leletu. I am priveledged (currently advantaged) to be part of this team. Thank you to Marita Guasco for the encouragement and helping me distill my thoughts and 'right-sizing' my priorities.

To my friends, thank you for encouragement whenever I wanted to give up. To my parents and family, thank you for believing that I can, even when my own words were contrary. To my wife, Brigetta. Together we endure lifes pain and celebrate its joy, and this project provided a lot of both. Thank you for believing on my behalf when I lose faith and hope, for dreaming with me and aligning everything (through good and bad times) to make those dreams a reality. To my beautiful daugthers, Nina and Sophia. You provide a reason to be better.

Contents

List of figures and tables

List of Abbreviations

AAIW	Antarctic Intermediate Water
ACC	Antarctic Circumpolar Current
AZ	Antarctic Zone
BGH	Bonus GoodHope
C:N ratios	Carbon to Nitrogen stoichiometric ratio
chl-a	Chlorophyll-a
CTD	Conductivity, Temperature, and Depth
CZCS	Coastal Zone Scatter Colorimeter
DIC/N	Dissolved Inorganic Carbon/Nitrogen
DOC/N	Dissolved Organic Carbon/Nitrgen
GPP	Gross Primary Production
HNLC	High Nutrient Low Chlorophyll
MIZ	Marginal Ice Zone
MLD	Mixed layer depth
MODIS	Moderate Resolution Imaging Spectroradiometer
NCP	Net Community Production
NPP	Net Primary Production
PAR	Photosynthetically Active Radiation
PF	Polar Front
POC/N	Particulate Organic Carbon/Nitrogen
SAF	Sub-Antarctic Front
SAMW	Sub-Antarctic Mode Water
SANAP	South African National Antarctic Programme
SAZ	Sub-Antarctic Zone

SeaWiFS	Sea-Viewing Wide Field-of-View Sensor
SIZ	Seasonal Ice Zone
SOCCO	Southern Ocean Carbon and Climate Observatory
SST	Sea Surface Temperature
STF	Sub-Tropical Front
STZ	Sub-Tropical Zone
UCDW	Upper Circumpolar Deep Water
VGPM	Vertrically Generalised Production Model
XBT	Expendable Bathythermographs

Chapter 1

Background and Context

1.1 The Southern Ocean CO_2 sink

The Southern Ocean is considered one of the most important oceanic sinks of atmospheric CO_2 (*Roy et al.*, 2003; *Sabine et al.*, 2004; *Takahashi et al*., 2002, 2012). In the industrial period (since ~ 1800), the ocean removed roughly 118 ± 19 PgC y^{-1} (1Pg = 1 billion tonnes = 1 x 10^{15} g) from the atmosphere amounting to roughly 50% of anthropogenic emissions (Sabine et al., 2004). The ocean holds the majority of the total inventory of carbon (~ 93%) due to the ability of CO_2 to form carbonic acid in seawater, along with its dissociation products namely, bicarbonate and carbonate ions (*Feely et al.*, 2001). The two principal mechanisms responsible for the uptake and storage of atmospheric CO_2 are the physical solubility pump and the biological pump. The solubility pump involves the CO_2 exchange at the surface ocean and sequestration of its chemical species in the ocean interior through the ocean thermohaline circulation. The biological pump, through photosynthesis, converts CO_2 to organic carbon thereby reducing the partial pressure of CO_2 in surface waters which drives the draw-down of CO_2 from the atmosphere into the ocean interior. Global (terrestrial and oceanic) annual total primary production, calculated from chl-a, sea surface temperature and surface irradiance is estimated at roughly 45 – 50 PgC yr^{-1} (*Behrenfeld and Falkowski*, 1997; Field et al., 1998; Carr et al., 2007).

Oceanic CO_2 uptake amounts to 1.4 - 2.2 PgC y^{-1}, up to 25% of the estimated anthropogenic releases of 9 PgC into the atmosphere annually (Gruber et al., 2009).

The Southern Ocean accounts for nearly 50% (~1 PgC) of the annual oceanic uptake of anthropogenic CO_2, primarily through the biological pump, particularly in the midlatitudes (30 – 50°S) (Fig.1.1) (*Metzl et al.*, 1999; Takahashi et al., 2002), accounting for ~ 80% of the Southern Ocean uptake (*Moore and Abbott*, 2000). The biological pump is affected by macronutrient and micronutrient (iron) availability, water column irradiance and stability (mixing) as well as grazing pressures at various spatial and temporal scales (ie. *Thomalla et al.*, 2011). The complex role of these multiple driving factors is emphasised by the large-scale spatial variability of chl-a (Fig. 1.1), which highlight regional differences in phytoplankton biomass attributed to variability in seasonal physics and biogeochemical dynamics (*Arrigo et al.*, 2008, *Moore and Abbott*, 2000). These studies all highlight the importance of drivers of phytoplankton production variability in the Southern Ocean. In order to better understand the drivers of productivity, these various controlling factors of phytoplankton production (biological pump) are investigated in this work. Of particular interest are the contrasting regions of elevated phytoplankton biomass whose annual cycles are dominated by seasonal and intra-seasonal scales of mixed layer variability (*Thomalla et al.*, 2011; *Fauchereau et al.,* 2011). There are important regional and basin scale differences in the way that ocean productivity responds to the otherwise regular seasonal forcing (*Thomalla et al.*, 2011). These knowledge gaps in this globally important region provided the opportunity for research focused on characterizing and understanding the drivers of variability of the seasonal cycle of phytoplankton in the Southern Ocean (*Monteiro et al*., 2011; *Thomalla et al.*, 2011; *Fauchereau et al*., 2011; *Joubert et al.*, 2014, *Swart et al*., 2014, *Thomalla et al*., 2014).

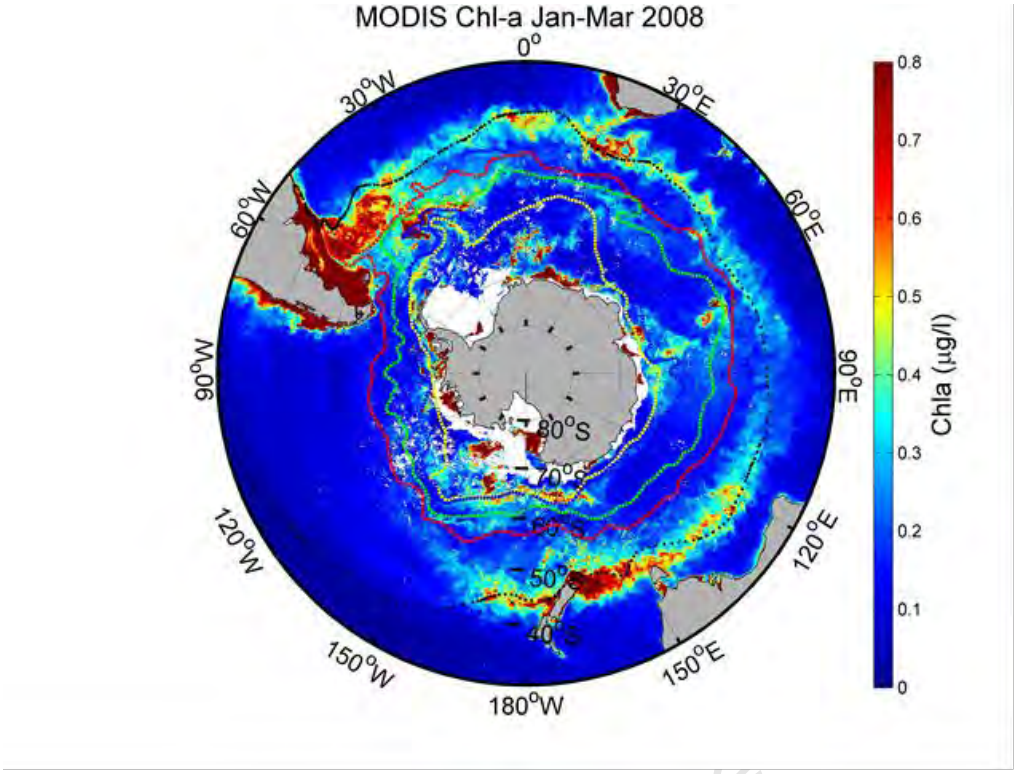

Figure 1.1. MODIS image of summer climatology (Jan – Mar 2008) for Chl-a concentration (µg l^{-1}) for the Southern Ocean. Climatological frontal positions (Sub-Tropical Front in black; Sub-Antarctic Front in red; Polar Front in green, and Southern Boundary in yellow) from Orsi et. al., (1996) are shown.

1.2 The Biological Pump

Primary production in the Southern Ocean plays a key role in the distribution of CO_2 at the ocean-atmosphere interface. Through the fixation of inorganic carbon to organic matter (particulate and dissolved) during photosynthesis, the partial pressure of CO_2 in the surface ocean is reduced, and equilibrium requirements results in a net uptake flux of CO_2 from the atmosphere. Carbon is exported from the surface to the deep ocean by foodweb transformation processes, physical mixing of dissolved organic carbon, transport and gravitational sinking of particles. This process is collectively referred to as the biological pump (Fig. 1.2). The Southern Ocean biological pump plays an

important role in regulating the supply of nutrients to thermocline waters (Subantarctic Mode Water and Intermediate Water) of the entire Southern Hemisphere and North Atlantic (Sarmiento et al., 2004), which in turn drives low latitude productivity (*Sigman and Boyle*, 2000, and supply the nutrients to the thermocline waters that support productivity in low latitude oceans (*Sarmiento et al.*, 2004). Factors that regulate phytoplankton growth (e.g. light and nutrients), physical sinking and remineralization (ie. grazing and bacterial activity) play a key role in regulating the efficiency of the biological pump and the strength of the Southern Ocean CO_2 sink.

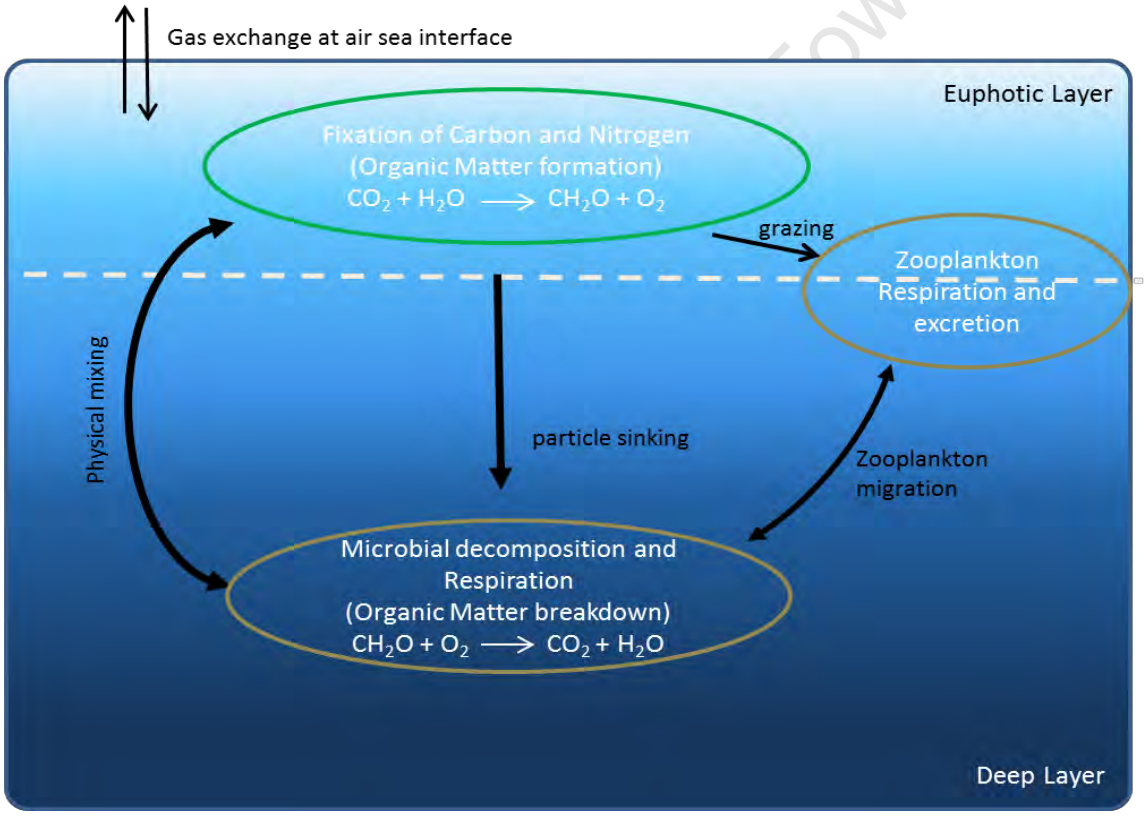

Figure 1.2: Simplified schematic of the components of the biological pump that converts Dissolved Inorganic Carbon (DIC) into organic biomass and export it as Particulate- or Dissolved Organic Matter to the deep ocean. Organic matter is remineralised at depth by bacteria and grazers to replenish dissolved nutrients, which is transported to the surface through vertical advection and diffusion processes and convective overturning. Figure adapted from Gruber and Sarmiento, (2006).

1.3 Phytoplankton biomass distribution in the Southern Ocean

Primary production estimates from *in situ* observations (*Banse*, 1996; *Bathmann et. al*., 1997; *Tremblay et. al*., 2002; *Honjo*, 2004), computational modelling (*Hense et. al.*, 2000; Schlitzer 2002) and remote sensing (*Behrenfeld and Falkowski*, 1997; *Moore and Abbott* 2000; *Arrigo et al.,* 2008) highlight the complex spatial and temporal variability of phytoplankton biomass in the Southern Ocean (Fig. 1.1). Satellites are particularly useful because they give high spatial resolution measurements, however remote sensing can only observe the surface to the first optical depth of the ocean, approximated by the euphotic depth divide by 4.6 (Kirk, 1994). Mean summertime (Dec – Feb) surface chl-a concentrations are in excess of 0.5 μg L^{-1} in the midlatitude region (30 – 50°S), but < 0.1 μg L^{-1} in the sub-tropics (equatorward of 40°S). Phytoplankton production is proposed to be highest in a circum-Antarctic band between 30 - 50°S (Fig. 1.1, eg. *Banse*, 1996), corresponding to the Sub-Antarctic Zone (*Metzl et al*., 1999; *Moore and Abbott*, 2000). Maximum phytoplankton biomass (chl-a) is observed during austral summer (*Hiscock et al.*, 2003; *Arrigo et al*., 2008; *Thomalla et al*., 2011) with localised annual blooms over regions of shallow bathymetry around and downstream of Sub-Antarctic islands (*Fiala et al.*, 1998; *Blain et al.*, 2001; *Pollard et al*., 2002; *Korb and Whitehouse*, 2004; *Pollard et al*., 2007), at hydrographic fronts (*Laubscher et al.*, 1993; *Hense et al.* 2000; *Sokolov and Rintoul*, 2007) and in the marginal ice zone (*Arrigo and van Dijken*, 2004; *Arrigo et al.*, 2008). Seasonal variability in chl-a concentration for the highly productive regions equatorward of 50°S is typically attributed to control by iron availability, and light limitation, associated with changes in mixed layer depth and water column stability (*Boyd*, 2002; *Thomalla et al.*, 2011). Lowest chl-a concentrations are associated with open ocean regions north of the sea ice zone, and

between hydrographic fronts, where phytoplankton biomass remains low (chl-a < 0.3 mg m^{-3}) throughout the year (Fig. 1.1), mainly due to a lack of iron and poor light conditions (*Boyd et al.*, 2001).

1.4 Drivers of phytoplankton productivity in the Southern Ocean

The low mean chl-a concentrations in the Southern Ocean, despite the high inventory of unused macronutrients, (*Chisholm and Morel*, 1991; *Sarmiento et al*., 2004) are maintained by bottom-up controls (available resources) of phytoplankton production through light, iron, and silicic acid limitation (*Martin et al.*, 1990; *Bathmann et al.*, 1997; *Boyd et al.*, 2001, 2002, 2007; *Moore and Abbott*, 2002; *Arrigo et al*., 2008*)* as well as the top-down controls by grazing (*Banse*, 1996; *Cullen*, 1991; *Price et al.*, 1991; *Smetacek et al.*, 2004; *Behrenfeld*, 2010). The challenge of how to unravel these various and inter-related regulating factors in the complex spatial domain of the Southern Ocean, remains a strong research focus in the Southern Ocean.

Bottom up controls of primary production

1.4.1 Macronutrients

Phytoplankton have certain cellular requirements that have been characterised by Redfield stoichiometric ratios of C:N:Si:P at 106:16:16:1 (*Redfield et al*., 1963; *Sarmiento and Gruber*, 2004), although some deviations from this are becoming increasingly apparent (eg. *Kortzinger et al.*, 2001; *Deutsch and Weber*, 2012). When a particular nutrient becomes depleted, phytoplankton growth is limited (Liebig's Law). Nutrient uptake can be described by Michaelis-Menton kinetics:

$$\mu = \frac{dP}{dt} = \mu_{max} \frac{S}{K_s + S} \qquad 1.1$$

Where μ is the growth rate, μ_{max} is the maximum specific uptake rate, K_s is the half-saturation constant, and S is the substrate concentration. Kinetic studies in the Southern Ocean are limited (*Collos and Slawyk* 1986; *Glibert et al.*, 1982; *Mengesha et al.*, 1998), and while some results suggest indicate a hyperbolic relationship between nitrogen concentration and uptake, statistically meaningful kinetic parameters are not yet available (*Cochlan*, 2008). Nitrogen in particular plays an important role as a building block for amino acids in phytoplankton growth. Despite the abundance of nitrate in the surface Southern Ocean (Fig. 1.3a, ~ 25 μmol L^{-1}), nitrogen uptake rates are generally low, which in some instances can be linked to silica limitation of diatom growth (*Martin-Jèzèquel et al.*, 2000). Silicate (SiO_4) derived from silicic acid is utilised by marine diatoms to form amorphous frustules. These diatom cells are disproportionately important in the export of organic matter to the deep ocean due to their size and mineral ballasting which are thought to enhance their sinking rate (*Buesseler*, 2001). A distinct latitudinal boundary in SiO_4 concentration is observed at the Polar Front (Fig. 1.3, *Levitus et al.*, 1994). Poleward of the Polar Front, surface SiO_4 concentrations are not limiting (up to 60 μmol L^{-1}), while equatorward, depleted SiO_4 concentrations (< 2 μmol L^{-1}) limit diatom production, and hence export production. The preferential removal of SiO_4 from the surface ocean due to its more efficient drawdown of SiO_4 relative to NO_3 (*Pondaven et al.*, 2000; *Brzezinski et al.*, 2001), results in high NO_3 concentrations in a band where SiO_4 is depleted. SiO_4 cycling differs from other nutrients in that it is mainly utilised by diatoms, and has minimal assimilation up the food chain, and is regenerated via dissolution kinetics rather than metabolic degradation (remineralisation). Under optimal environmental conditions, diatoms assimilate NO_3 and SiO_4 in a ratio of approximately 1:1

(*Brzezinski*, 1985). However, when diatoms become stressed for instance under iron or light limitation, large deviations from this ratio have been observed (*Hutchins and Bruland*, 1998; *Franck et al.*, 2000). For example, iron addition to iron limited phytoplankton, showed a twofold decrease in SiO_4:NO_3 (and SiO_4:PO_4) consumption ratios despite the benefit of Fe addition to diatom growth (*Takeda*, 1998).

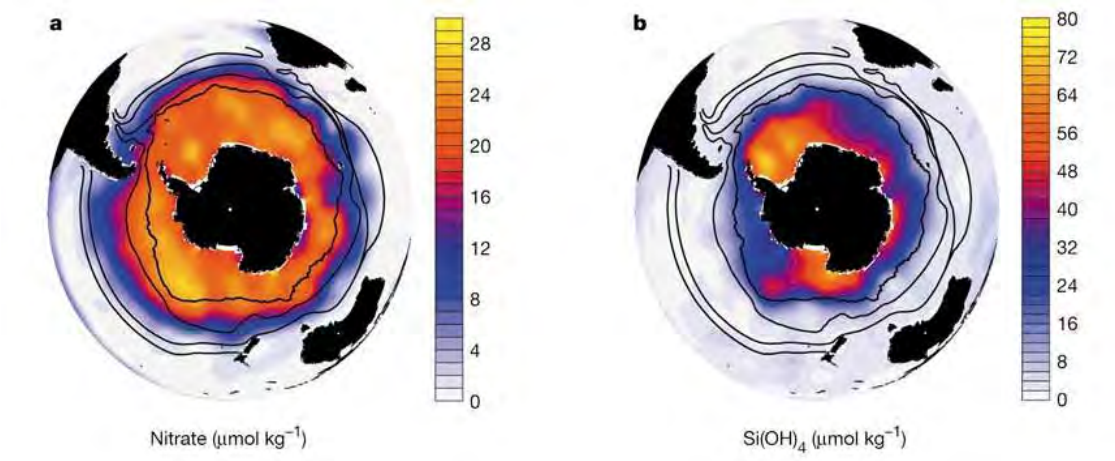

Figure 1.3. Annual mean Nitrate (a) and Silicic acid (b) concentrations in the Southern Ocean. Black lines from north to south indicate the northern Sub-Tropical Front, southern Sub-Tropical Front and Subantarctic Front. Figure from *Sarmiento et.al*., (2004).

1.4.2 Iron limitation

The micronutrient iron has long been considered as a bio-limiting factor in the underutilization of surface macronutrients (*Gran*, 1931), due to its low solubility in seawater and low concentrations in the Southern Ocean (*De Baar et al.*, 1995). Iron addition experiments in the late 1980's showed that iron supply to iron limited phytoplankton cause an increase in both carbon fixation and nitrogen utilization rates (*Marin et al.*, 1990), as well as an increase in phytoplankton biomass (*de Baar et al.*, 1995; *Boyd et al.*, 2007), photosynthetic efficiency (as shown by elevated F_v/F_m values) (*Suggett et al.,* 2009; *Hiscock et al*., 2008) and primary production

(*Timmermans et al.*, 1998). Convincing evidence for enhanced phytoplankton biomass upon iron addition has also been shown using *in situ* iron enrichment experiments in the Southern Ocean (ie. SOIREE, EISENEX, EIFEX, SAGE, SOFeX, *Boyd et al.*, 2007; *De Baar et al*., 2005). Without exception, these experiments resulted in increased chl-a biomass. Furthermore, the 'iron hypothesis' of John Martin (*Martin*, 1990) assign glacial-interglacial cycles of atmospheric CO_2 from ice core records (*Sigman and Boyle*, 2000) to be controlled by changes in iron supply in the Southern Ocean.

Dissolved iron (dFe) concentrations in the open Southern Ocean surface waters typically range between < 0.2 – 0.5 nmmol L^{-1} (*Martin et al*., 1990; *Sedwick and DiTullio*, 1997; *Croot et al*., 2004; *Tagliabue et al*., 2012). In the Atlantic Southern Ocean, dFe concentrations increase with depth up to 1.1 nmol L^{-1} (*Chever et al*., 2010; *Klunder et al.*, 2011). The sources of iron in the water column include upwelling (*de Baar et al.* 1995), airborne dust deposition (*Cassar et al*., 2007), shelf sediment entrainment (*Blain et al.,* 2007; *Bowie et al.*, 2009), hydrothermal activity (*Klunder et al*., 2011; *Tagliabue et al.,* 2010), bottom pressure torque (*Sokolov and Rintoul*, 2007), vertical diffusive fluxes (*Boyd et al.*, 2005; *Frants et al.*, 2013) with a minor contribution from ice-berg melting (*Smith et al.,* 2007; *Lancelot et al.*, 2009).

The cycling and distribution of iron is controlled by a variety of physical, chemical and biological processes. For instance redox chemistry and dissolution are important drivers of iron speciation between soluble (< 0.02 μm), colloidal (0.02 – 0.2 μm) and particulate (> 0.2 μm) iron fractions. The majority of iron in the ocean is present in the particulate fraction (> 0.2 μm), which upon acidification allow the study of the "labile" particulate pool sources and distribution (*Chever et al.*, 2010). Iron binding ligands, which account for 99% of dFe form iron complexes of soluble and colloidal

fractions (*Boye et al.,* 2010), which minimise losses due to precipitation and scavenging. It remains unclear how iron-ligand exchange between dissolved, colloidal and particulate pools, and photochemical reduction and biological processes facilitate these interactions in the upper ocean (*Boyd and Ellwood*, 2010). As a result of these processes together with the biological uptake of dFe by phytoplankton in surface waters, the water column profile of dissolved iron resembles that of nutrients (*Boyd and Ellwood*, 2010).

Iron is an essential element for phytoplankton growth as it is required for metabolic processes such as nitrate reduction and carbon fixation, and in the photosynthetic and respiratory electron transport system and the synthesis of chl-a. Assimilatory enzymes (such as ferredoxin within the membranes of eukaryotes) have a high demand for iron (*Morel et al.*, 1991). Cellular metabolic iron demand predicts that phytoplankton growth utilizing NO_3 requires 60% more iron than those growing on NH_4 (*Raven*, 1990). This is because extracellular iron reduction increase with smaller cell size (*Sunda*, 2001) typical of NH_4 based production. This additional iron in NO_3 based production is required to reduce NO_3 to NH_4 before being assimilated into amino acids (*Raven et al.*, 1990). It has also been reported that mixotrophic phytoplankton can directly assimilate colloidal iron (*Nodwell and Price*, 2001). Low levels (< 0.1 nmol L^{-1}) of iron affect the intracellular iron concentrations and specific growth rates of various phytoplankton species (*Greene et al.,* 1992; *Strzepek et al*., 2011; *Behrenfeld and Milligan,* 2013). Open ocean diatoms for instance have a low intracellular Fe:C ratio of 0.67 µmol mol^{-1} (*Lane et al*., 2009), compared to values between 4 – 1770 µmol mol^{-1} in coastal diatom species (*Sunda and Huntsman,* 1995). Photosynthetic organisms have adapted strategies to cope with low iron concentrations such as reducing biogeochemical requirements (*Strzepek et al.,* 2002) or increasing

bioavailable iron through the use of iron complexing ligands called siderophores (*Boye et al.,* 2001; *Maldonado et al.,* 2005). Siderophores (an iron chelating agent) released by bacteria are used to acquire iron, generally under iron limiting conditions, and can easily solubilise mineral iron (*Sunda*, 2001). The strategy of reducing iron requirements has been shown to manifest through over-expression of pigment-protein complexes which do not partake in photosynthesis, decreasing the photosynthetic assimilation efficiency, and concurrently the light-limited rate of photosynthesis (*Behrenfeld et al.,* 2004; *Hiscock et al.,* 2008). Eukaryotes such as diatoms have been shown not to produce siderophores per se, and instead use reductase enzymes to reduce soluble iron at the cell surface from Fe(III) to Fe(II) valence state, before taking it up (*Shaked et al*., 2005).

Fluxes of new iron from the subsurface into the euphotic zone range from ~3 µmol Fe m^{-2} y^{-1} for vertical diffusive supply in HNLC regions (*Boyd et al.,* 2012), to 300 µmol Fe m^{-2} y^{-1} from sediment resuspension (*Moore et al.*, 2008). *Boyd et al*., (2005) defined the contribution of new iron to total iron supply (*fe-ratio = new iron / (new + regenerated iron)* which range from 10% in HNLC regions (*Boyd et al., 2005)*, to 50% in waters with higher iron concentrations (*Sarthou et al.,* 2008). The *fe*-ratio was found to scale positively with increased iron supply (*Karl et al*., 2003), with low *fe*-ratios indicative of high rates of recycling. These high recycling rates have been proposed to drive the elevated productivity sustained throughout summer in the Southern Ocean (*Tagliabue et al.,* 2014). The authors argue that deep winter mixing (or entrainment) and diapycnal diffusion (across density surfaces) are the two main physical process supplying iron to the surface waters. Diapycnal diffusion depends on vertical diffusivity (k_z) and the dFe concentration gradient at the base of the mixed layer ($\partial Fe/\partial z$). Due to deep ferricline depths (ferricline is defined as the depth where

(∂Fe/∂z) is maximum) in the Atlantic Sub Antarctic Zone (SAZ), diapycnal diffusion was shown to be ten times smaller than deep winter mixing. During the spring bloom, the annual pulse of iron which was replenished from deep winter mixing is depleted, and then subsequently (during late spring and summer) replenished by iron recycling (*Tagliabue et al.* 2014). These authors do not consider the importance of sub-seasonal vertical fluxes of dissolved iron concentration at shorter spatial scales (meso- and sub-mesoscales), and its influence on phytoplankton productivity which are considered here in Chapter 4. Iron limitation, notwithstanding the co-limitation of diatoms by Fe and light (*Boyd et al.*, 2001; *Hiscock et al.,* 2008), must not be understated, particularly in the HNLC Southern Ocean, which has the strongest wind stresses (and mixing energy) of the world ocean (*Trenberth et al.,* 1990).

1.4.3 Light availability

Light utilized by phytoplankton during photosynthesis is separated into two interrelated processes. Firstly, during the 'light reaction' of photosynthesis, phytoplankton pigments absorb light energy (photons) and convert it to stored chemical energy in the form of reduced molecules such as ATP (adenosine triphosphate) and NADPH (nicotinamide adenine dinucleotide phosphate-oxidase) (eg. *Behrenfeld and Milligan*, 2013). Secondly, the 'dark reaction', which does not require light, utilises the reduced molecules to reduce CO_2 to organic matter (*Behrenfeld and Milligan*, 2013). The photosynthetically available radiation (PAR) is affected in the atmosphere by absorption, scattering and reflection so that perceived light varies with latitude and season (Fig. 1.4) (*Kirk*, 1984).

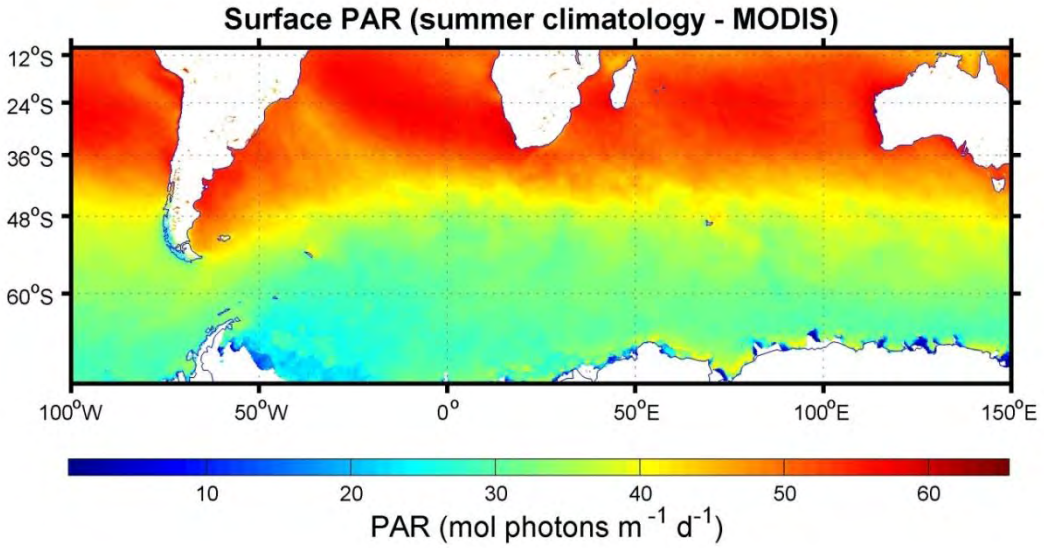

Figure 1.4. Modis summer climatology (December – February, for years 2002 - 2012) of surface photosynthetically active radiation (PAR) showing the latitudinal gradient in surface irradiance for the Southern Ocean.

Furthermore, at the surface ocean, the penetration of light is attenuated through the water column by selective absorption and scattering, following an approximate exponential relation with depth (*Morel*, 1988). Irradiance at a certain depth level below the surface (I_z) can be expressed by the following equation:

$$I_z = I_0 . e^{-K.z} \qquad (1.2)$$

Where I_0 is the irradiance at the surface (in terms of quanta per unit time per unit area), K_d is the diffuse attenuation coefficient (in units of m^{-1}), and z is the depth in m. An empirical relationship for K_d is given by K_d = 0.121 x [chl-a]$^{0.428}$ (*Morel*, 1988) and represents most oceanic environments reasonably well (*Sarmiento and Gruber*, 2006). The bottom of the euphotic zone is nominally defined as the depth where the light level is 1% of surface light (*Kirk,* 1984). Below the euphotic zone it is considered that

light is insufficient for photosynthesis to continue. As phytoplankton biomass (and pigments) increases in the euphotic zone, the attenuation of light also increases resulting in a shoaling of the euphotic depth.

Prior to the evidence for iron limitation described above, the prevailing understanding for control of primary productivity in the Southern Ocean was that relatively weak water column stability (turbulent mixing) would mix phytoplankton deeper than the euphotic zone resulting in sub-optimal time integrated irradiance conditions (*Holm-Hansen et al.*, 1977). The "Critical Depth Hypothesis" first formulated by Harald Sverdrup proposed a depth where the light requirements for net growth would exceed the total community consumption (respiration) in order for a bloom to develop (*Sverdrup*, 1953). Assuming constant water column respiration, net water column production and respiration are in balance at the compensation depth (Fig. 1.5). The depth of the mixed layer relative to the critical depth predicts whether a bloom will develop or not (*Sverdrup*, 1953; *Mitchell et al*., 1991). The critical depth hypothesis predicts that if the depth of the well mixed surface layer is greater than the depth of the euphotic zone, phytoplankton will spend part of their time without sufficient light for growth to exceed respiration. This means that the phytoplankton community cannot sustain net positive growth (*Sverdrup, 1953*; *Mitchell et al*. 1991). Conversely, shoaling of the surface mixed layer to above the critical depth (Z_{cr}) will result in phytoplankton spending all of their time in an environment with sufficient light for growth to exceed respiration (Sverdrup, 1953; *Holm-Hansen et al*., 1977). In such circumstances, provided nutrients are sufficient, net primary productivity can increase, allowing phytoplankton blooms to occur. The concept of light limitation within nutrient replete oceanic mixed layers has been applied to predict the spring development of phytoplankton blooms due to light supply and depth of the mixed

layer (*Siegel et al.*, 2002). In the Southern Ocean, where the mixed layer depths are particularly deep in winter, the shoaling of the mixed layers in spring is thought to be one of the main drivers for the observed spring blooms (*Metzl et al.*, 1999, 2006, *Nelson and Smith*, 1991).

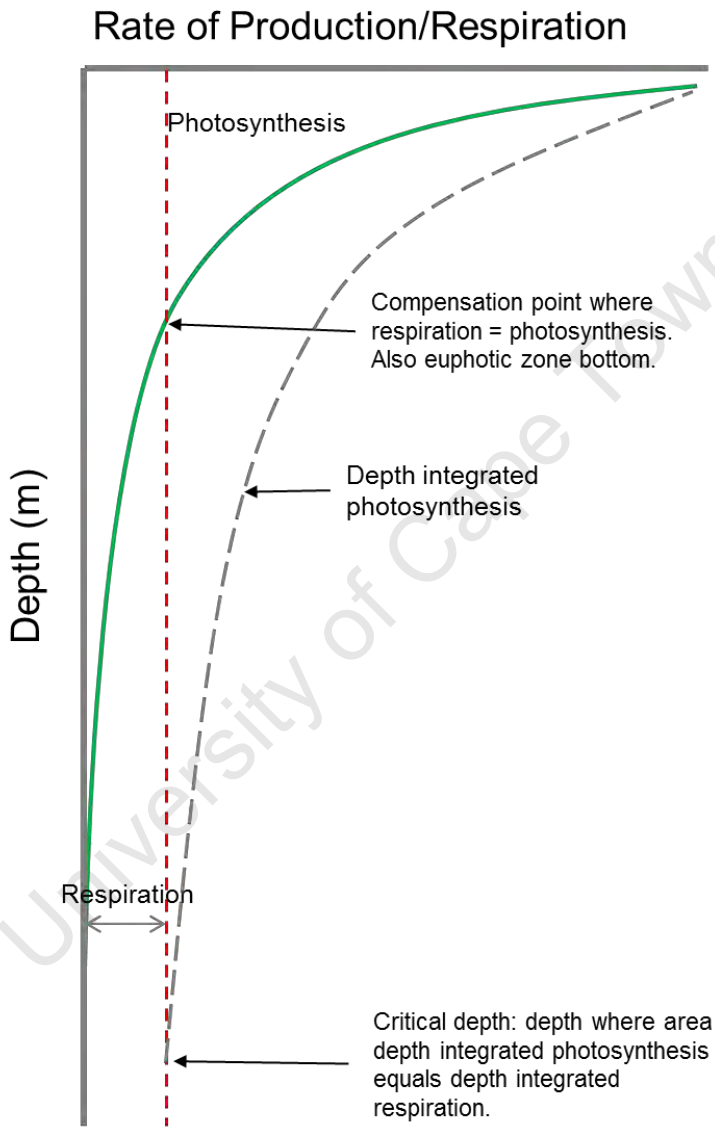

Figure 1.5. Schematic representation of the critical depth hypothesis (*Sverdrup*, 1953). Photosynthesis (green line) decrease exponentially following light attenuation with depth, while respiration is assumed to be constant. The compensation point is the depth where photosynthesis and respiration rates balance each other. Above the compensation depth net photosynthesis rates exceed respiration rates. The critical depth indicates the mixed layer thickness required for depth integrated photosynthesis (area under the photosynthesis curve) to

exceed depth integrated respiration (area under the respiration curve), hence where light irradiance is great enough to give net positive growth.

However, application of the Sverdrup hypothesis can be problematic in a highly dynamic, natural, mixed community (*Nelson and Smith*, 1991; *Smetacek and Passow*, 1990), where a mixed phytoplankton assemblage can have varying growth and loss rates with depth. Loss terms, which are assumed constant with depth in the Sverdrup Hypothesis, are difficult to measure, and are often dependent on growth rates, species physiology (community size structure), plankton seeding strategies and grazing pressure (*Smetacek and Passow*, 1990; *Behrenfeld,* 2010). The accurate determination of the compensation and critical depths is also difficult because of fluctuations in the underwater light field, resulting from self-shading or a time-dependent light field (*Nelson and Smith*, 1991). Finally, the definition of the critical depth means that it is averaged over 24 hours and is limited to the initiation of the spring bloom. This means that Sverdrup (1953) should be applied cautiously when describing light limitation in relation to phytoplankton productivity.

Several other models have been proposed for the onset of the spring bloom. The dilution-recoupling hypothesis proposed by *Behrenfeld* (2010) highlights the role of the balance between phytoplankton growth and losses through grazing. According to this model, net population growth in the North Atlantic is initiated in winter when mixed layers are deepest, prior to the onset of spring stratification (*Behrenfeld*, 2010). This revised theory focuses on the balance between phytoplankton growth and grazing and proposes that maximum phytoplankton growth rates are observed during winter, when mixed layers are deepest and phytoplankton most diluted (*Behrenfeld*, 2010). It proposes that positive growth begins during winter when mixed layers are at its

deepest, decoupling predator-prey interaction (diluting encounter rates), and allowing phytoplankton growth to exceed losses. This is in direct contrast to Sverdrup's hypothesis which assumes losses are constant with time and predicts highest phytoplankton growth in shallow mixed layers, however it is equally difficult to assess.

Another model to predict the onset of the spring bloom is the shutdown of turbulent convection (*Taylor and Ferrari*, 2011). This model showed that phytoplankton growth increases when the water column mixing rate is slower than the net phytoplankton growth rate, and hypothesises that the onset of the bloom occurs when atmospheric cooling decreases, resulting in a surface heat flux increase (*Taylor and Ferrari*, 2011). This model still requires a mixed layer shallower than the critical depth in order for positive productivity (in other words Sverdrup conditions), but proposes changes in surface heat flux as a better predictor of the annual spring bloom instead of mixed layer depth (MLD) only. *Chiswell* (2011) proposes the onset of stratification model from winter to spring resulting from strong vertical mixing conditions (increased wind stress, surface cooling and convective overturning) that deepen the seasonal thermocline in winter. A deepening thermocline (to depths deeper than the critical depth) implies high rates of vertical mixing, resulting in negative net production. Subsequently, in spring, wind stress generally decreases, causing a weakening of convective overturning, resulting in slowing down of mixing processes. Phytoplankton blooms can then initiate when mixing ceases, even if the thermocline is deeper than the critical depth (*Chiswell*, 2011) provided they are no longer mixed out of the surface euphotic waters. This complex interaction between the mixed layer depth and water column production remains a topic of debate.

1.4.3.1 Photosynthesis light response curves

Light-dependent response of photosynthesis can be examined using photosynthesis vs. irradiance (*PvsE*) curves (*Platt and Jassby*, 1976; *Platt et al.*, 1980, *Sakshaug et al*., 1991). An idealised *PvsE* curve is shown in Fig. 1.6. At low irradiance photosynthesis is proportional to available light, while cell respiration processes exceed photosynthesis. The irradiance at which photosynthesis balances respiration is the compensation irradiance (I_c), and net photosynthetic production is positive at irradiances greater than I_c. As light increases, photosynthesis increases until photosynthetic capabilities become saturated and it becomes constant at high irradiance where maximum photosynthetic production (P_{max}) is maintained. When light intensities increase further, damage to photopigments ensue and photoinihibition occurs (*Alderkamp et al*., 2010). The saturation irradiance (I_k) is estimated by P_{max}/α. The initial slope (α) of the light-limited portion of the *PvsE* curve is a measure of the efficiency with which a plant harvests light (*Kirk*, 1994) and represents the amount of photosynthesis per incident photon. Photoinhibition generally occurs at elevated irradiances, where the *PvsE* curve tapers off (*Sakshuag et al*., 1997). P_{max} reflects the efficiency of photosynthesis and shows significant variation between phytoplankton species. It is dependent on enzyme-dependent processes like the transfer of reductants from the light reactions and their use in organic matter synthesis (dark reactions).

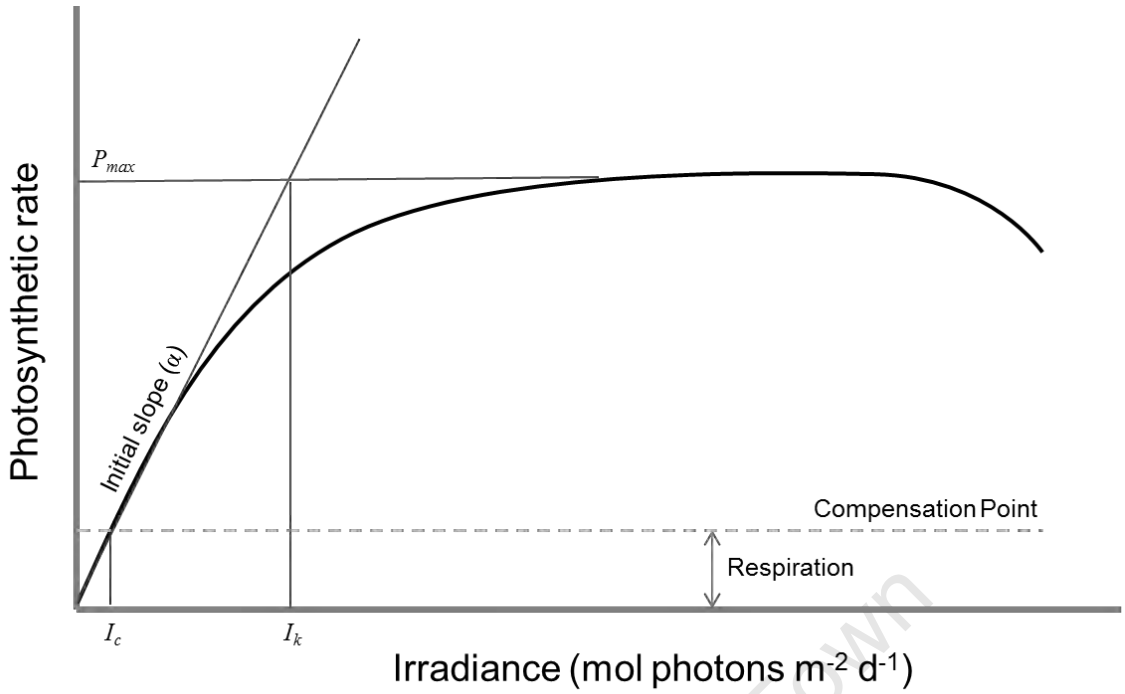

Figure 1.6. Idealised schematic of photosynthesis vs. irradiance (*PvsE*), where α is the initial light limited slope, P_{max} is the light saturated rate of photosynthesis, I_c is the compensation irradiance and I_k the saturation irradiance.

These processes are temperature sensitive (i.e. *Coté and Platt*, 1984, *Davidson*, 1991), and are related to the availability of nutrients, resulting in acclimation to specific environments. For instance, diatoms proliferate at light sufficient environments while flagellates are more adept in the lower light region of the water column (*Chan,* 1980; *Jones and Gowan,* 1990). Diatoms are non-motile, hence favoured by high turbulent mixing which enhance nutrient flux in the proximity of the cells, while more motile dinoflagellates can exploit optimum nutrient and light conditions through swimming in calmer less turbulent conditions (*Smayda,* 1997; *Peters et al.*, 2006). Iron addition experiments during SOFeX have shown that increased iron results in doubling light-limited photosynthetic rates (in other words increased α), but have little impact on light-saturated photosynthetic rates (*Hiscock et al.*, 2008). In low temperature

conditions, organisms are adapted to reduce cellular chl-a (*Davidson*, 1991), which decrease the light harvesting capacity. The effect is that photosynthetic efficiency (in terms of P_{max}) can be maintained at reduced temperatures.

1.4.4 Temperature

The near-zero water temperatures of the Southern Ocean have been proposed as a controlling factor of phytoplankton growth rates (*Priddle et al*., 1992; *Raven and Geider*, 1988; *Laws et al*., 2000). Early radioactive tracer studies revealed increases in photosynthetic rates with increasing temperature up to 7^{o}C, followed by rapid decreases at higher temperatures. This suggested that rates of photosynthesis are limited by thermodynamic effects on metabolic reactions (*Neori and Holm-Hansen*, 1982), which relate to enzyme reactivity processes. *Laws* et al., (2000) showed that while export production was insensitive to total production rates at elevated temperatures (> 25^{o}C), maximum export occurred at temperatures between 0 – 10^{o}C. *Geider et al*. (1987) observed an empirical relationship between the carbon:chl (C:Chl) ratio with temperature and light, using laboratory cultures of phytoplankton and cyanobacteria. The authors showed that C:Chl ratios increased linearly with increasing light at constant temperature, and decreased exponentially with increased temperature at constant light. Low-temperature chlorosis was proposed as an adaptive response in the allocation of cell resources between temperature-independent biophysical reactions (i.e. light harvesting), and temperature-dependent biochemical reactions (nutrient assimilation). Stated more simply, water temperature sets an upper limit on phytoplankton growth rates that are subsequently modified by other environmental factors (*Smith and Sakshaug*, 1990). Therefore, although temperature

impacts on photosynthesis rates, the patchy nature of phytoplankton blooms and the high range of production rates across small temperature ranges, suggest that temperature is not the primary controlling factor of production in the Southern Ocean (*Holm-Hansen et al*. 1977).

1.4.5 Top down controls of primary production

Low chl-a concentrations in the Southern Ocean are also proposed to be maintained by grazing by zooplankton (*Banse*, 1996; *Smetacek et al.*, 2004). A strong link between small phytoplankton size classes (pico and nano phytoplankton) and small microzooplankton grazers (ie protozoans) suggests a close relationship between phytoplankton growth rates, cell division rates and grazers (*Banse*, 1996). Small phytoplankton cells (with high growth rates) cannot evade microzooplankton grazers with relatively fast growth rates (*Banse*, 1996). Under these conditions, most organic matter will be remineralised within the microbial loop, resulting in limited carbon export from surface waters. An alternate scenario can occur when larger diatom cells escape grazing pressure from the larger metazoan zooplankton grazers that take a long time to grow (*Banse*, 1996). Such conditions favour the occurrence of phytoplankton blooms, with consequent export of organic matter through sinking of larger cells and faecal pellets (*Falkowski et al*., 1998).

1.5 Estimating primary production

Primary production and the downward flux of particulate material from the upper mixed layer of the ocean have a major effect on biogeochemical processes in the

oceans and on the earth system as a whole. There are a variety of direct and indirect methods that exist which enable the estimation of rates of primary production and carbon export. These include chemical ^{15}N tracer studies (i.e. *Dugdale and Goering*, 1967), seasonal drawdown of nutrient stocks in the euphotic zone (ie. *Sweeney et al.*, 2000), carbon budgets based on concentration changes in oxygen (*Bender et al*., 1987) or total CO_2 (*Bender et al*., 2005), continuous measurement of biological oxygen supersaturation (*Hendricks et al.,* 2005; *Reuer et al.,* 2007; *Cassar et al.*, 2009), export of sinking particles using sediment traps (*Berelson et al*., 1997) and ^{234}Th disequilibrium (*Buesseler et al.*, 1992; *Lampitt et al.,* 2008), as well as production rates calculated from remotely-sensed properties (e.g. chl-a, temperature and PAR) (see *Behrenfeld and Falkowski*, 1997; *Arrigo et al.*, 2008). These methods have individual strengths and weaknesses depending on the environment conditions, the logistical constraints inherent in the study and the underlying assumptions associated with each method.

Before providing estimates of primary productivity, it is necessary to clarify the various types of 'productivity' referred to throughout this study. Definitions described in *Cullen*, (1991) include the following:

Gross Primary Production (GPP), is the total rate of CO_2 fixation during photosynthesis.

Net Primary Production (NPP), is GPP minus autotrophic respiration.

Net Community Production (NCP) is NPP minus losses due to heterotrophic respiration by microorganisms and metazooplankton.

A variety of productivity estimates are used in this work, and the following section describes the uncertainties and assumptions associated with each method.

1.5.1 New production and the f-ratio

Measurements of phytoplankton production in the euphotic layer using ^{15}N stable isotopes (*Dugdale and Goering*, 1967) can be used to infer carbon export into the ocean interior based on the *f*-ratio (*Eppley and Peterson*, 1979; *Savoye et al.*, 2004). The *f*-ratio represents the fraction of new production fuelled by uptake of nitrogen which is "new" to the euphotic layer (NO_3, N_2), introduced primarily by seasonal overturning or upwelling and from "regenerated" phytoplankton production fuelled by uptake of other nitrogen compounds (urea, NH_4 and dissolved organic nitrogen (DON)) which have been recycled within the euphotic layer (*Eppley and Peterson*, 1979). As nitrogen flux into surface waters must ultimately be balanced by equivalent losses, the *f*-ratio is a measure of that fraction of primary production, which is potentially available for export to the deep ocean or to higher trophic levels; which is surplus to phytoplanktonic community maintenance requirements (*Goeyens et al.*, 1998). NO_3 uptake can thus provide an indirect estimate of downward carbon flux when Redfield ratio stoichiometry is inferred or measured (*Eppley and Peterson*, 1979). This approach to measuring carbon export relies on a number of underlying assumptions which include steady state conditions (uptake flux approximately balanced by particulate nitrogen flux out of the surface), no storage of nitrogen in surface waters (*Eppley and Peterson*, 1979), and minimal euphotic layer nitrification (*Bianchi et al*., 1996; *Yool et al.*; 2007). For instance, in order for the uptake of new nitrogen (NO_3) to balance the upward flux of NO_3 into the surface there has to be no storage of nitrogen in the surface waters. This would exclude the release of DON through heterotrophic activity (*Bronk et al*., 1994), which if present in surface waters will result in an underestimation of gross nitrogen uptake rates (*Bronk et al*., 1994; *Slawyk & Raimbault,* 1995). Nitrification is the major route by which

heterotrophically regenerated nitrogen is remineralised by bacteria through the oxidation of ammonium to nitrite and nitrate (*Yool et al.*, 2007). Unlike nitrate that originates from below the nutricline (the depth in the water column where nutrient concentrations show the steepest gradient), nitrate derived from nitrification in the euphotic zone should be considered as regenerated nitrogen. Nitrification can therefore substantially distort estimates of "new" and export production when based on bulk nitrate uptake (*Yool et al*., 2007). Although nitrification in surface waters is particularly important in oligotrophic ocean regions, this process may not be significant in nitrate replete environments such as the Southern Ocean (*Yool et al.*, 2007; *Lucas et al.*, 2007; *Clark et al.*, 2008). Another problem is the use of particular stoichiometric ratios to convert nitrogen uptake (ρN) to carbon equivalents, which may be compromised by non-Redfield behaviour in the cellular response to available light, iron and nutrients (*Brzezenski et al*., 2003; *Arrigo*, 2005). Despite its limitations, the *f*-ratio remains a useful proxy for estimating potentially "exportable production" (*Sambrotto and Mace*, 2000) in nutrient rich polar oceans, particularly when used in conjunction with other export proxies.

1.5.2 Seasonal drawdown of nutrients

Although the seasonal drawdown of nutrients to estimate seasonal productivity is not used in this work, a brief description is outlined here. Depth-integrated seasonal decreases in the nitrate reservoir over an annual cycle can be used to estimate new production rates (eg. *Garside and Garside*, 1993). In this method, seasonal NCP is calculated using the depth integrated difference of nitrate between winter and summer reservoirs and converting this to carbon using a stoichiometric ratio of organic matter.

The depth integration is usually performed to the nutricline, or a standard depth below the euphotic zone or MLD. This estimate however, does not account for the amount of nitrate that has been converted to dissolved organic nitrogen (DON) that accumulates over the productive season before mineralisation in winter (*Williams*, 1995). The fraction of accumulated DON converted to NO_3 prior to winter, would represent new production which is not exported. Again, nitrate input and removal through nitrogen fixation, nitrification, atmospheric deposition, sub-mesoscale diapycnal mixing, and denitrification are similarly not considered and as such this method tends to overestimate export production. In this method, the choice of the integration depth representing the winter reservoir is important in order to ensure that only euphotic zone processes are considered. In addition, this method assumes that the water column above the integration depth is completely mixed in winter. Finally, this method is largely dependent on the stoichiometric ratios that are used to convert nitrogen to carbon equivalents. It also relies heavily on independent estimates of primary production, over the same time period in order to scale new production estimates to total production (*Sanders et al*., 2007). Carbon to Nitrogen (C:N) ratios can range from 5.3 – 9.1 (e.g. in the Pacific sector between the Antarctic Polar Front and the ice edge), and are generally related to taxonomic variability (*Rubin*, 2003). Such differences in C:N ratios can introduce uncertainty in this production estimate. This method also estimates production over the entire productive season and complicates direct comparison of N uptake estimates from daily/hourly incubation experiments.

1.5.3 Thorium/Uranium disequilibrium

Carbon export estimates are also possible using $^{234}Th/^{238}U$ disequilibrium (*Coale and Bruland,* 1985, 1987). This technique is based on radioisotope concentration measurements instead of particle traps (*Buesseler*, 1992). It is based on the high particle reactivity of ^{234}Th which is rapidly scavenged onto particles in the water column. ^{234}Th is produced from the radioactive decay of its soluble, long-resident parent ^{238}U (Uranium-238). Lower activities of particle-reactive ^{234}Th relative to its conservative parent ^{238}U in surface waters are associated with sinking particles. In other words, adsorption of ^{234}Th onto particles leads to a deficit of its activity, which magnitude is proportional to its removal rate on sinking particles. Particulate Organic Carbon (POC) export is calculated as the product of the ratio of $POC/^{234}Th$ on settling particles and the ^{234}Th disequilibrium flux (*Coale and Bruland*, 1985). Uncertainties associated with this method relate to varying measurement techniques and choice of models (steady-state vs non-steady state). In addition, arguably the largest uncertainty in the application of the thorium approach lies in reliably characterising the ratio of $POC:^{234}Th$ on settling particles, which varies with time, depth, particle type, size and sinking velocity (for review see *Buesseler et el*., 2006). The half-life of ^{234}Th is 24.1 days, resulting in this disequilibrium to reflect the net rate of particle export from the surface on timecales of days to weeks (*Coale and Bruland*, 1985, 1987; *Buesseler et al.*, 1992). A multi-proxy approach of carbon export is most useful and recommended to compare a variety of export estimates as they access different time and space scales.

1.5.4 Primary production from satellite observations

Ocean colour remote sensing has significantly increased our observing ability of spatial and temporal variations in upper ocean productivity on a global scale. Early empirical relationships related chl-a concentrations, as a proxy for photosynthesis, to integrated photosynthesis at various irradiance levels in the water column (*Ryther and Yentsh*, 1957). A number of models have been proposed to estimate primary productivity (PP) from the optical properties of water (see review of *Behrenfeld and Falkowski*, 1997), the simplest of these estimates depth integrated water column primary production as a function of surface chl-a (*Eppley et al.*, 1985). More complex (and complete) models estimate primary productivity as a function of biomass profiles, surface irradiance, water column quantum yield for photosynthesis (*Morel*, 1978), and the spectral attenuation of PAR (400 – 700nm; *Morel*, 1991, *Platt and Sathyendranath*, 1995). Using surface chl-a as the sole factor for the determination of depth integrated primary productivity is problematic since nutrient limitation, depth distribution of biomass and temperature also influence productivity rates (*Behrenfeld and Falkowski*, 1997). Vertically and spectrally explicit models can incorporate algal physiological processes related to environmental factors (e.g. *in situ* light conditions). The implementation of these models may be hindered by the limited availability of the photosynthesis-irradiance parameters (ie. initial slope and assimilation number) at global scale (*Carr et al*., 2006). However, alternative approaches have been developed to provide estimates of the photosynthesis-irradiance parameters ar regional and global scales (e.g. *Platt et al.,* 2008*; Huot et al.,* 2013; *Saux Picart et al.,* 2014). The model presented in *Behrenfeld and Falkowski* (1997) calculate PP using chl-a biomass and the maximum observed photosynthetic rate representing the effective photo-adaptive yield under certain light conditions. This method is highly dependent

on incident radiation, and is mathematically described by the *PvsE curve*, making it sensitive to knowledge about the physiological state or species composition of the phytoplankton community (*Falkowski and Raven*, 1997). A typical depth and time integrated model described by *Behrenfeld and Falkowski*, (1997) is as follows:

$$\sum PP = Chl \times Z_{eu} \times P^{b}_{opt} \times DL \times f(I^{m}_{*}) \quad (1.3)$$

Where ΣPP is the daily carbon fixation rate (mg C m^{-2} d^{-1}) integrated from the surface to the euphotic depth (Z_{eu}) in meters (m), Chl is the chl-a concentration in the surface (mg m^{-3}), $P^{b}_{opt}$is the maximum chlorophyll specific carbon fixation rate observed within the water column under variable irradiance (mg C (mg Chl)$^{-1}$ h^{-1}), DL is the day length, (h), and $f(I^{m}_{*})$ is an irradiance function dependent on the light saturation of photosynthesis and is given by $I^{m}_{*} = I^{m}_{o} / I^{m}_{K}$, where I^{m}_{o} is the local irradiance at noon and I^{m}_{K} is the photoadaptation parameter (*Platt and Sathyendranath,* 1993). The main limitation with this method is that PP is heavily dependent on surface chl-a and the euphotic depth (*Behrenfeld and Falkowski*, 1997), both of which are difficult to estimate from satellite.

In the modes described in equation 1.3, the variables are ranked according to their ecological variability range (*Behrehnfeld and Falkowski*, 1997). For instance depth integrated chl-a biomass (Chl-a × Z_{eu}) ranges between ~ 2 – 500 mg Chl m^{-2}, making chl-a and Z_{eu} the main contributors to variability of PP (~ 38%) (*Behrenfeld and Falkowski*, 1997). P^{b}_{opt} varies by a factor of 40 (~ 0.5 - 20 mg C mg Chl^{-1} h^{-1}), while estimates of the dimensionless f(I_{*}^{m}) potentially cause PP to change by a factor of ~ 4. Day length (DL) has a more limited effect on the PP (*Behrenfeld and Falkowski,* 1997). It is worthy to note that $P^{b}_{opt}$is distinct from P^{b}_{max} described in the PvsE curve, in that the latter can be measured using 2 hr *PvsE* experiments in the laboratory, and

the former is measured in the field, and governed by a balance of light limitation, light saturation and photoinhibition over a 24 hr period. They are however functionally similar in that they both describe light-saturated photosynthesis (*Hiscock et al*., 2008).

According to *Arrigo et al.*, (2008), estimates of total annual production in the Southern Ocean (> 50^{o}S) from 1997 – 2006 is 1.95 Pg C y^{-1}, roughly 50% lower than estimates by *Behrenfeld and Falkowski*, (1997) and *Moore and Abbott,* (2000). These differences were attributed to differences in the algorithms for chl-a between SeaWiFS (in the former) and Coastal Zone Scatter Colorimeter (CZCS) data in the latter. Higher and less accurate chl-a concentrations were determined from CZCS resulting from longer atmospheric optical path length in the Southern Ocean and unique bio-optical properties for Southern Ocean phytoplankton species (*Arrigo et al.,* 2008). An increase in abundance of *in situ* observation of high quality (High Performance Liquid Chromotography derived) chl-a data has since improved chl-a detection algorithms from space and hence further improved NPP estimates presented in *Arrigo et al.*, (2008). The errors associated with retrieving individual PP parameters from space (e.g. chl-a, Z_{eu}) and their associated influence on the modelled results highlights the difficulties faced when using satellite derived estimates of primary productivity.

1.5.5 Net community production (NCP)

NCP can be estimated through the simultaneous measurement of dissolved gasses (O_2 and Ar) in the surface mixed layer (*Cassar et al*., 2009; *Hendricks*, 2004; *Reuer et al.*, 2007) together with a gas exchange parameterization from wind speeds (eg. *Wanninkof*, 1992). As O_2 and Ar have similar solubility properties (*Garcia and Gordon*, 1992) the simultaneous measurement of these two gases provides an estimate

of the biological O_2 supersaturation. This is because Ar is inert and only affected by physical saturation processes (ie. temperature, bubble entrainment and atmospheric pressure), whereas O_2 is affected by both physical and biological processes. GPP can be constrained by the isotopic composition (^{16}O, ^{17}O, and ^{18}O) of dissolved O_2 (*Luz and Barkan*, 2000), based on the difference between atmospheric and photosynthetic O_2 in surface waters. Biological O_2 supersaturation in the mixed layer gives a measure of net community O_2 production (NCP = NPP minus community respiration). NCP (in units mmol m^{-2} d^{-1}), under steady state conditions, can thus be estimated by

$$NCP = k_w \,.\, (\Delta O_2/Ar) \,.\, [O_2]_{sat} \,.\, \rho \qquad (1.4)$$

Where k_w is the weighted gas transfer velocity for O_2 (m d^{-1}), $[O_2]_{sat}$ is the saturation concentration of oxygen in the mixed layer (μmol kg^{-1}) and ρ is the density of seawater (kg m^{-3}) (*Reuer et al.*, 2007; *Cassar et al.*, 2009).

1.6 Mixed layer processes affecting NCP

The mixed layer is the depth of the surface layer where the density, temperature and salinity are essentially uniform. The mixed layer depth (MLD) in the ocean is maintained by a balance between processes that create stratification (ie solar heat flux, low mixing condition, density gradients) and processes that destroy stratification (wind, surface cooling, convective instabilities that lead to turbulent mixing). In the Southern Ocean during summer, the MLD can be less than 20 m, while in winter MLD can reach more than 500 m in sub-polar latitudes (*Monterey and Levitus*, 1997; *DeBoyer-Montegut et al*., 2004). Soluble gases within the mixed layer are exchanged at the air-sea interface. Physical transport processes in the mixed layer affect the availability of nutrients that sustain biological productivity (*Lewis et al*., 1984;

Williams and Follows, 2003), and the export of organic material from the euphotic zone (*Ruiz et al*., 2001). These include entrainment/detrainment due to shoaling and deepening of the mixed layer, horizontal advection across a sloping mixed layer, vertical diffusion at the base of the mixed layer, diapycnal mixing across density surfaces and mixing due to mesoscale eddies (Fig. 1.6, modified from *Levy et al*., 2013).

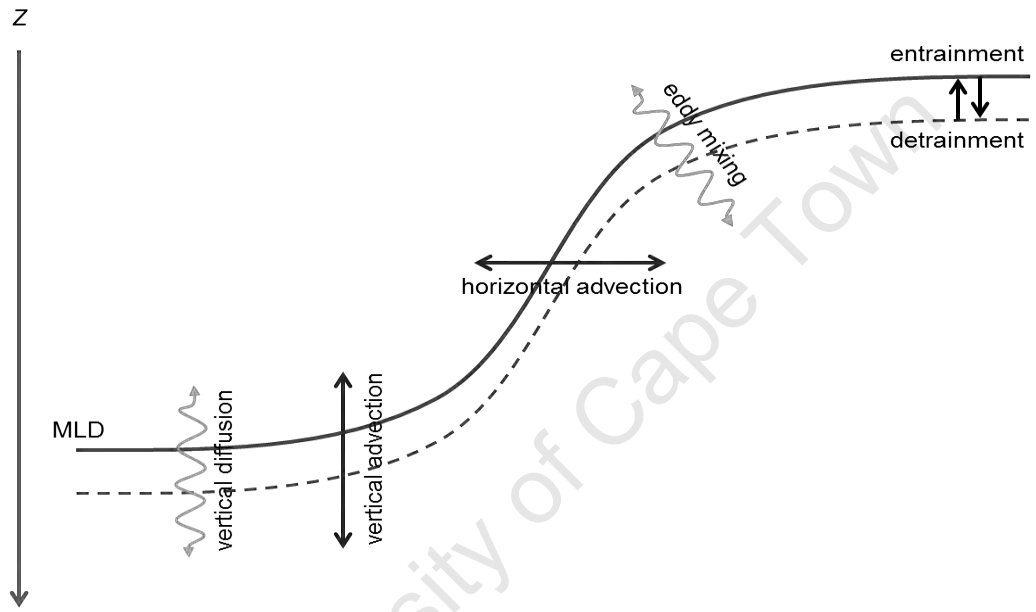

Figure 1.7. Mixed layer processes affecting the nutrient concentration and primary productivity (taken from *Levy et al.* 2013).

All the processes listed above operate at a range of different spatial and temporal scales. For example, winter convective overturning increases surface nutrient concentrations in the seasonal thermocline (*Williams and Follows*, 2003) to sustain primary productivity over the growing season. At shorter time and spatial scales, episodic mesoscale eddies (10 – 100 km in size) upwell nutrients into the euphotic zone that can support phytoplankton blooms in subtropical regions (*Levy et al.*, 2009; *McGillycuddy et al.*, 2007; *Oschlies and Garcon*, 1998). Rapid eddy-driven

stratification (on timescales of weeks) has also been proposed as a driver for the early initiation of the spring bloom (*Mahadevan et al.*, 2012). The mechanism proposed by *Mahadevan et al.*, (2012) is that unstable lateral density gradients ('fronts') generate mixed layer eddies which move less dense water over denser water increasing rates of stratification. However, when wind conditions are along the frontal current, Ekman transport moves denser water over lighter water, favouring convective mixing. When re-stratifying mechanisms (mixed layer eddies, solar heating) overcome mixing (downfront winds, surface cooling), vernal blooms are initiated (*Mahadevan et al*., 2012). A slightly different example is given by *Taylor and Ferrari* (2011) who proposed that during winter, when deep convection is present, frontal restratification, caused by frontal instabilities, can stimulate productivity by reducing the rate of vertical mixing and increasing the re-stratification rate.

Sub-mesoscale processes at horizontal scales of 1 – 10 km, vertical scales of 100 m and timescales of 1 day are also important in stimulating phytoplankton production and export (*Lévy et al.*, 2001). Within an oligotrophic production regime, short term wind-driven sub-mesoscale eddies will increase vertical inputs (advection and diffusion) of nutrients (*Klein and Coste,* 1984), which stimulate new production in the surface (*Lévy et al.*, 2009). An additional mechanism is that stratification at sub-mesoscale fronts and a reduction of vertical mixing (e.g. *Taylor and Ferrari*, 2011) also stimulate primary productivity. Sub-mesoscale frontal dynamics are implicated in not only changing the primary and export production, but also the structure and functioning of phytoplankton communities (*Lévy et al.*, 2012). Phytoplankton response to sub-mesoscale dynamics depend mainly on whether the community is light limited or nutrient limited. Alleviation of nutrient limitation by increased vertical inputs stimulates productivity in a nutrient limited regime, while stratification in light

limited conditions dampen the rate of vertical mixing (through mixed layer shoaling or reduction in mixing intensity), increasing the light exposure for phytoplankton.

Previous work using satellite chl-a data has proposed that phytoplankton productivity variability during spring and summer in the Southern Ocean can be influenced by intra-seasonal adjustments of the mixed layer physics that modulate light and nutrient limitation (*Fauchereau et al*., 2011, *Thomalla et al*., 2011). In the Southern Ocean, the limiting nutrient dFe can be supplied vertically into the euphotic zone by once off wintertime convective overturning (entrainment), and year-round diapycnal diffusion, as well as Ekman upwelling (*Boyd and Ellwood*, 2012; *Tagliabue et al*., 2014). *Fauchereau et al.* (2011) investigated the response of surface chlorophyll concentrations to subseasonal variability in MLD. The authors show showed that transient episodes of increased chlorophyll in summer were related to both a shoaling of the mixed layer when light conditions were suboptimal and a deepening of the mixed layer particularly when nutrients (in particular iron) were limited.

1.7 Hypotheses and outline

Hypothesis one

Context: In this work the dynamics of primary productivity in the Southern Ocean are investigated with a focus on *in situ* observations of primary productivity in the Atlantic Sector of the Southern Ocean between Cape Town and Antarctica. The following section outlines the hypotheses tested in this work. The Southern Ocean is an HNLC region due to the constraints of light and iron co-limitation as well as zooplankton grazing (*Chisholm and Morel*, 1991; *Boyd*, 2002). Iron affects

phytoplankton growth rates and is essential for nitrate reduction in phytoplankton cells (*Raven*, 1988). In addition, cellular iron demand from nitrate reduction is energy expensive and requires more iron than regenerated based production for photosynthetic redox reactions (*Maldonado and Price*, 1996).

Hypothesis: Regions of elevated summer biomass result from relief of iron and light limitation that will be evident in high f-ratios while the contrary holds for low biomass regions.

Hypothesis two

Context: The characteristics of seasonal cycle of primary production have recently been shown to be sensitive to sub-seasonal modes of variability in upper ocean dynamics that regulate iron and light availability (*Fauchereau et al*., 2011; *Thomalla et al.*, 2011; *Swart et al.,* 2012; 2014).

Hypothesis: Sub-seasonal dynamics in the summer MLD are central to explaining the observed variability primary productivity during summer.

Finally, primary productivity is driven by co-limitation by light and iron (*Boyd et al*., 2001). Under conditions where productivity is influenced by irradiance, iron relief affects the slope of the productivity response to light conditions (*Hiscock et al.,* 2008). This idea is further extended to explore relationships between *in situ* observations of NCP and mean water column irradiance.

Outline of the Thesis

In this work, the area of interest spans all the major frontal zones from the subtropics in the north, across the Antarctic Circumpolar Current, to the Weddell Sea region near the Antarctic Continent (Fig. 1.1). Chapter 2 introduces the methods. In Chapter 3 estimates of new and regenerated primary productivity using nitrogen tracer experiments in late summer 2008 are used to investigate the potential carbon export from the surface to the deep ocean in the Atlantic Southern Ocean. In this research, spatial and temporal variability in primary productivity estimates are considered in relation to variability in the physical and biogeochemical environment.

In Chapters 4 and 5, the nature of the interplay between phytoplankton productivity and iron and light limitation is investigated in the SAZ to gain a better understanding of their impact on the Southern Ocean's carbon cycle. In this research the role of meso- and sub-mesoscale variability of the MLD is investigated with respect to its impact on the availability of light and nutrients to support phytoplankton growth and biological productivity in Southern Ocean. This was achieved using high resolution *in situ* observations of NCP and MLD in summer along the Goodhope transect.

Chapter 6 integrates chapters 3 – 5 and discusses the major gaps in the research of Southern Ocean productivity with respect to climate change and provides a summary of the implications of this work in the context of ocean productivity.

Chapter 2

Methods

This chapter descrtibes the study area for this research with respect to the hydrographic and biogeochemical settings as well as the methods employed throughout this study to estimate primary productivity for samples collected in the surface mixed layer of the Atlantic Southern Ocean during several cruise campaigns in the Atlantic Southern Ocean, mainly in late summer, between 2008 and 2013.

2.1 Study Area

The uninterrupted nature of the ACC transports water, heat and salt between the three ocean basins and ensures continuity among a narrow range of environmental characteristics (*Smetacek et al.*, 2004). This inter-ocean basin exchange links the global Meridional Overturning Circulation, which regulates the global climate system (*Gordon*, 1986; *Speich et al.,* 2007), particularly through Agulhas Rings at the Agulhas retroflection South of Africa (*Lutjeharms*, 1996; *Speich et. al.,* 2007). The Weddell Sea Gyre on the other hand, interacts with the Antarctic Continental shelf, which is considered to be a deep water formation region (*Orsi et. al.*, 1993; *Gordon*, 2001). The biogeochemical zonation of the Southern Ocean (*Thomalla et. al.*, 2011) is mainly controlled by wind-driven upwelling and transport of the Antarctic Circumpolar Current (ACC) (*Pollard et. al.*, 2002). Upwelled Circumpolar Deep Water (UCDW) closes the global ocean nutrient cycle and provides the nutrient supply to support primary productivity in the sub-Antarctic as well as in the ocean basins to the north (*Marinov et*

al., 2006). This is mainly due to the formation of Sub-Antarctic Mode Water (SAMW) and Antarctic Intermediate Water (AAIW), which originates in the winter water layers that encircle Antarctica. The formation of SAMW is particularly strong in the Subantarctic Zone (40 – 45°S) and Polar Front Zone (45 – 55°S) in the western South Atlantic (*Sarmiento et al.*, 2004).

2.2 Hydrographic and biogeochemical setting

Hydrographic ocean fronts are associated with strong currents and gradients in temperature and salinity (*Swart et. al.*, 2008), and expose different water masses to the surface layer and allow surface biogeochemical zonation (*Pollard et. al.,* 2002). It is worth noting that, rather than being a fixed circumpolar continuum, fronts are thought to be localised jet-like features steered by bathymetry, which carry the majority of the transport of the ACC (*Belkin and Gordon*, 1996; *Sokolov and Rintoul*, 2007). At the fronts upward sloping isopycnal surfaces (layers of relatively uniform density) outcrop, resulting in a north-south latitudinal distribution of surface macronutrient concentrations (*Sarmiento et. al.*, 2004). This stepwise characteristic has been used to demarcate biogeochemical zones across the ACC (*Pollard et al.,* 2002). The biogeochemical zones outlined in *Pollard et al.*, (2002) are used throughout the text, based on the changing balance of temperature and salinity to the stratification confined by physical frontal positions (*Orsi et al.*, 1995; *Swart et al.*, 2010).

A sharp zonal decrease in temperature and salinity is observed on crossing the across the STF from the SAZ (Fig. 2.1). Between the STF and the Sub-Antarctic Front (SAF, ~ 44°S) lies the Subantarctic Zone (SAZ). Here, temperature dominates the stratification north of the SAF (*Whitworth and Nowlin*, 1987). The SAZ is a highly

productive zone (*Moore and Abbot*, 2000; *Thomalla et. al.*, 2011), and its water characteristics are mostly influenced by surface waters that have been carried northwards by wind driven Ekman transport from the Polar Front Zone (PFZ) in the surface layer (*Pollard et. al*., 2002). The PFZ has the SAF as its northern limit and the Polar Front (PF, ~ 50°S) at its southern limit. The PF is classically defined by the 2°C subsurface temperature minimum at a depth of 200 m (*Belkin and Gordon*, 1996, *Orsi et. al*., 1995). The unstable subsurface temperature minimum is compensated for by fresh surface salinities which dominate stratification southward of the PF (*Pollard et. al.*, 2002). South of the PF lies the Antarctic Zone (AAZ), confined by the Southern Boundary of the ACC (SBdy, ~ 56°S). *Orsi et. al.,* (1995) defined the Southern Boundary (SBdy) as the southern terminus of Upper Circumpolar Deep Water (UCDW) or the vertical extent of the 1.5°C isotherm. Southward of the SBdy lies the Southern Antarctic Circumpolar Zone (SACCZ), identified by the absence of UCDW.

2.3 Underway in situ sampling in the Atlantic Southern Ocean.

Seven crossings of a meridional cruise transect in the Atlantic Southern Ocean were conducted in austral summers of 2008 - 2011, on board the *RV Marion Dufresne* (Feb/Mar 2008) and *MV S.A. Agulhas* (Dec2008 - Mar2009 and Dec2009 - Mar2012). The first process study cruise the BONUS-GOODHOPE (BGH) cruise (http://www.univ-brest.fr/IUEM/BONUS-GOODHOPE/start.php) formed part of the International Polar Year (IPY-GEOTRACES) programme aiming to understand large scale inter-ocean exchanges, characterising biogeochemical processes in carbon cycling and trace elements, and assessing the impact of coastal open ocean exchanges on geochemical properties. The subsequent cruises formed part of SOCCO (the Southern

Ocean Carbon and Climate Observatory) that ustilises the logistic voyages of the South African National Antarctic Programme (SANAP) with the aim of continuing long term time series observations in the Southern Ocean to link surface CO_2 flux and net primary production variability to the underlying physical and biogeochemical drivers. The cruise tracks followed the GOODHOPE-A21 repeated hydrographic section from the World Ocean Circulation Experiment (WOCE), along the Greenwich meridian between Cape Town and Antarctica (Fig. 2.1).

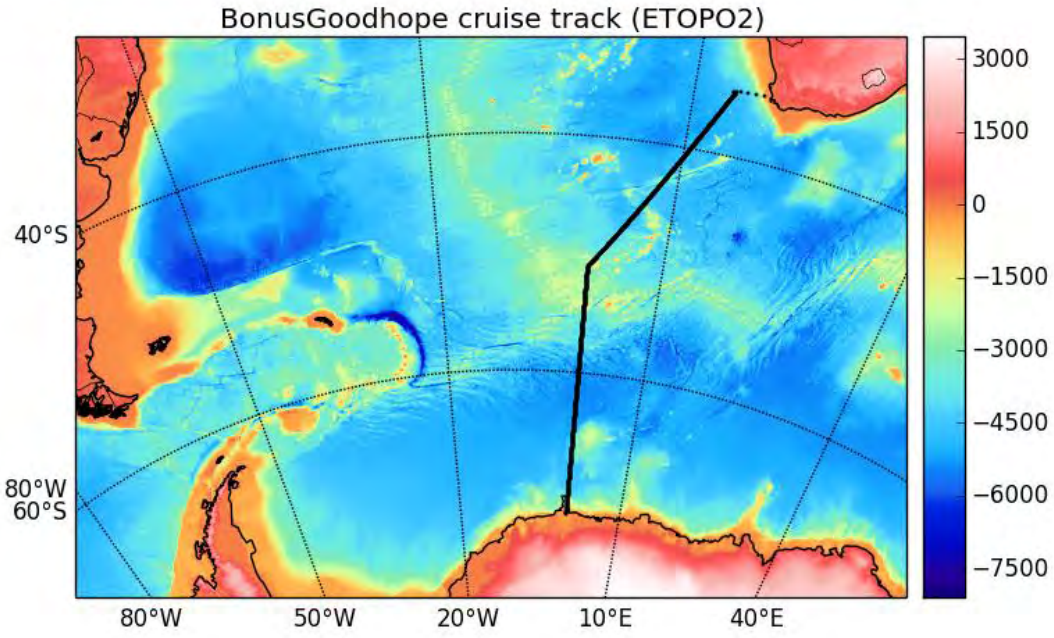

Figure 2.1. Bonus Goodhope Cruise repeat transect in the Atlantic Southern Ocean between 2008 and 2010, overlaid on the bathymetry (units in meters).

2.3.1 Hydrographic measurements

High resolution water column temperature and salinity profiles were collected using conductivity temperature and depth (CTD; only in Feb/Mar2008), Expendable

Bathythermographs (XBT) and underway Conductivity Temperature and Depth (uCTD) profilers. XBTs were deployed at ~20 nautical miles intervals. uCTDs were deployed between XBT stations. CTD (SEABIRD 911plus with auxiliary sensors) mounted on a SEABIRD rosette was deployed on average every 20 nautical miles on the BGH cruise. Auxiliary sensors included a SBE43 Dissolved Oxygen sensor, Fluorometer and Turbidity sensor, Altimeter, and Underwater PAR sensor. Mixed layer depths were determined using the temperature criteria of *De Boyer-Montégut et al*., (2004), ($\Delta T <$ 0.2 ^{o}C in reference to the temperature at 10 m depth). Climatological MLD data were also derived using temperature and salinity profiles (from Argo and hydrographic data) from the Met Office Hadley Centre EN3 v.2a (at www.metoffice.gov.uk/hadobs/en3/). The EN3 dataset objectively analyses all available *in situ* temperature and salinity profiles into a monthly, one degree resolution global grid (*Ingleby and Huddleston*, 2007).

2.3.2 Nutrient analyses

Ambient NO_3 and $Si(OH)_4$ concentrations were analyzed on a Bran and Lubbe AAIII autoanalyser, as by described in *Tréguer and Lecorre* (1975). Ambient and experimental concentrations of NH_4 and urea were determined manually by the colorimetric method of *Grasshoff et. al.,* (1983) scaled to 5ml samples (*Probyn*, 1985).

2.3.3 Dissolved Oxygen

Samples for Dissolved oxygen (DO) were collected from CTDs and the uncontaminated underway seawater intake for all underway legs of the cruises. DO concentrations were determined using the Winkler iodometric method (*Grasshoff et. al.*, 1999). DO bottles

were filled from the bottom with a siphon to minimise cavitation. Samples were fixed immediately after sampling with $MnCl_2$ and NaOH/NaI and precipitated as $Mn(OH)_2$ in an alkaline medium. Samples were acidified with sulphuric acid (H_2SO_4) and titrated using a standardised solution of sodium thiosulphate dispensed by a Dosimat™ autotitrator. Oxygen sensor results from the CTD were compared with those analysed using the Winkler method for quality assurance and outliers were removed from the CTD dataset.

2.4.4 Particulate organic carbon and nitrogen

Particulate organic carbon (POC) and –nitrogen (PON) were determined by filtering 1 L samples collected from surface casts, through pre-ashed 25mm Whatman GF/F filter papers. Filtered samples were frozen at -20^{o}C until analysis ashore. Samples were oven-dried at 60^{o}C, acid fumed with sulphuric acid and pelleted into aluminium/tin cups (8x5 mm) for analysis on a Thermo Finnegan Flash EA1112 elemental analyser.

2.4 Chlorophyll-a (Chl-a)

Chlorophyll-a (Chl-a) samples were determined after filtration of 250 mL seawater using 25 mm Whatman GF/F filters. Chl-a pigments were extracted from the filter using 7 mL of a 90% aqueous acetone solution (*Strickland and Parsons,* 1963) over 24 hours followed by centrifugation. Sample fluorescence was measured using a Turner designs 10AU fluorometer after calibration using pure chl-a from spinach (Sigma-Aldrich). Phaeopigments were determined upon acidification with 10% HCl and reading on the fluorometer.

2.5 Remote sensing measurments

2.5.1 Photosynthetically Active Radiation

PAR was taken from MODIS climatology for summer months in units of mol photons m^{-2} d^{-1} (http://oceancolor.gsfc.nasa.gov/cgi/l3) from 2002 to 2012. Mean water column irradiance ($\bar{I}_{MLD}$) was determined using monthly PAR integrated over the mixed layer and exponential attenuation of light, and then dividing by the MLD. The diffuse attenuation coefficient (K_z) was calculated using *in situ* chl-a concentrations (*Morel et al.*, 1988).

2.5.2 Chlorophyll-a

Chl-a concentrations from MODIS/Aqua, using the Level-3 9 km × 9 km grid. 8-day satellite composites from 2002 to 2012 were aggregated to a seasonal climatology. Satellite data, particularly in the Southern Ocean, suffers from a high frequency of days where clouds, light conditions, sea-ice, or other problems compromise the observations. The relative frequency of such 15 days for our dataset is between 5 % and 15 % on this grided data product (*Jonsson et al*., 2014)

2.5.3 Wind speed data

Wind speed data were obtained using daily averages of NESDIS 0.5° resolution based on the QuickSCAT satellite (*Ebuchi et al*., 2002). Gas transfer velocities are typically determined using a daily 10 m wind speed observations (u_{10}), weighted to account for prior wind speed variability. The weighting technique developed by *Reuer et al.,* (2007), where the fraction of the mixed layer ventilated on collection day (f_1), and the gas transfer velocity on the collection day (k_1) is calculated as $f_1 = k_1 .1$ day/MLD. The

weight on sample collection day (ω_1) was assigned a value of $\omega_1 = 1$. Subsequent days have a weighting reduced proportional to the fraction ventilated on day 1 according to $\omega_2 = \omega_1(1-f_1)$ up 60 days prior to sample collection (*Reuer et. al.,* 2007). As such, although wind speeds of 60 days prior to the collection date are considered, it is only the first 10 days that has the strongest influence on the NCP.

2.6 Nitrogen uptake measurements

To determine depth integrated nitrogen uptake, samples were collected at 5 water column irradiance levels (100%, 50%, 25%, 10% and 1%) within the euphotic layer using a Seabird 911plus CTD-rosette, equipped with 12 litre Niskin bottles. Light levels were measured using a hand held Biospherical radiation sensor. Three bulk samples (2 L each) from each light level were pre-screened through a 200 µm plankton mesh to exclude zooplankton grazers and then transferred into 2 L washed borosilicate glass bottles. Aliquots of 200µl stock solutions ($K^{15}NO_3$ (1 µmol/100µl), $^{15}NH_4Cl$ (0.1 µmol/100µl) and $CO(^{15}NH_2)_2$ (0.1 µmol/100µl)) were added separately to three bottles from each light depth for nitrogen uptake incubations, while 420 µl stock solution $NaH^{13}CO_3$ (0.5 µmol/100µl) was added to the NO_3 incubation bottle only, for carbon fixation measurements. Incubation bottles were placed inside a polycarbonate incubation tubes covered with Panalux^{TM} neutral density filters to simulate appropriate water column light absorption at different depths. Sea surface temperatures were maintained by circulating surface water through the incubation tubes. Samples were incubated for 24 hours and terminated by filtration onto ashed 47 mm GF/F filters, which were then dried at 50^{o}C before later isotopic analyses.

2.7 Size fractionated uptake

Size fractionated N uptake and C fixation experiments were conducted using ~ 20 L bulk surface samples obtained using either a clean plastic bucket or from CTD Niskin bottles. The bulk sample was pre-screened through a 200 µm plankton mesh screen to remove zooplankton grazers and then divided into 3 x 6 L sub-samples, contained in clear polycarbonate incubation cylinders. The sub-samples were spiked with $^{15}NO_3$-N, $^{15}NH_4$-N, and ^{15}urea-N salts as described previously to a final spike concentration of 0.25 µM. The 3 x 6 L samples were incubated at 50% ambient light for 24 hours. After incubation, each 6 L experiment was post-fractionated into 3 equal 2 L fractions. The first 2 L was passed through a 200 µm mesh, a further 2 L through a 20µm plankton mesh screen and finally, 2 L was passed through a 2 µm Nuclepore membrane filter. The three size fractions (< 2 µm, 2 - 20 µm and 20 - 200 µm) were finally filtered onto ashed 47 mm GF/F filters for later isotopic analyses.

2.8 Isotope analyses

As entire 47mm diameter filters are too large to be pelleted into tin capsules for analyses, 10 small-diameter discs (~ 2 mm) were punched from the large filters and placed into 8x5mm tin capsules prior to analysis on a Delta V Plus stable light isotope mass spectrometer interfaced to a Thermo Finnegan Flash EA1112 Elemental Analyser for simultaneous POC/N and ^{15}N, ^{13}C measurements. Natural abundance for N and C were 0.3663 atom% ^{15}N and 1.1056 atom% ^{13}C respectively. Values were scaled upwards to reflect the proportion of the sub-sampled area relative to the total filtered area. Sulphanilamide and urea were used as a calibration standard for C and N determinations. Uptake rates for C and N were calculated as described by *Dugdale and*

Wilkerson (1986), without correction for isotopic dilution in the case of NH_4 uptake. The atom% ^{15}N excess in the sample was corrected for the natural abundance of ^{15}N (N_{nat}):

$$^{15}N_{xs} = {}^{15}N_{sample} - {}^{15}N_{nat} \quad (2.1)$$

Specific uptake rates (N taken up per unit particulate N) were calculated from the isotopic ratio upon termination of the incubation:

$$V_{(t)} = \frac{{}^{15}N_{xs}}{\left({}^{15}N_{init} - {}^{15}N_{nat}\right) \times T} \quad (2.2)$$

Where T is the incubation time of the experiment, $^{15}N_{init}$ is the atom% ^{15}N in the initially labelled fraction added to the incubation experiment. $^{15}N_{init}$ is dependent on the nutrient concentration of the sample. The transport rate, $\rho_{(t)}$ (the N uptake in concentration units) is calculated from $V_{(t)}$ and the $PON_{(t)}$ concentration at the end of the incubation:

$$\rho_{(t)} = V_{(t)} \text{ x } PON_{(t)} \quad (2.3)$$

Using this method often yields an underestimate of *V* since it remains constant as PON increases during the incubation and does not account for the uptake of non-labelled nutrients during the incubation (*Dugdale and Wilkerson*, 1986), or the presence of detrital nitrogen (*Dugdale and Goering*, 1967). Several other methods/models are proposed for calculating the uptake rates. For instance taking account of the initial concentration of PON in the sample, or assuming that the *V* is constant throughout the incubation period (*Dugdale and Wilkerson,* 1986). Note that isotope ratios and PON were measured on the same sample during mass spectrometry analysis (*Dugdale and Wilkerson*, 1986).

2.9 Underway O_2/Ar measurements and Net Community Production

High resolution measurement of the spatial variability of net community production using the ΔO_2/Ar ratio was conducted underway on all the abovementioned cruises. A continuous flow system that draws from the ship's scientific seawater supply was linked to a micro capillary equilibrator that separates the gas and water phases (*Cassar et al.,* 2009). The gas phase was analyzed on board using a Pheiffer quadrupole mass spectrometer. The system included an Aanderraa oxygen optode and a number of thermocouples used to continuously monitor the temperature at each stage of the sampling cycle. The sampling period was < 10 seconds, and data was averaged for 2 minutes. Small differences in the oxygen concentrations were monitored through periodic simultaneously sampling of both lab supply and surface waters for Winkler analysis. NCP was calculated as described in the equation 1.4.

The underlying assumptions inherent in this calculation are that NCP is equal to the gas exchange flux, NCP has been constant over the mixed layer residence time (~10 days), and finally, that argon saturation concentration is the same in the water and atmosphere. The latter assumption introduces an error of approximately 1% to the magnitude of NCP estimates, due to deviation from the saturation concentrations between water and air (*Cassar et al*., 2011). NCP approximates carbon export production, due to the stoichiometric link between oxygen and carbon during photosynthesis. Because of these assumptions stated above NCP may be significantly different from the actual carbon export production.

A simple box model calculation for a hypothetical MLD of 40 m, net O_2 production rate of 60 mmol O_2 m^{-2} d^{-1}, and dissolved oxygen concentration of 249.5 μmol kg^{-1}, was used to test the wind speed weighting technique by randomly varying the wind speed

between 1 – 20 m s^{-1}. This result show that using a 60 day wind speed weighting technique is more robust for NCP calculation than using 7 day mean wind speed prior to sampling (*Reuer et. al.,* 2007). A complication with this method is that in the absence of net production, O_2 would still commonly be supersaturated in seawater because of the physical processes of temperature or pressure changes and bubble entrainment. Breaking waves produce bubbles which induce supersaturation by partly dissolving in seawater, causing $\Delta O_2/Ar$ ratios to increase according to the atmospheric ratio (*Emerson*, 1987). Uncertainties associated with this process are small and usually neglected in calculations (*Reuer et al.*, 2007). Warming of the mixed layer causes supersaturation by lowering the solubility of oxygen. Uncertainties in the gas exchange parameterisation will introduce the largest error (~30 – 40 %) in estimates of NCP (*Reuer et al*., 2007; *Cassar et al*., 2009). Entrainment or upwelling of O_2-undersaturated waters causes the O_2 bioflux to underestimate NCP (*Jonsson et al.*, 2012). Finally, although diffusive gas exchange is the dominant physical process affecting dissolved O_2 concentrations in the mixed layer, diapycnal mixing at the base of the mixed layer and horizontal advection complicates the O_2 mass balance of NCP within the mixed layer.

2.10 Autonomous high resolution hydrographic data (gliders)

High resolution hydrographic measurements were conducted in the SAZ between September 2012 and February 2013 using autonomous gliders as part of the Southern Ocean Seasonal Cycle Experiment (SOSCEx, *Swart et al.*, 2012, 2014). Two gliders were deployed near Gough Island in the South East Atlantic Ocean, at 42.4°S, 9.9°W and 43.0°S, 11°W respectively, and followed an eastward trajectory for approximately

5.5 months. Measurements included conductivity, temperature, pressure, dissolved oxygen, chl-a fluorescence (proxy for phytoplankton biomass), PAR and two wavelengths of optical backscattering by particles. The upper water column was sampled continuously to a depth of 1000 m, at a nominal vertical velocity of 10 cm s^{-1}, at an average data measurement rate of 0.2 Hz. Each dive cycle took approximately 5 hours and covered a horizontal distance of approximately 2.8 km. Data was transmitted using the Iridium Satellite system. All glider sensors were cross-calibrated using ship-based CTD casts, conducted within 3 km and 4 hours of deployment and retrieval of each glider. Bottle samples were also collected at these casts for chl-a, salinity and dissolved oxygen cross-calibration. All sensors were despiked and evaluated for sensor drift. Biofouling by Goose-neck barnacle occurred on the glider fearing and sensor platforms of SG574 towards the end of the mission (final 3 weeks). The final 22 days of temperature and salinity data, affected by the bio-fouling was excluded from the analysis in this study. Only minor biofouling was observed on temperature and salinity data of SG573 and no data were discarded from this glider. Only data from SG573 were used to determine MLD variability from daily temperature profiles (see Chapter 4).

Chapter 3

Nitrogen uptake by phytoplankton in the Atlantic sector of the Southern Ocean during late austral summer.

The work in this chapter is based on the following peer-reviewed publication:

Joubert, W.R., S.J., Thomalla, H.N.Waldron, M.I.,Lucas, M., Boye, F.A.C., LeMoigne., F., Planchon, and S. Speich., 2011, Nitrogen uptake by phytoplankton in the Atlantic sector of the Southern Ocean during late austral summer, Biogeosciences, 8, 2947–2959, 2011, doi:10.5194/bg-8-2947-2011.

3.1 Introduction

Primary productivity in the Southern Ocean plays a key role in the biological uptake of atmospheric CO_2 (*Metzl et al*., 1999; *Takahashi et al*., 2002). Phytoplankton biomass typically shows low chl-a (<0.5 mg m^{-3}) in open ocean waters of the Southern Ocean (*Tréguer and Jacques*, 1992; *Banse*, 1996; *Moore and Abbott*, 2000), while localised elevated chl-a (> 1 mg m^{-3}; *Moore and Abbott*, 2000) is often associated with mesoscale upwelling at hydrographic fronts (*Laubscher et al*., 1993; *Comiso et al*., 1993; *Moore and Abbott*, 2002; *Sokolov and Rintoul*, 2007), the marginal ice zone (MIZ) (*Smith and Nelson*, 1986; *Sedwick and DiTullio*, 1997) and regions of shallow bathymetry around Subantarctic islands (*Blain et al*., 2001; *Pollard et al*., 2002; *Korb and Whitehouse*, 2004; *Seeyave et al*., 2007; *Whitehouse et al.*, 2008). Under-utilization of available macronutrients by phytoplankton production results in the prevalent HNLC condition

(*Chisholm and Morel*, 1991) of the Southern Ocean. Despite a high inventory of available macronutrients, low chl-a concentrations are maintained by bottom-up controls of phytoplankton production through light, iron, and silicate limitation (*Martin et al*., 1990; *Bathmann et al*., 1997; *Boyd et al*., 2001, 2002, 2007; *Moore and Abbott*, 2002; *Arrigo et al*., 2008), as well as by top-down grazing control (*Banse*, 1996; *Cullen*, 1991; *Price et al*., 1994; *Smetacek et al*., 2004; *Behrenfeld*, 2010). These factors regulating primary production all modify carbon export and thus play a key role in determining the strength of the Southern Ocean biological carbon pump.

Measurements of phytoplankton production throughout the euphotic layer using ^{15}N stable isotopes (*Dugdale and Goering*, 1967) have often been used to infer carbon export into the ocean interior based on the *f*-ratio (*Eppley and Peterson*, 1979; *Savoye et al*., 2004). Carbon export estimates are also possible using $^{234}Th/^{238}U$ disequilibrium (e.g. *Buesseler*, 1992). Lower deficiency of particle-reactive ^{234}Th relative to its conservative parent ^{238}U in surface waters are associated with sinking particles. Particulate Organic Carbon (POC) export is calculated as the product of the ratio of $POC/^{234}Th$ on settling particles and the ^{234}Th disequilibrium flux (*Coale and Bruland*, 1985). Uncertainties associated with this method relate to varying measurement techniques and choice of models (steady-state vs non steady state). In addition, arguably the largest uncertainty in the application of the thorium approach lies in reliably characterising the ratio of $POC:^{234}Th$ on settling particles, which varies with time, depth, particle type, size and sinking velocity (for review see *Buesseler et el*., 2006). Despite all the uncertainties associated with the various proxies of carbon export (see section 1.5), it is nonetheless useful to compare a variety of export estimates as they assess different time and space scales.

This work reports measurements of new and regenerated uptake rates and *f*-ratios (as a proxy for export) in surface waters of the Atlantic sector of the Southern Ocean in late austral summer 2008 as part of the BGH programme. The cruise crossed a number of mesoscale features and major hydrographic fronts; namely the STF, SAF, PF, the Southern Antarctic Circumpolar Current Front (SAccF) and Sbdy (Fig. 2.1). Results from this study characterise ρN dynamics and *f*-ratios across different hydrographic regions and investigates their relation to MLD, light, macro-nutrient and dissolved surface iron concentrations. We compare our data with ^{15}N estimates of production in other areas of the Southern Ocean, as well as with ^{234}Th based estimates of carbon export measured during the BGH cruise.

3.2 Sampling and cruise track

The analytical methods utilised in this chapter is described in Chapter 2 above. The sampling cruise on board the *R/V-Marion Dufresne* was conducted from Feb 8 - Mar 18, 2008. The cruise transect (Fig. 3.1) started on the shelf outside Cape Town (South Africa) at the 200 m isobath and followed the GoodHope – A21 transect in a south-westerly direction towards the 0^{o} meridian, then continued south to $58^{o}S$ (Fig. 3.1). A total of 79 sampling stations were completed (Speich et al., 2008), 12 of which were targeted for *ρ*N incubations using ^{15}N tracer techniques (*Slawyk and Collos*, 1977; *Dugdale and Wilkerson*, 1986).

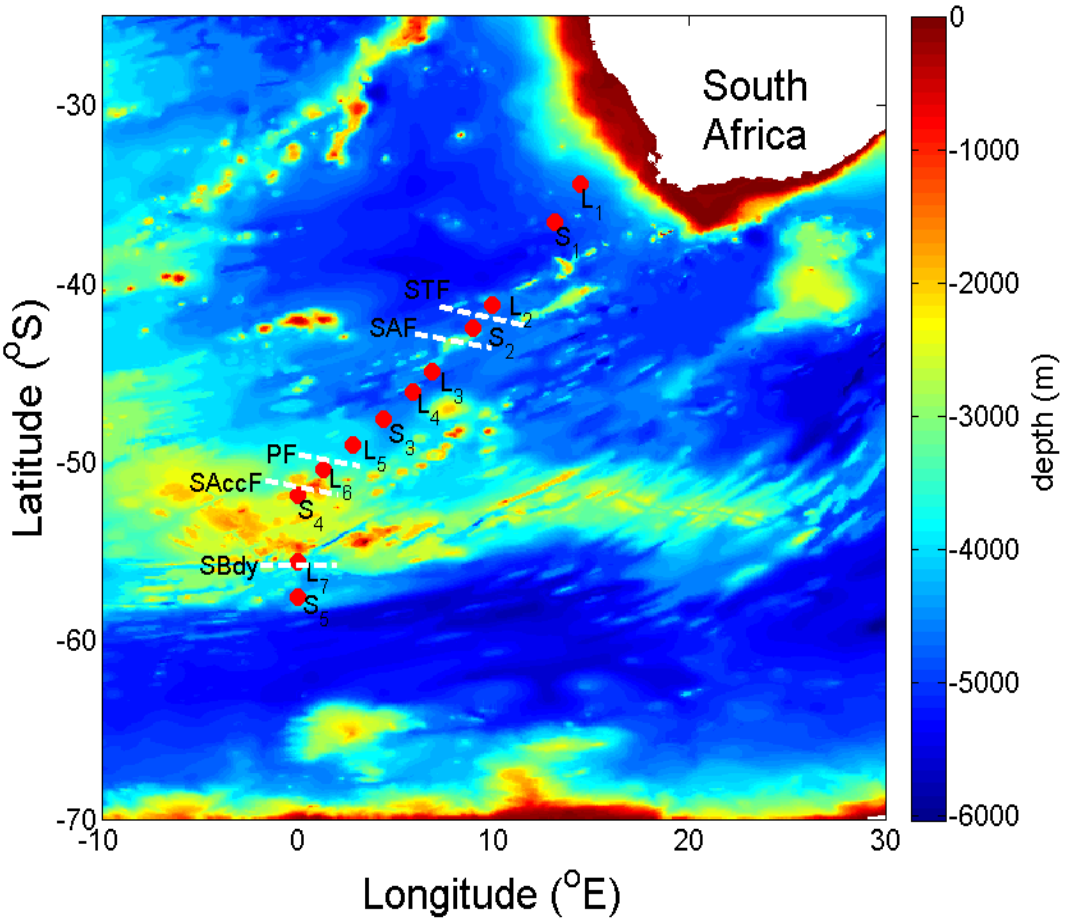

Figure 3.1. Cruise track during the Bonus Goodhope 2008 campaign. Red dots indicate the sampling positions for ^{15}N uptake experiments. The hydrographic fronts, Subtropical Front (STF), Sub-Antarctic Front (SAF), Polar Front (PF), South Antarctic Circumpolar Current Front (SAccF) and Southern Boundary (Sbdy) are indicated by dotted white lines.

3.3 *Results*

3.3.1 Hydrography

The BGH meridional cruise track crossed all the major hydrographic fronts and open ocean regions commonly recognised in the Southern Ocean (*Orsi et al.*, 1995) (Fig. 3.1). The frontal positions during the cruise were determined using potential temperature criteria (*Speich et al.*, 2011). The region north of the STF was defined as

the STZ where SST exceeded 14°C and salinity exceeded 35 psu (Fig. 3.2). The SAZ was between the STF (42.2°S) and the SAF (44.2°S), where SST fell in the range 9 - 14°C, and surface salinity between 34 – 35 psu. In this zone, an intense anticyclonic eddy ("anticyclone M"; *Arhan et al*., 2011) of Indian Ocean origin was observed (at 42.9°S – 44°S) over the Agulhas Ridge (Fig. 3.2). The PFZ extended from the SAF to the PF (*Pollard et al*., 2002) at 50.1°S, where SST decreased from 10 - 5°C and surface salinity was <34 psu (Fig. 3.2). The AZ was found south of the PF where temp was <3°C and salinity was ~34 psu. The following results are presented according to the four zones defined above (STZ, SAZ, PFZ and AZ).

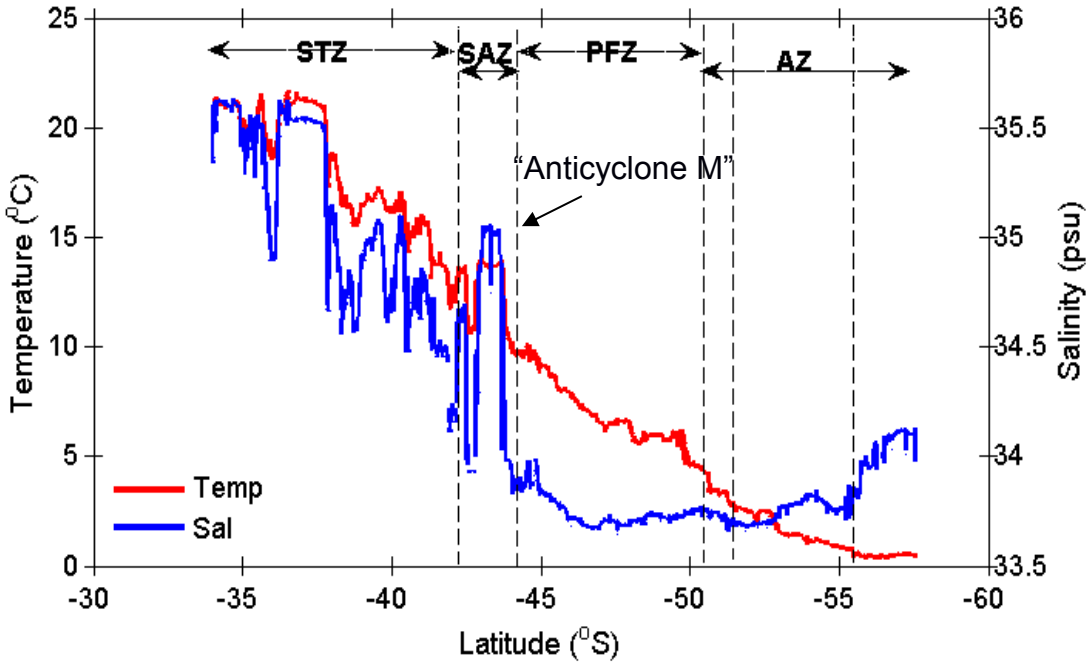

Figure 3.2. Surface temperature (red line) and surface salinity (blue line) with latitude along the cruise track. It shows the zonal description of the regions during the cruise (STZ, SAZ, PFZ and AZ. The position of Anticyclone M is indicated by the increase in temperature and salinity in the SAZ.

3.3.2 Nutrients

Nutrient concentrations shown in Fig. 3.3(a,b) are from the upper 200 m of the BGH cruise track (*LeMoigne et al*., 2011). In the STZ, surface nutrient concentrations (Fig. 3.3 a,b) showed typical oligotrophic conditions, with surface NO_3^- concentrations < 0.05 µmol L^{-1} (Fig. 3.4a), while surface $Si(OH)_4$ concentrations were typically < 2 µmol L^{-1} (Fig. 3.3b). Surface NH_4^+ concentrations were depleted (< 0.1 µmol L^{-1}), while urea concentrations were variable, ranging from 0.22 – 1.51 µmol L^{-1} (Table 3.1). In the SAZ, a gradual increase in surface NO_3^- concentrations was observed ranging from 5 – 15 µmol l^{-1}, but reaching 20 µmol l^{-1} below 100 m depth (Fig. 3.3a, Table 3.1). $Si(OH)_4$ concentrations were depleted (<2 µmol l^{-1}) throughout the surface 250 m (Fig. 3.3b). NH_4^+ concentrations were < 0.25 µmol l^{-1}, but reached concentrations of up to 0.4 µmol L^{-1} between 40 - 70 m depth (Table 3.1), while urea concentrations ranged from 1 – 1.5 µmol L^{-1} (Table 3.1). In the PFZ, surface NO_3^- concentrations reached > 20 µmol L^{-1} (Fig. 3.3a), while $Si(OH)_4$ concentrations remained < 2 µmol L^{-1} in the upper 100 m of the water column (Fig. 3b). From north to south, surface NH_4^+ concentrations (above 100 m) gradually increased from below 0.25 µmol L^{-1} to greater than 1.0 µmol L^{-1} (Table 3.1). Urea concentrations were higher than in the STZ and ranged from ~ 1 µmol L^{-1} to a maximum of 3.27 µmol L^{-1} (at ~ 60 m, station S3). Ubiquitously high nutrient concentrations were observed in the AZ. NO_3^- concentrations exceeded 30 µmol L^{-1} in the surface ~ 100 m and continued to increase to a maximum of ~ 40 µmol L^{-1} with depth (Fig. 3.3a). $Si(OH)_4$ concentrations showed a steep north-south gradient from < 2 µmol L^{-1} north of the PF to > 60 µmol L^{-1} at the southern margin of the region (Fig. 3.3b). NH_4^+ and urea concentrations in the AZ reached 0.8 and 2 µmol L^{-1} in the euphotic layer.

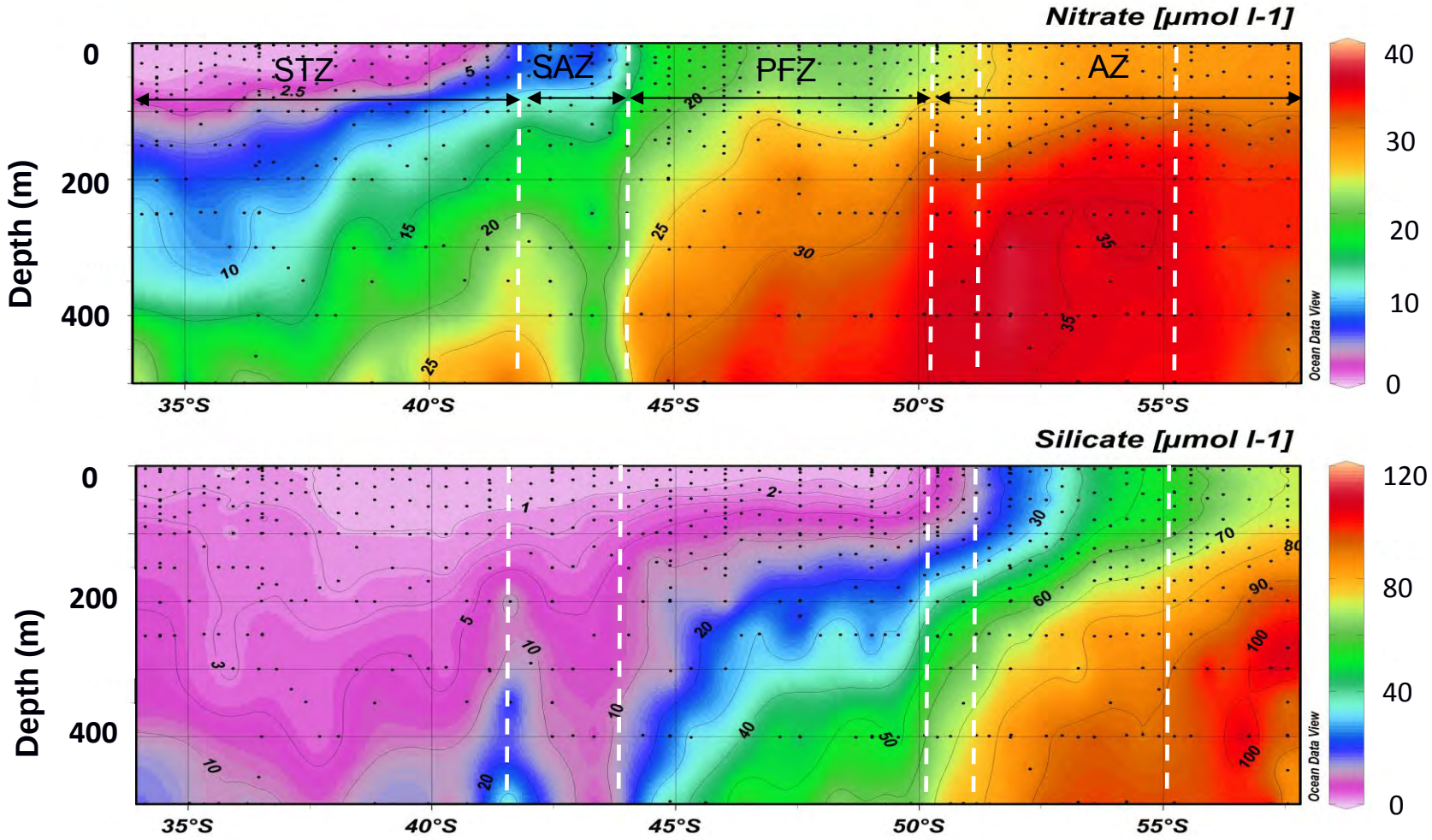

Figure 3.3 a, b. Profiles of NO_3 and $Si(OH)_4$ in the upper 500 m along the Bonus Goodhope Cruise track. It shows increasing surface nutrient concentrations with increasing latitude. Frontal positions measured during the cruise are indicated by the white vertical dotted lines.

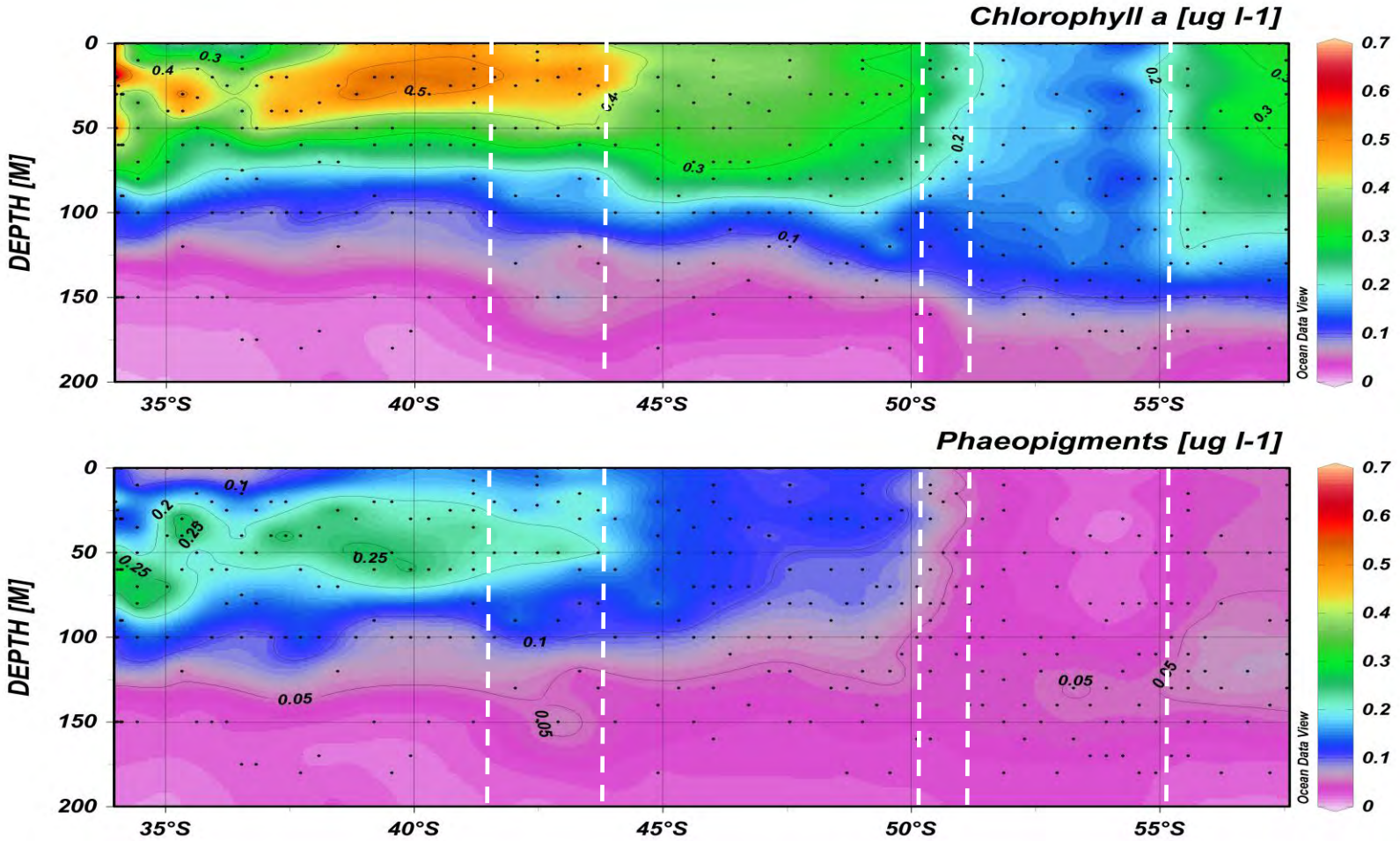

Figure 3.3 c, d (cont.). Profiles of chl-a and phaeopigments in the upper 200 m of the water column along the Bonus-Goodhope cruise track. Elevated pigment concentrations were observed in equatorward of the Subtropical Front. Frontal positions measured during the cruise are indicated by the white vertical dotted lines.

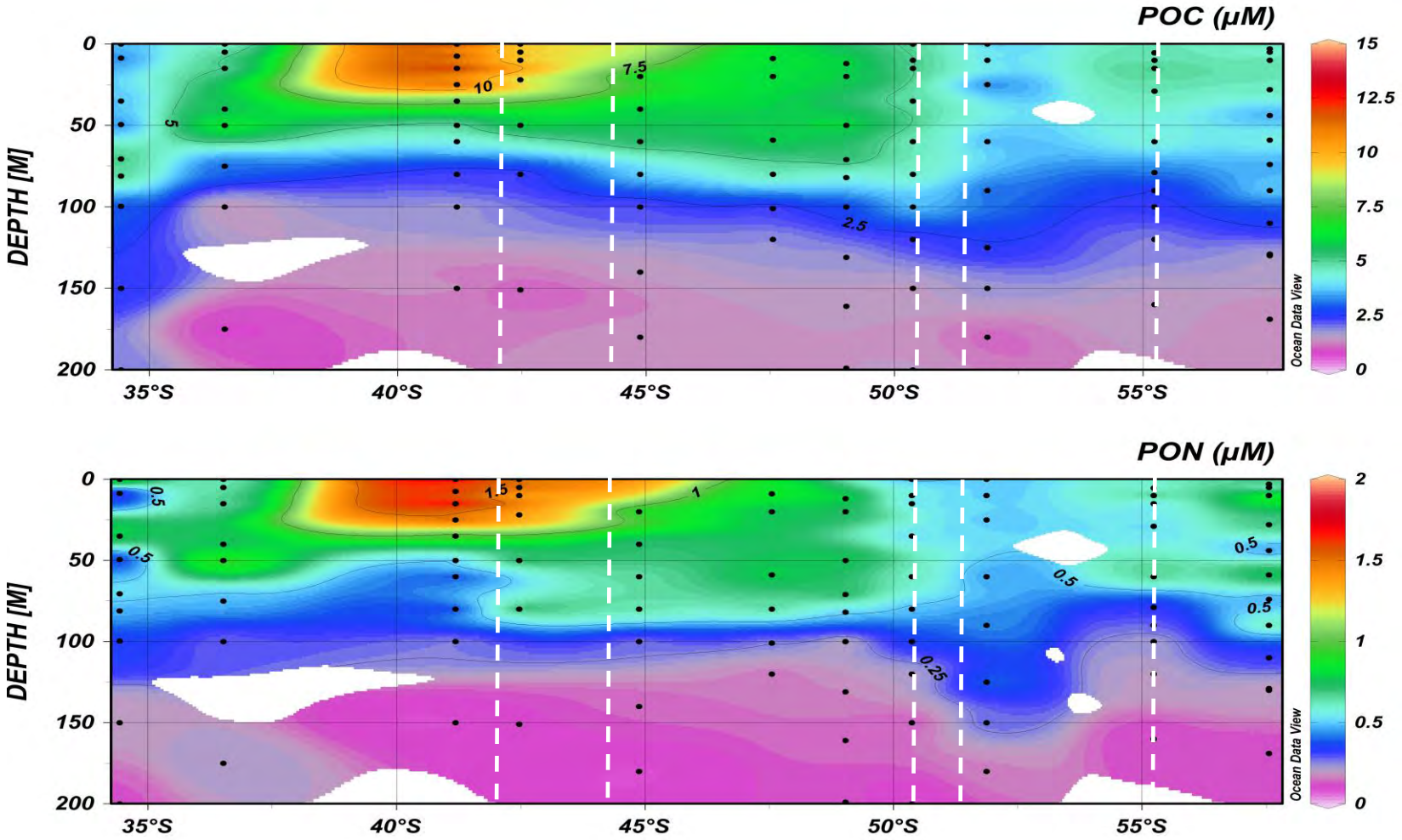

Figure 3.3 e, f. (cont.) Profiles of Particulate Organic Carbon (POC) and Particulate Organic Nitrogen (PON) in the upper 200 m of the water column along the Bonus Goodhope cruise track. Highest concentrations were observed equatorward of the Sub-Antarctic Front. Frontal positions measured during the cruise are indicated by the white vertical dotted lines.

Table 3.1: List of data at each sampling station (including latitude positions) during the BGH cruise (MLD; m, sample depth; m, chl-a, µg L^{-1}; POC and PON, µmol L^{-1}; nutrients, µmol L^{-1}; ρN, nmol L^{-1} d^{-1}). *f*-ratio is dimensionless. The five sample depths at each station represent, with increasing depth, the 100%, 50%, 25%, 10% and 1% light depths. nd indicates no data.

Station	MLD	Depth	Chl-a	POC	PON	NO_3	NH_4	Urea	ρNO_3	ρNH_4	ρUrea	*f*
STZ												
L1	42	1.0	0.05	5.36	0.94	<0.05	0.06	0.22	14.4	12.7	10.7	0.38
(34.4°S)		5.0	0.05	8.13	0.68	<0.05	0.05	0.33	9.5	26.0	30.5	0.14
		9.1	0.06	1.80	0.25	<0.05	0.01	0.11	13.9	29.0	20.0	0.22
		35.0	0.11	4.78	0.82	<0.05	0.02	0.33	21.2	34.5	49.8	0.20
		80.9	0.47	3.36	0.46	3.24	0.01	0.33	4.9	2.7	61.7	0.07
S1	10	1.0	0.14	4.36	0.59	<0.05	0.02	0.86	5.5	17.4	245.1	0.02
(36.5°S)		7.3	0.16	4.50	0.62	<0.05	0.01	0.76	20.1	18.4	280.2	0.06
		14.0	0.17	4.56	0.64	<0.05	0.06	0.32	17.8	20.3	133.5	0.10
		40.2	0.20	5.42	0.71	<0.05	0.10	0.86	18.2	16.3	347.5	0.05
		53.6	0.37	7.06	0.99	<0.05	0.17	0.76	5.0	4.9	264.7	0.02
L2	17	1.0	0.49	12.26	1.93	2.01	0.08	1.51	1.4	32.0	330.5	0.00
(41.2°S)		3.3	0.54	12.26	1.93	2.01	0.08	0.65	37.5	37.7	169.0	0.15
		7.8	0.55	12.27	1.77	2.50	0.10	1.08	53.2	42.8	294.2	0.14
		15.3	0.56	14.12	1.88	3.86	0.03	0.76	56.6	17.6	105.0	0.32
		35.4	0.40	6.07	0.90	3.99	0.51	0.65	7.0	5.9	41.6	0.13
SAZ												
S2	75	1.0	0.35	7.70	1.30	11.04	0.09	1.26	41.0	15.9	50.0	0.38
(42.5°S)		5.0	0.35	7.24	1.48	10.80	0.09	2.11	157.2	30.1	197.2	0.41
		9.6	0.35	7.68	1.15	10.80	0.09	0.84	96.7	21.8	57.6	0.55
		21.9	0.34	7.48	1.30	10.80	0.09	1.37	132.2	25.9	105.1	0.50
		50.6	0.38	5.78	0.89	6.03	0.09	1.26	54.7	1.8	46.7	0.53
PFZ												
L3	47	1.0	0.25	4.78	0.78	17.79	0.31	0.71	30.7	23.4	26.4	0.38

(44.9°S)		10.0	0.25	4.57	0.64	nd	nd	1.29	nd	nd	50.7	nd
		20.2	0.25	4.78	0.68	nd	0.31	0.82	nd	25.8	34.0	nd
		40.0	0.26	4.65	0.78	nd	nd	0.59	nd	nd	35.6	nd
		60.9	0.25	4.57	0.64	17.67	0.31	nd	56.8	5.1	nd	0.92
L4	81	1.0	0.40	6.97	0.78	18.68	0.67	1.37	17.6	6.3	36.0	0.29
(46.0°S)		10.6	0.40	6.67	0.80	18.68	0.67	0.91	33.1	22.0	18.2	0.45
		18.9	0.40	6.51	0.88	18.44	0.68	0.91	53.4	29.4	44.1	0.42
		20.3	0.40	5.63	0.75	18.44	0.68	1.03	45.6	35.7	15.3	0.47
		48.9	0.40	6.04	0.78	18.92	0.69	1.94	43.0	26.7	8.0	0.55
S3	84	1.0	0.36	6.04	0.86	21.12	0.60	0.24	124.0	39.6	13.0	0.70
(47.6°S)		5.0	0.36	6.04	0.86	21.12	0.60	0.85	72.0	24.6	16.9	0.63
		9.5	0.36	5.89	0.88	20.88	0.60	0.85	40.2	21.0	14.0	0.53
		19.7	0.36	5.58	0.74	21.12	0.60	1.58	28.3	48.1	106.8	0.15
		60.1	0.36	5.56	0.80	20.88	0.62	3.27	22.2	8.4	108.5	0.16
L5	97	1.0	0.26	5.17	0.47	20.93	0.73	0.39	37.1	8.2	5.6	0.73
(49.0°S)		3.9	0.26	5.17	0.47	20.93	0.73	0.39	20.6	9.3	3.0	0.63
		10.1	0.26	5.49	0.53	20.93	0.73	2.06	21.0	14.4	13.2	0.43
		13.9	0.28	5.19	0.47	20.93	0.73	1.42	39.1	18.8	15.3	0.53
		60.4	0.25	5.16	0.60	20.93	0.73	0.77	15.5	15.3	10.5	0.38
L6	78	1.0	0.31	5.37	0.54	22.80	1.26	nd	14.6	4.3	nd	0.77
(50.4°S)		5.7	0.31	5.37	0.54	22.80	1.26	1.58	18.1	6.2	20.1	0.41
		9.4	0.30	9.04	0.74	22.80	1.25	1.33	22.9	7.4	28.3	0.39
		15.2	0.30	5.23	0.47	22.80	1.26	1.94	23.5	11.5	48.4	0.28
		78.5	0.30	3.43	0.31	24.51	1.89	1.33	13.6	5.5	13.3	0.42
AZ S4	107	1.00	0.16	2.67	0.50	nd	0.80	2.00	nd	11.0	24.7	nd
(51.8°S)		1.90	0.16	2.67	0.50	25.71	0.80	2.00	28.8	11.6	16.9	0.50
		13.50	0.17	2.72	0.50	25.71	0.79	2.19	20.9	8.5	12.5	0.50
		23.60	0.16	2.98	0.50	25.71	0.80	1.62	19.7	9.2	16.8	0.43
		88.30	0.16	2.60	0.40	25.96	0.79	1.43	10.8	7.1	8.7	0.41

L7	69	1.0	0.25	5.37	0.54	28.08	0.46	0.83	28.0	14.4	11.0	0.52
(55.6°S)		5.3	0.25	9.04	0.74	28.08	0.46	0.41	51.1	13.0	8.0	0.71
		13.5	0.24	5.23	0.47	28.08	0.43	1.33	42.3	15.0	19.4	0.55
		25.1	0.27	5.39	0.52	28.08	0.43	1.94	53.3	3.7	41.5	0.54
		109.9	0.28	2.05	0.19	29.76	0.31	1.33	45.4	14.3	18.4	0.58
S5	90	1.0	0.33	4.48	0.76	27.81	0.61	1.68	47.5	20.0	29.3	0.49
(57.6°S)		3.2	0.33	4.48	0.76	27.81	0.61	1.29	41.2	23.8	29.3	0.44
		8.5	0.33	4.63	1.03	27.81	0.61	2.06	45.2	27.6	43.4	0.39
		28.8	0.30	4.06	0.69	28.06	0.63	3.10	33.3	19.5	73.0	0.26
		90.0	0.21	3.55	0.68	28.06	0.62	1.16	36.1	22.8	21.1	0.45

27 Table 3.2: Comparison of depth integrated values of ^{15}N uptake (mmol m^{-2} d^{-1}) by phytoplankton in various regions of the Southern Ocean.

Region/Description	$\int\rho NO_3$	$\int\rho NH_4$	$\int\rho$Urea	$\Sigma\int\rho N$	*f*-ratio	
Atlantic Sector (Summer 2008, BGH)						this study
STZ (34 - 41°S)	1.01 (0.3)	0.69 (0.3)	6.47 (6.7)	8.18 (6.8)	0.24 (0.22)	
SAZ (42 - 44°S)	5.11	0.92	4.31	10.34	0.49	
PFZ (45 - 50°S)	1.97 (0.5)	1.16 (0.4)	2.13 (1.8)	5.26 (2.2)	0.41 (0.11)	
AZ (51 - 57°S)	3.39 (1.9)	1.27 (0.6)	2.86 (1.6)	7.51 (3.5)	0.45 (0.11)	
Australian Sector (Spring 2001, CLIVAR-SR3)						Savoye et al. (2004)
SAZ/STF (49 - 51.0°S)				4.4 (0.3)	0.53 (0.26)	
PFZ (54 - 57°S)				5.6 (0.1)	0.56 (0.02)	
AZ (61 - 65°S)				9.6 (2.2)	0.61 (0.08)	
Bellinghausen Sea						Waldron et al., (1996)
SIZ (56 - 64°S)	1.8 (1.2)	10.9 (3.9)	9.9 (0.4)	18.0 (11.9)	0.1 (0.01)	
Indian Sector (CROZEX, Summer 2004)						Lucas et al., (2007)
Crozet-M3 bloom	20.3 (5.7)	3.6 (1.3)	6.1 (2.0)	30.1 (7.5)	0.67 (0.08)	
Crozet-South of Plateau (HNLC)	1.8 (0.8)	3.2 (0.5)	1.1 (0.2)	6.0 (1.5)	0.28 (0.07)	
Indian Sector (Summer 1994, ANTARES3)						Mengesha et al., (1998)
Kerguelen Plateau (PFZ, Stn A18; 49°S)	5.7	3.5	2.8	11.9	0.48	
Kerguelen Plateau (PFZ, Stn A16; 52°S)	7.7	2	1	10.7	0.72	
Indian Sector (late Summer 1999, MIOS-4)						Thomalla et al., (2011)
STZ (31 - 40°S)	3.76 (4.2)	19.83 (15.0)	22.30 (17.8)	46.07 (33.5)	0.07 (0.03)	
SAZ (41 - 46°S)	0.94(0.2)	5.26 (2.3)	6.48 (5.4)	12.67 (7.9)	0.09 (0.04)	
Pacific Sector (Summer 1997, US-JGOFS)						Sambrotto and Mace, (2000)
PFZ (57 - 61°S)	2-5 (2.3)				0.05 - 0.48	

3.3.3 Chlorophyll-a

In the STZ, euphotic zone chl-a concentrations were highest, exceeding 0.4 µg L^{-1} with a sub-surface chl-a maximum (> 0.5 µg L^{-1}) at 30 – 40 m (Fig. 3.3c See also *Beker et al*., 2011). A similar sub-surface maximum was observed for phaeopigments, although slightly deeper in the water column at 40 – 60 m (Fig. 3.3d). Size-fractionated chl-a showed that picophytoplankton (< 2 µm) contributed 50.4% to total chl-a (Fig. 3.4b,). In the SAZ, chl-a concentrations in the surface ~ 40 m exceeded 0.4 µg L^{-1} (Fig. 3.3c), whereas a sub-surface maximum in phaeopigments (> 0.3 µg L^{-1}) was observed at ~ 50 m (Fig. 3.d). Size-fractionated chl-a indicated that nano- (2-20 µm) and picophytoplankton contributed 60.2% and 39.8% respectively to total chl-a concentrations, while no microplankton (20 – 200 µm) were measured (Fig. 3.4) in the SAZ. In the PFZ, chl-a concentrations of ~ 0.3 µg L^{-1} were found in the upper 70 m, (Fig. 3.3c). Phaeopigments typically exceeded 0.1 µg L^{-1} in the upper 50 m of the water column, and remained <0.1 µg L^{-1} below this depth (Fig. 3.3d). Size-fractionated chl-a in surface samples was dominated by nanophytoplankton (54.3%) throughout this region (Fig. 3.3), followed by picophytoplankton (30.6%) and microphytoplankton (15%). Chl-a concentrations in the AZ between the PF and the SAccF, as well as south of the SBdy, ranged from 0.2 to 0.3 µg L^{-1}, while a band of low chl-a (< 0.2 µg L^{-1}) was evident between the SAccF and the SBdy (Fig. 3.3c). Phaeopigments appeared completely absent in this region (Fig. 3.3d). In the AZ, nanoplankton comprised 61.9% of the phytoplankton community, while micro and picoplankton comprised 18.9 and 19.2% respectively (Fig. 3.4).

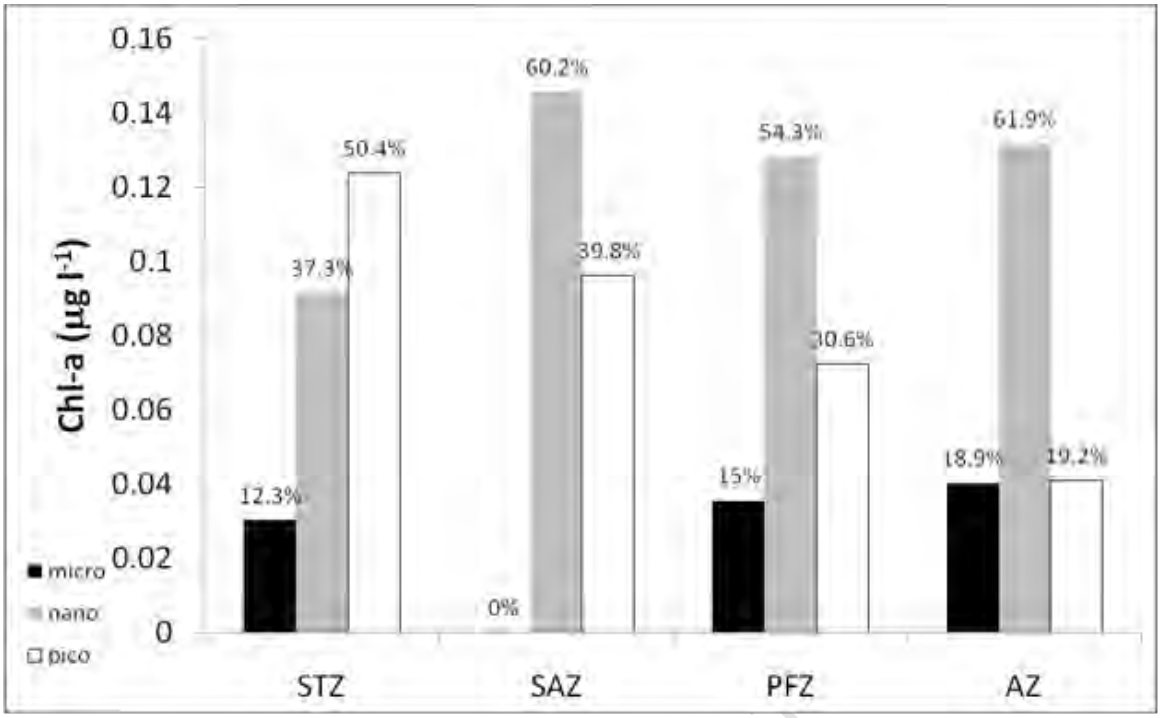

Figure 3.4. Size fractionated chl-a of surface samples in each region along the BGH cruise track. Percentage of the total is presented at the top of each bar. It shows the decreasing contribution of picophytoplankton from north to south along the cruise track.

3.3.4 Particulate Organic Carbon and Nitrogen

Maximum concentrations of POC (14.1 µmol L^{-1}) and PON (1.9 µmol L^{-1}) were found in the STZ just north of the STF (Fig. 3.3e,f) and confined to the upper 25 m. Average PON concentrations over the euphotic layer of the STZ were 1.0 ± 0.6 µmol L^{-1}, with a mean euphotic zone C:N ratio of 7.16 ± 2.29. In the SAZ, POC and PON concentrations in the surface 40 m reached a maximum of 7.7 and 1.5 µmol L^{-1} respectively (Fig. 3.3e,f, modified from *Beker et al.*, 2011), with a mean euphotic zone C:N ratio of 6.0 ± 0.7. In the PFZ, POC and PON averaged 5.3 ± 0.5 µmol L^{-1} and 0.7 ± 0.2 µmol L^{-1} respectively in the upper 60 m of the water column (Fig. 3.3e,f), with both decreasing below this depth. The average C:N ratio in the euphotic zone was 8.2 ± 1.7. In the AZ, POC and PON were typically < 4 µmol L^{-1} and < 0.5 µmol l^{-1} respectively (Fig. 3.3e,f) in the euphotic zone, with a mean C:N ratio of 7.4 ± 2.7.

3.3.5 Nitrogen uptake

In the STZ (n = 3), ρurea dominated depth integrated nitrogen uptake ($\int\rho$N) by ~80% (Fig. 3.5), reaching a maximum rate of 347 nmolN L^{-1} d^{-1} at 40 m at station S1 (Table 3.1). ρurea was on average 8 times greater than ρNO_3^- or ρNH_4^+ yielding a mean *f*-ratio of 0.24 ± 0.22 (Fig. 3.5). Specific uptake of urea (V_{urea}) was on average 10 times greater than that of nitrate (V_{NO3}) or ammonium (V_{NH4}) (Fig. 3.6). In the SAZ (n = 1) ρNO_3^- and ρurea reached maximum rates at 5 m of 157.3 and 197.2 nmolN L^{-1} d^{-1} respectively (Table 3.2). These values decreased to 54.7 and 46.4 nmol L^{-1} d^{-1} respectively at the 1% euphotic depth. $\int\rho$N was 10.3 mmolN m^{-2} d^{-1}, with the highest contribution from $\int\rho NO_3^-$ (49.4%) followed closely by $\int\rho$urea (43%) (Table 3.2). The depth-integrated *f*-ratio for this station was 0.47 (Table 3.2). Specific uptake rates of nitrate (V_{NO3}) and urea (V_{Urea}) over the euphotic zone were 0.12 ± 0.05 $d^{-1}$and 0.13 ± 0.08 d^{-1} (Fig. 3.6), while V_{NH4} was lower (0.02 ± 0.02 d^{-1}). In the PFZ (n=5), euphotic zone ρNO_3^-, ρurea and ρNH_4^+ remained below 50 nmol L^{-1} d^{-1} (Table 3.2) and were typically lower than uptake rates in the STZ and SAZ. Station S3 exhibited the highest ρN rates, compared to adjacent stations to the north or south. At station S3, ρNO_3^- decreased from 124.0 nmolN L^{-1} d^{-1} in the surface to 22.2 nmolN L^{-1} d^{-1} at the base of the euphotic zone (Table 3.1). Conversely, ρurea increased from 13.0 nmolN L^{-1} d^{-1} in the surface to 108.5 nmol L^{-1} d^{-1} at depth. Average $\int\rho$N for the PFZ was 5.26 ± 2.2 mmolN m^{-2} d^{-1} (Table 3.2), with the majority being due to $\int\rho NO_3^-$ (1.97 ± 0.46 mmolN m^{-2} d^{-1}) and $\int\rho$urea (2.13 ± 1.78 mmolN m^{-2} d^{-1}), while $\int\rho NH_4^+$ averaged 1.16 ± 0.41 mmolN m^{-2} d^{-1}, resulting in a mean *f*-ratio of 0.41 ± 0.11 (Table 3.2). Average euphotic zone V_{NO3}, V_{NH4} and V_{Urea} were 0.07 ± 0.07, 0.03 ± 0.1 and 0.04 ± 0.03 d^{-1} respectively (Fig. 3.6). In the AZ (n = 3), ρNO_3^-, ρNH_4^+ and ρurea also remained below 50 nmol l^{-1} d^{-1} (Table 1). Mean $\int\rho$N for the AZ was 6.46 ± 4.21 mmolN m^{-2} d^{-1} (Table 3.1), with up

to 50% being derived from $\int \rho NO_3^-$ (3.43 ± 2.68 mmolN m^{-2} d^{-1}) (Table 3.2). Mean *f*-ratio in the AZ was 0.45 ± 0.11 (Table 3.2). Specific nitrogen uptake rates in the AZ were similar to those observed in the PFZ (Fig. 3.6).

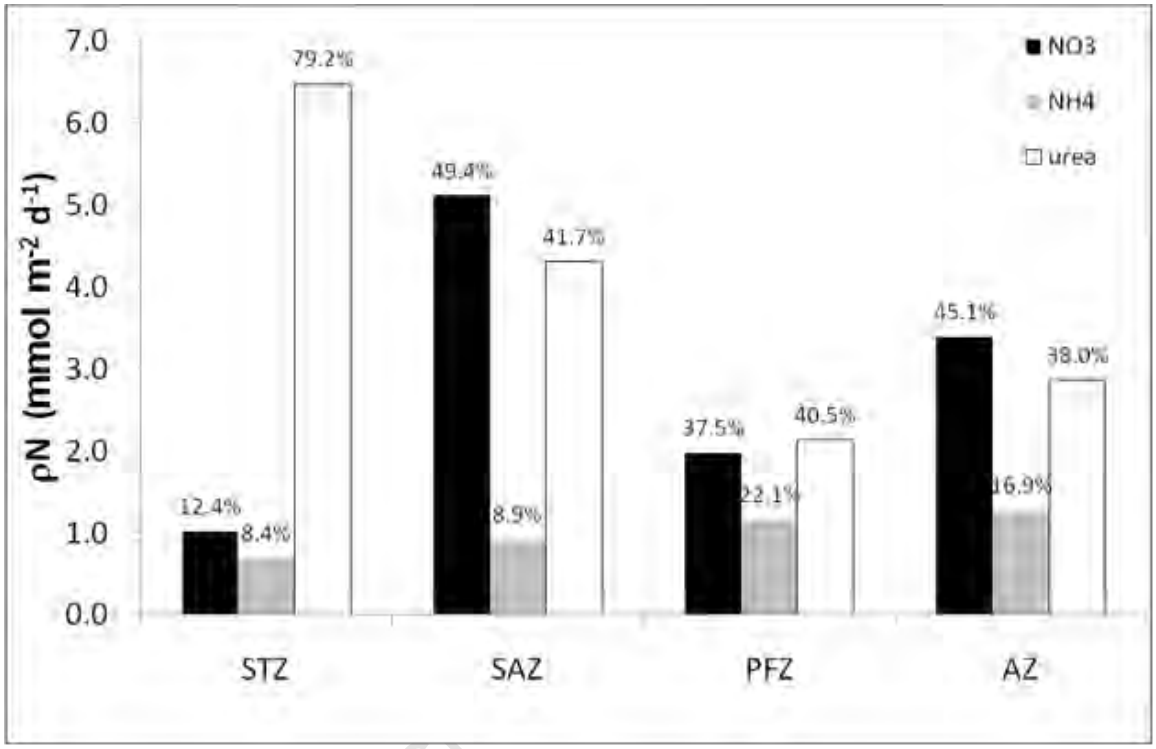

Figure 3.5. Depth integrated nitrogen uptake (∫ρN) in each zonal region. It shows the contribution $\int \rho NO_3$ (black), $\int \rho NH_4$ (grey) and ∫ρUrea (white) as % of total uptake.

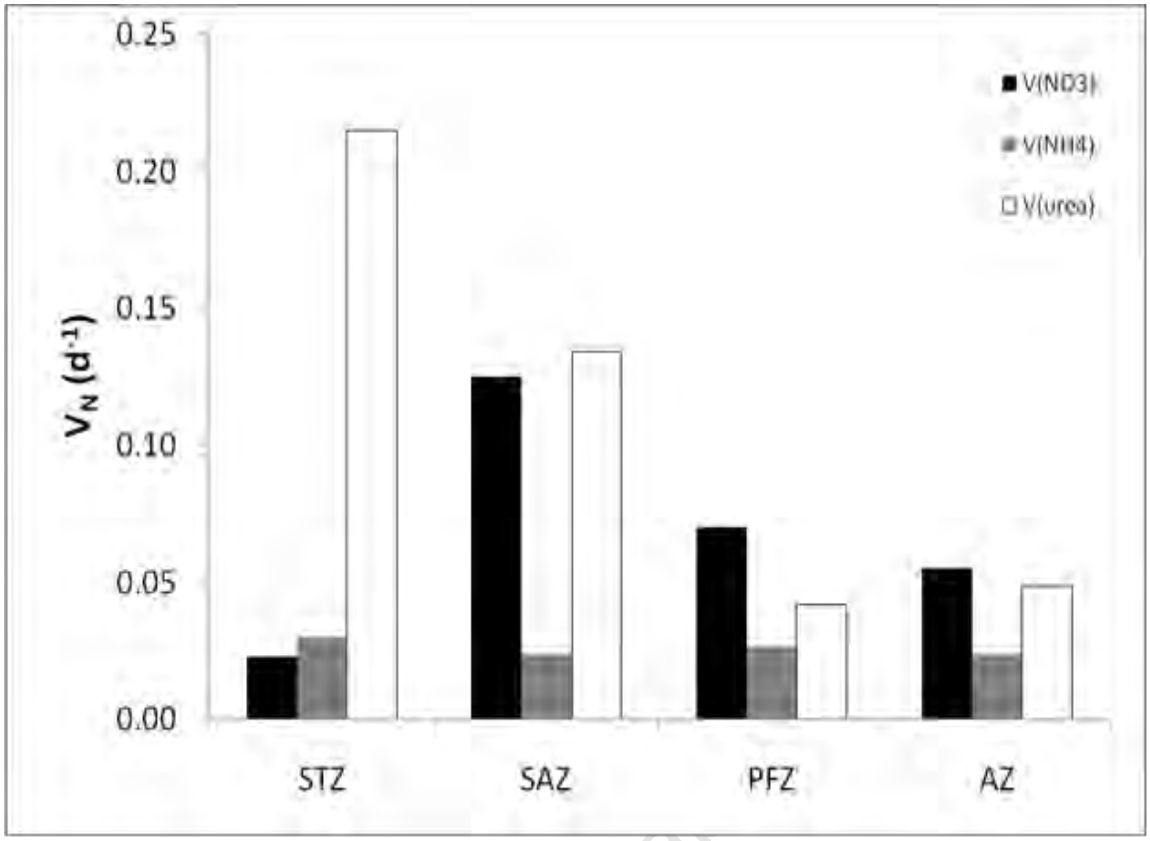

Figure 3.6. Specific uptake (V, h^{-1}) averaged over the euphotic zone for each region. It shows the contribution V_{NO3} (black), V_{NH4} (grey) and V_{Urea} (white) as % of total uptake, and a decreasing trend V_{Urea} from north to south.

3.4 Discussion

In this section we discuss nitrogen uptake dynamics across four different hydrographic regions in the Atlantic sector of the Southern Ocean. We highlight regional differences in uptake rates, *f*-ratios and community size structure and investigate how these change in relation to MLD, temperature, nutrients and surface dissolved iron concentrations. We compare our data with other ^{15}N estimates of production in the Southern Ocean, as well as with ^{234}Th based estimates of carbon export measured during the BGH cruise.

3.4.1 Regional comparisons of nitrogen uptake

The Subtropical Zone

Relatively high $\int\rho$N in the STZ (8.18 ± 6.8 mmolN m^{-2} d^{-1}) was dominated by $\int\rho$urea (~ 79%), with V_{urea} being ten times higher than V_{NO3} or $V_{NH4,}$ (Fig. 3.6), indicating significant regenerated production, as reflected by low *f*-ratios (0.24 ± 0.22). It is unlikely that all the urea uptake is through phytoplankton production, as urea is easily assimilated by heterotrophic bacteria (*Kirchman*, 2000) which can contribute up to 25% of nitrogen uptake (*Fouilland et al*., 2007). Low new production rates in this region are likely due to limiting surface NO_3 concentrations (<0.05 µmol L^{-1}). Phytoplankton community structure was consistent with a typically regenerated-based community (*Tremblay et al*., 2000) with picophytoplankton dominating by ~51% (Fig. 3.4). This is consistent with previous results of low *f*-ratios in the Indian (*f* = 0.07 ± 0.03) (*Thomalla et al*., 2011) and Pacific basins (*Sambrotto and Mace*, 2000) (Table 3.2). These results imply that this region of the Southern Ocean is dominated by urea re-cycling within the microbial loop, with little carbon export, little atmospheric CO_2 "draw-down", and conservation of nitrogen in surface waters (*LeFevre et al*., 1998; *Smetacek et al*., 2004).

The Subantarctic Zone

Station S2 in the SAZ exhibited only slightly higher total $\int\rho$N rates compared to those observed in the STZ, however this station showed a greater contribution of ρNO_3^- (49.4%), which increased the *f*-ratio from 0.24 to 0.49 (Table 3.2). V_{NO3} (0.12 d^{-1}) at this station was double that found in other regions (Fig. 3.6) along with the highest concentrations of chl-a (> 0.5 µg l^{-1}), POC (> 7 µmol L^{-1}) and PON (> 1 µmol L^{-1}) (Fig. 3.3c,e,f). Specific uptake rates are known to provide information on the potential for

macronutrient, light or iron limited growth, with higher values being characteristic of faster growth rates in nutrient and light replete environments. These high V_{NO3} values thus suggest possible alleviation of iron stress (*Lucas et al.*, 2007), along with sufficient light availability (MLD = 45.2 ± 17.1 m). $\int\rho$N rates in the SAZ of the Atlantic measured in this study (10.3 mmolN m^{-2} d^{-1}) were slightly higher than those measured in the Australian sector in late spring/early summer (4.4 ± 0.3 mmolN m^{-2} d^{-1}) (*Savoye et al*., 2004) and were comparable to the Indian sector in late summer (12.7 ± 7.9 mmol N m^{-2} d^{-1}) observations (*Thomalla et al*., 2011) (Table 3.2).

It has been shown for oligotrophic regions that new production is enhanced within mesoscale eddy activity through the vertical injection of nutrients into the euphotic layer (*Greenwood*, 2007; *Strass et al.*, 2002; *Levy et. al.*, 2009). This station was on the edge of a mesoscale hydrographic feature, 'anticyclone M' (*Arhan et al*., 2011), observed just north of the SAF (Fig. 3.2). The proposed mechanism for the enhanced production and higher *f*-ratios at this station is enhanced vertical nutrient injection (including iron) at the edges of the anticyclone (*Levy et al*., 2009) along with an improved light environment associated with persistent shallow and stable mixed layers associated with the warm core eddy (*Llido et al*., 2005). Mesoscale eddies such as these provide important areas for local but significant POC export and biological CO_2 draw-down in an overall HNLC Southern Ocean. This mechanism is addressed in Chapter 4 using high resolution NCP and concomitant MLD measurements along the same cruise track.

The Polar Front Zone

Total $\int\rho$N rates in the PFZ were the lowest of the four regions (Table 3.2), with low *f*-ratios of 0.41 ± 0.11. $\int\rho$urea and V_{urea} were substantially lower than in the STZ and

SAZ to the north (Fig. 3.5; Fig.3.6). High concentrations of ammonium and urea (Table 3.2) were observed in the PFZ indicating very active regeneration processes. Dilution of the isotopic $^{15}NH_4^+$ and ^{15}N-urea uptake due to high regenerated nutrients released by bacteria and zooplankton grazers can potentially lead to an underestimation of the uptake rates of these substrates and consequently an overestimation of the *f*-ratio. Early work in the Scotia Sea showed that ammonium uptake can be underestimated by a factor of 2 – 3 in summer (*Glibert et al*., 1982). Although no NH_4^+ regeneration experiments were conducted during the cruise, one can expect that underestimation of regenerated uptake would further reduce the *f*-ratio's presented here. Although our cruise was in late austral summer, deep mixed layers in this region (MLD = 68.7 ± 18.9 m) relative to the 1% light depths (61 ± 11 m) make light a potentially limiting factor to primary production and to NO_3^- uptake in particular considering its high light demand in comparison to NH_4^+ and urea uptake (*Lucas et al.*, 2007, *Cochlan*, 2008). In addition, low surface Fe concentrations < 0.2 nmol L^{-1} (*Chever et al.*, 2010) likely limit new production (*Timmermans et al*., 1998) promoting the dominance of small cells as size confers a competitive advantage for nutrients at low concentrations (*Leynart et al.*, 2004). Smaller cells are however more susceptible to grazing by microzooplankton (*Raven*, 1986), which controls their biomass and at the same time contributes to potential regenerated production through NH_4^+ excretion (*Glibert and Garside*., 1992). Size-fractionated chl-a concentrations showed the PFZ to be dominated by nanophytoplankton (54%, Fig. 3.3).

Several authors have found an increase in diatom concentration to be associated with the PF and attribute this to an increase in $Si(OH)_4$ (*Laubscher et al*., 1993; *Bathmann et al*., 1997, *Smetacek et al*., 1997; *Tremblay et al*., 2002). Although it is possible for diatoms to fall within the nanophytoplankton size range, substantial increases in $Si(OH)_4$ were

only found south of the SACCF (Fig. 3.3b). Thus, although the percentage of microphytoplankton increased from 0% in the SAZ to 15% in the PFZ, the continued dominance by nanophytoplankton (54%) was likely due to $Si(OH)_4$ limitation of diatom growth and low surface Fe concentrations (< 0.2 nmol L^{-1}, *Chever et al*. 2010) favouring smaller cells. Similarly, low $Si(OH)_4$ concentrations have been shown to play an important role in regulating nitrate uptake (*Dugdale and Wilkerson*, 1998, *Sambrotto and Mace*, 2000) such that the low $Si(OH)_4$ concentrations in this region may have contributed to the low NO_3^- uptake rates (1.97 mmolN m^{-2} d^{-1}) and *f*-ratios found here. $\int\rho$N rates in the Atlantic PFZ from this study (5.26 mmolN m^{-2} d^{-1}) were similar to those in the Australian sector (5.6 mmolN m^{-2} d^{-1}) and the HNLC Crozet sector (6 mmolN m^{-2} d^{-1}), but lower than the bloom region associated with naturally Fe fertilized Crozet (30.1 mmolN m^{-2} d^{-1}) and Kerguelen (11.9 mmolN m^{-2} d^{-1}) Islands (Table 3.2). High concentrations of regenerated nutrients, low *f*-ratios and nanophytoplankton dominated communities at this particular time of year implies an inefficient biological pump for this region which appears to be controlled by nutrient (Fe and $Si(OH)_4$) and light co-limitation and microzooplankton grazing.

The Antarctic Zone

A slight increase in $\int\rho$N was observed in the AZ (7.5 mmolN m^{-2} d^{-1}) relative to the PFZ (5.3 mmolN m^{-2} d^{-1}). The contribution of $\int\rho NO_3^-$ to total $\int\rho$N increased with a simultaneous increase in *f*-ratios to 0.45 indicating a slightly higher potential for carbon export. As with the SAZ, high ambient regenerated nutrient concentrations (Table 3.1) imply active regeneration processes occurring in the surface, however a decrease regenerated uptake rates, particularly urea uptake (Fig. 3.5) were observed relative to regions further north. An underestimation of the regenerated production in this region,

could thus lead to an overestimate of the *f*-ratio. Although $Si(OH)_4$ concentrations increase south of the SACCF (Fig. 3.3b), lowest chl-a concentrations are found in the region between the SACCF and the SBdy and it is only south of the Sbdy that chl-a concentrations increase (Figure 3.3c). Although the mixed layer tends to deepen (MLD = 93.9 ± 14.7 m) in the AZ, so too does the 0.1% light depth (96 ± 12 m), indicating unlikely control through light limitation in deeper mixed layers. More likely, low surface iron concentrations (*Chever et al*., 2010) characteristic of the late summer season are limiting phytoplankton growth despite sufficient irradiance (see also *Boyd et al.*, 2001; *Lucas et al*., 2007). $\int\rho$N from this study (7.5 mmolN m^{-2} d^{-1}) was in a similar range to the $\int\rho$N (9.6 mmolN m^{-2} d^{-1}) of the permanently open AZ in the Australian sector (*Savoye et al*., 2004). As expected however, these open ocean $\int\rho$N rates are up to 60% lower than those observed during bloom conditions in the Seasonal Ice Zone (SIZ) of the Bellinghausen Sea (18.0 ± 11.9 mmolN m^{-2} d^{-1}) (Table 3.2). Lower open ocean $\int\rho$N rates compared to the SIZ can be ascribed to the lack of dissolved iron inputs from melting ice (*Sedwick and DiTullio*, 1997; *Gao et al*., 2003; *Grotti et al*., 2005) and a less favourable light environment through deep mixed layer depths (93.9 ± 14.7 m) (*Smith and Nelson*, 1986). Although there is a slight increase in production and *f*-ratios in the AZ, relative to the PFZ, the ice free regions of this sector appear to have a relatively low potential for carbon export particularly in the late summer season due predominantly to Fe limitation.

3.4.2 Comparison ^{15}N estimates and ^{234}Th export flux

Carbon export derived from ^{234}Th deficits at 100 m revealed a north-south gradient, with the highest export fluxes (up to 6 mmolC m^{-2} d^{-1}) found south of the PF (Fig. 3.7, *Planchon et al.*, 2013). Although the latitudinal trend in *f*-ratio estimates of carbon

export were not as clear, with high export being associated with the eddy in the SAZ, there was a similar tendency for carbon export to increase with latitude (Fig. 3.7). New production estimates of carbon export were however 2 – 20 times greater in magnitude (Fig. 3.7) than ^{234}Th derived estimates. Reasons for this are numerous. Firstly, the two methods used to estimate carbon export are not intended to measure the same process. Although the rates are expected to be comparable in a steady state system or when averaged over large enough time and space scales, there is otherwise no *a priori* reason why the rates should be identical, bearing in mind *f*-ratio estimates of new production is potentially overestimated as the *f*-ratio is only estimated from ρNO_3^-.

Stable isotope incubations measure NO_3^- uptake at a discrete site over 12 – 24 hours in the euphotic layer (typically < 60 m) and may therefore not be representative of mesoscale averages. ^{234}Th deficit derived estimates of carbon export (at 100 m) on the other hand encompass large spatial scales of 10s to 100s of kilometres (*Buesseler et al*., 1992) and a time period of ~31 days. Hence, in this instance ^{234}Th derived carbon fluxes more than likely represents a considerable averaging of episodically lower fluxes when compared to the short-term ^{15}N incubations. Furthermore, ^{234}Th carbon flux estimates are derived by considering the POC/^{234}Th ratio of particles > 50 µm and may well ignore a significant export flux within the < 50 µm fraction. During BGH however, the POC/^{234}Th ratios of particles > 50 µm and < 50 µm were not very different. New production estimates, on the other hand do not discriminate on a size basis and represents the potential export of both dissolved and particulate material. This is consistent with other observations in both the Indian (*Mengesha et al.*, 1998) and Pacific sector (*Savoye et al*., 2004) of the Southern Ocean and highlights the important role of this region of the ocean in the global carbon cycle.

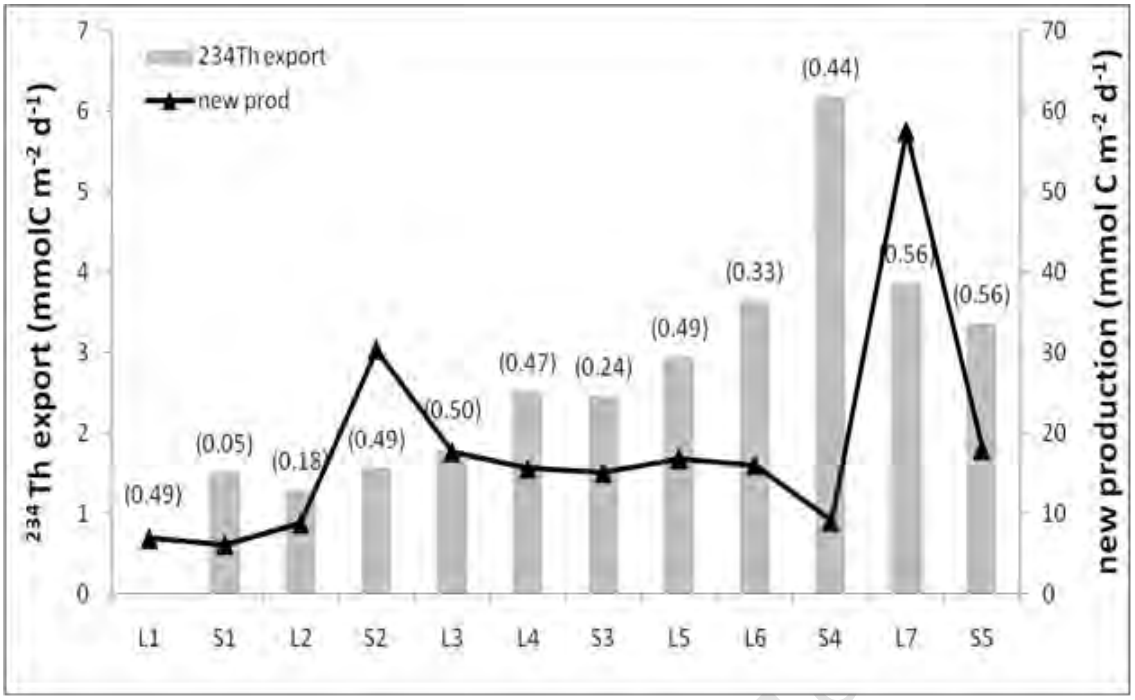

Figure 3.7. Comparison between ^{234}Th export (at 100 m) (grey bars) and 'new production' estimates (black triangles) during BGH. New production calculated from $\int \rho NO_3$ and the C:N ratio. It shows the difference in magnitude of these proxies of carbon export. *f-ratios* are indicated in brackets above the ^{234}Th export estimates.

3.5 Conclusions

This work presents ^{15}N-labelled nitrogen uptake measurements in the Atlantic Southern Ocean in late austral summer, 2008. It shows that ρN in the oligotrophic STZ was dominated by ρurea, resulting in low *f*-ratios (f = 0.24). Size fractionated chl-a data is dominated by picophytoplankton (> 50%) and also indicative of a community based on regenerated phytoplankton production. It is unlikely that the measured NH_4^+ and urea uptake rates reflect only regenerated production in the STZ, given that the uptake estimates based on ^{15}N uptake does not account for heterotrophic bacterial activity. This probably results in an overestimation of urea uptake and underestimation of the *f*-ratio in the STZ. However, given the low concentrations of NO_3^- in the surface waters of the STZ (< 0.05 µmol L^{-1}) the dominance of urea recycling within the microbial loop

(*Taylor and Joint*, 1990) potentially result in lower carbon export. The greatest $\int\rho N$ was observed in the SAZ and ascribed to enhanced nutrient supply and favourable light conditions associated with an anticyclonic eddy. Higher *f*-ratios were observed in the SAZ (*f* = 0.49), Polar Frontal Zone (PFZ, *f* = 0.41) and Antarctic zone (AZ, *f* = 0.45) relative to the STZ (*f* = 0.24) and indicate a higher contribution of ρNO_3^- relative to total ρN and higher export potential in regions further south. New production estimates of carbon export (calculated from ρNO_3^- and the C:N ratio) were lowest in the STZ (7.3 ± 0.43 mmol C m^{-2} d^{-1}; n = 3), compared to 30.4 mmolC m^{-2} d^{-1} in the SAZ (n = 1), 16.3 ± 1.03 mmolC m^{-2} d^{-1} in the PFZ (n = 5) and 28.2 ± 25.8 mmolC m^{-2} d^{-1} in the AZ (n=3). These carbon export estimates are comparable to observations carried out in the other sectors of the Southern Ocean (*Waldron et al.*, 1995; *Sambrotto and Mace,* 2000; *Savoye et al.*, 2004; *Lucas et al.*, 2007). The Southern Ocean accounts for nearly 50% (~1 PgC) of the annual oceanic uptake of anthropogenic CO_2, primarily through the biological pump, particularly in the midlatitudes (30 – 50°S) (Fig.1.1) (*Metzl et al.*, 1999; *Takahashi et al*., 2002), accounting for ~ 80% of the Southern Ocean uptake (*Moore and Abbott*, 2000). Increasing trends in ambient water column nutrient and surface iron concentrations corresponded with higher $\int\rho NO_3^-$ rates. Higher *f*-ratios south of the SAF reflects this, however, we suspect this to be an overestimation of the *f*-ratio given the elevated regenerated nutrient concentrations which indicate active regeneration processes assuming regeneration of nitrate in the euphotic layer. The relatively low total *ρ*N rates are ascribed to late summer season sampling when nutrients are depleted prior to the winter re-supply. Comparison of our *f*-ratio based estimates of carbon export with those from ^{234}Th data collected during the cruise revealed a similar tendency for carbon export to increase with latitude but no clear correlation was observed. In addition, new production estimates were 2 – 20 times greater in magnitude

and likely the result of the different integration time scales for the two different methods.

This work showed relatively high new production estimates in the SAZ in late summer. The high *f*-ratios measured in the SAZ were considered to be indicative of a potential source of an intraseasonal replenishment of iron supporting new production in this region. Furthermore, it also highlighted the role of mesoscale eddy activity as a potential supply mechanism of new iron into the euphotic zone. This meridional *f*-ratio gradient study highlighted the need to further examine the role of fine space and temporal scale dynamics in understanding the drivers of primary production in the SAZ. This could be achieved through high resolution observations of the productivity and its drivers which is furher investigated in the following chapter.

Chapter 4

The Sensitivity of Net Community Productivity to Intra-Seasonal Mixed Layer Variability in the Sub-Antarctic Zone of the Atlantic Ocean.

The work in this chapter is based on the work submitted to Biogeosciences for peer-reviewed publication:

Joubert, W. R., Swart S., Tagliabue, A.,Thomalla S. J., Monteiro, P.M.S.,2014, The Sensitivity of Primary Productivity to Intra-Seasonal Mixed Layer Variability in the Sub-Antarctic Zone of the Atlantic Ocean., Biogeosciences, BG2014-71, under review.

Preface

The previous chapter highlighted the importance of mesoscale eddies in the SAZ, enhancing the vertical injection of nutrients including iron as a driver of elevated new production in this region. Recent work has however implicated the additional role of sub-seasonal modes in modulating the Fe and light supply in summer and thus contributing to the seasonal characteristics of primary production in the SAZ south of Africa (*Fauchereau et al*., 2011; *Thomalla et al.*, 2011; *Swart et al.,* 2012; 2014). Meso- and submesoscale features give rise to variable rates of biogeochemical processes, depending on whether production is light or nutrient (iron) limited. When nutrients are the limiting factor, meso- and submesoscale features can provide a source of nutrients into the euphotic layer which stimulate productivity. Under light limiting conditions, meso and submesoscale eddies drive stratification that shoals the mixed layer thereby decreasing the depth of vertical mixing and increasing the light exposure

for enhanced phytoplankton growth. This chapter examines the physical control mechanisms responsible for supplying surface waters with Fe and modulating light that are ultimately responsible for controlling variability in the NCP in the Atlantic Southern Ocean.

4.1 Introduction

Two of the principal drivers of the HNLC characteristics (*Chisholm and Morel*, 1991) of the Southern Ocean are limitation by light (*Mitchell et al.*, 1991) and iron (*Martin et al*., 1991; *Boyd et al*., 2007). Exceptions occur at frontal regions, near islands and the marginal ice zone (*Arrigo*, 2010) where chl-a biomass can be elevated due to enhanced stratification and increased iron supply. The impact of these limiting factors on primary production varies over the growing season (*Boyd*, 2002). For instance during winter, increased light limitation is observed due to deep mixed layers caused by high rates of convective overturning (*DeBoyer-Montégut*, 2004). However, deep winter mixing also restores the Fe supply to the euphotic zone and relieves iron limitation for the onset of the spring bloom (*Boyd,* 2002; *Thomalla et al*., 2011; *Tagliabue et al*., 2014). Throughout spring and summer, the iron supplied to the euphotic zone from the pulse of winter convective overturning is depleted in the euphotic zone (*Boyd*, 2002; *Tagliabue et al.*, 2014). The complex role of these multiple driving factors is emphasised by the large-scale spatial variability of chl-a, which highlight regional differences in phytoplankton biomass attributed to variability in seasonal physics and biogeochemical dynamics (*Arrigo et al.*, 2008, *Le Quéré et al.,* 2002; *Moore and Abbott*, 2000). Broadly, elevated chl-a concentrations in the open Southern Ocean during the summer are associated with regions of upwelling and downstream of islands and bathymetric features (eg. *Pollard et al*., 2007), with the hydrographic fronts delineating zones with

similar mean chl-a concentrations (*Sokolov and Rintoul*, 2007). Previous work using satellite chl-a data has proposed that phytoplankton productivity variability during spring and summer in the Southern Ocean can be influenced by intra-seasonal adjustments of the mixed layer physics that modulate light and nutrient limitation (*Fauchereau et al*., 2011, *Thomalla et al*., 2011).

In the Southern Ocean, the limiting nutrient dFe can be supplied vertically into the euphotic zone by once off wintertime convective overturning (entrainment), and year-round diapycnal diffusion, as well as Ekman upwelling (*Boyd and Ellwood*, 2012; *Tagliabue et al*., 2014). Determining vertical supply rates of dFe requires knowledge of the water column dFe distribution and the depth of the ferricline. Using dFe measurements, *Tagliabue et al*. (2014), reported the depth of the ferricline in the SAZ to be between 200 – 500 m, which results in weak diapycnal diffusive fluxes (up to 15 nmolFe m^{-2} d^{-1}) in the region (*Tagliabue et al*., 2014). Based on the dFe gradient with depth and monthly mixed layer changes, *Frants et al*. (2013) calculated entrainment due to mixed layer deepening of 5 – 25 nmolFe m^{-2} d^{-1} in the Drake Passage. Lower diffusive fluxes of 15 nmolFe m^{-2} d^{-1} were observed in the SAZ south of Tazmania, calculated using vertical diffusivity from *in situ* microturbulence observations (*Boyd et al.*, 2005). All these estimates largely exclude synoptic or sub seasonal scale processes in their assessments of iron input.

A number of physical processes, varying at sub-seasonal scales, are known to modulate MLD variability and primary production (*Lévy et al*., 2012). For example, mesoscale (10 – 100 km) and submesoscale dynamics (1 – 10 km), have been shown to stimulate ocean productivity at similar scales through the vertical transport (advection and diffusion) of subsurface nutrients in oligotrophic ocean regions (*Lathuiliere et al.*, 2011, *Lévy et al*., 2009, *McGillicuddy et al*., 2007, *Oschlies and Garcon*, 1998). Under low

light conditions, enhanced rates of re-stratification associated with lateral advection from sub-mesoscale eddy and frontal instabilities (e.g., *Taylor and Ferrari*, 2011a; *Mahadevan et al*, 2012) reduce the depth of the mixed layer, thereby increasing the exposure of phytoplankton to light and favouring photosynthesis (*Sverdrup*, 1953). These findings indicate strong links between fine temporal (seasonal to sub-seasonal) and spatial (mesoscale to sub-mesoscale) scales of mixed layer dynamics and their influence on primary production.

NCP reflects the balance between net primary production and heterotrophic respiration (*Siegel et al*., 2002). In a steady state system, NCP is equivalent to new production, and approximates organic carbon export from the surface ocean (*Falkowski et al*., 2003). In order for net autotrophy to occur, in other words a positive NCP, the mixed layer is required to be shallower than a critical depth where water column integrated growth and loss rates are equal (*Sverdrup*, 1953). Furthermore *Sverdrup et al.,* (1953) defined the compensation depth (I_C) as the depth in the water column at which the light intensity is such that photosynthetic production balances losses by respiration (see chapter 1 for review). The I_C differs from the Z_{eu} (euphotic depth defined as the 1% light level, *Kirk,* 1994) in that it takes into account the physiological processes of photosynthesis as well as respiration. According to *Sverdrup et al.,* 1953, net growth is expected to occur when mean water column irradiance exceed I_C (e.g. *Siegel et al.*, 2002). Variability in MLD in the context of mean water column irradiance and I_C may affect the response of net community productivity.

Iron addition process studies (e.g., *Boyd et al.*, 2005) have demonstrated that productivity can be sustained by recycled iron, highlighting the importance of the so-called 'ferrous wheel' (*Strzepek et al*., 2005). When viewed as 'fe-ratios' (uptake of new iron/ uptake of total iron) new iron has been shown to account as little as 10% or as

much as 50% (from low to high iron waters) of the overall iron demand (*Boyd et al*., 2005; *Bowie et al*., 2009; *Sarthou et al*., 2008). Nevertheless, NCP has been shown to be consistently low when mixed layers are deep, regardless of iron sufficiency (*Cassar et al*., 2011). What remains uncertain is the response of NCP to intraseasonal variability in the MLD, which may influence the inputs of iron into the euphotic zone.

In this study, high resolution NCP estimates based on continuous shipboard measurements of ΔO_2/Ar ratios (and NCP) (*Cassar et al*., 2009) collected from several repeat transects in the Atlantic SAZ during austral summer are presented. The relationship between NCP and co-located MLD across the STZ, SAZ and the PFZ are investigated. Finally, the role of intraseasonal mechanisms that drive the variability of NCP in the context of mixed layer dynamics are highlighted to explore a link between summer entrainment of dFe and phytoplankton blooms sustained throughout summer blooms (*Swart et al*., 2014).

4.2 Sampling and cruise track

Five crossings in the Atlantic sector of the Southern Ocean were conducted between 2008 and 2010 (Fig. 4.1) along the GoodHope monitoring line (*Swart et al*., 2008; *Arhan et al.,* 2011). The transects crossed the major hydrographic fronts of the Southern Ocean, namely the STF (~ 40^{o}S), the SAF (~ 44^{o}S), and the PF (~ 50^{o}S) (Fig. 4.1).

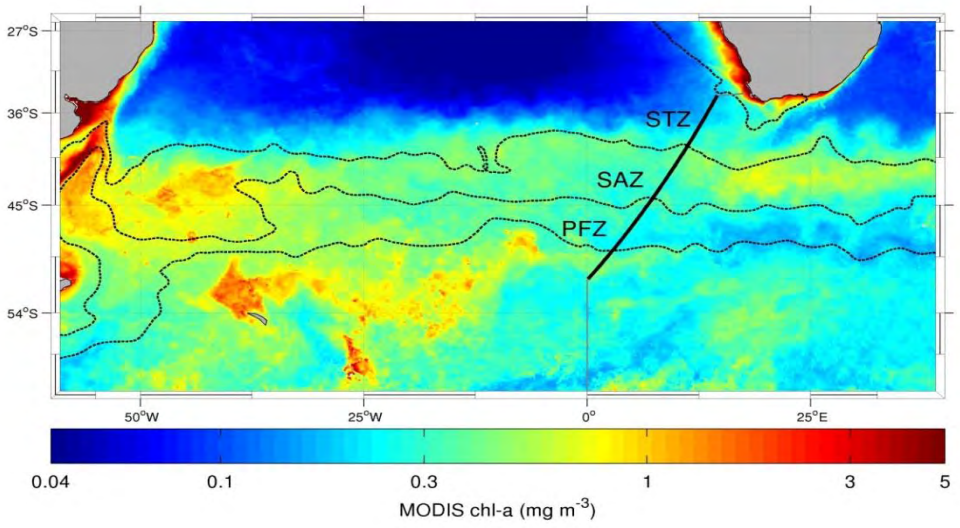

Figure 4.1. Sampling track of cruises overlaid on the summer climatology of chlorophyll-a observations from MODIS satellite over the period 2002 – 2012. Also depicted are the STZ, SAZ and the PFZ. Frontal positions (black dotted lines) are calculated from mean absolute dynamic topography.

NCP was estimated using continuous measurements of $\Delta O_2/Ar$ described in chapter 2. The underlying assumption inherent in this calculation is that NCP has been constant over the mixed layer residence time (~ 10 days). Sporadic data gaps in the wind speed product means that we cannot calculate gas transfer velocities at all locations for which we have $\Delta O_2/Ar$ measurements. Therefore more $\Delta O_2/Ar$ data are available. Lastly, entrainment or upwelling of O_2-undersaturated waters causes the biological O_2 flux to underestimate mixed layer NCP (*Jonsson et al.*, 2013). This effect is strongest south of the PF where undersaturated Circumpolar Deep Water upwells and reaches the base of the mixed layer (*Pollard et al.*, 2002). This study therefore focuses on the area between the STF and PF where the influence of this process is likely minimal.

Besides the in situ MLD from CTD, uCTD and XBT profiles described in Chapter 2, summer MLD fields were also derived using the same temperature criteria from temperature profiles from the Hadley EN3 v.2a dataset (*Ingleby and Huddleston*, 2007). Although MLD from Hadley EN3 is monthly data, it was preferred since it is based on *in situ* observations. Monthly mean EN3 MLDs (MLD_{EN3}) are not ideal to assess shorter timescale variability, but it was preferable to use this data-based product instead of higher resolution modelled data sets. Accordingly, we only use MLD_{EN3} to represent the approximate magnitude and range of intraseasonal MLD variability in summer between 1998 – 2011 (i.e. the period best constrained by observations in the EN3 dataset). PAR was taken from the standard monthly MODIS climatology product for summer months in units of mol photons m^{-2} d^{-1} (http://oceancolor.gsfc.nasa.gov/cgi/l3) from 2002 to 2012.

To assess short timescale in situ MLD variability, we used continuous water column temperature and salinity profiles of an autonomous glider deployed in the SAZ between September 2012 and February 2013 (described in *Swart et al*., 2014). Four hourly profiles were binned into 1 day bins to assess daily shoaling and deepening of the MLD. Deepening events along with mean iron profiles from the literature (*Tagliabue et al*., 2012) were used to calculate synoptic entrainment rates of dissolved iron from below the mixed layer.

4.3 Results

4.3.1 Meridional gradients and variability in MLD and $\Delta O_2/Ar$ ratios

Between 35°S – 50°S, $\Delta O_2/Ar$ ratios tend to be low (0 – 2%) when the MLD exceeds 45 m, but are generally elevated and highly variable (0 – 8%) when the MLD is less than

45 m (Fig. 4.2a). A similar relationship of elevated and variable NCP is observed with shallow MLD, albeit with a reduced dataset (Figure 4.2c). These results are consistent with earlier studies which show elevate primary production and NCP in shallow mixed layers, (e.g. *Sakshaug and Holm-Hansen,* (1986) (MLD < 40 m) and *Cassar et al.*, (2011) (MLD < 50 m)) and support the canonical control of phytoplankton production by irradiance (*Sverdrup*, 1953). Geographically speaking, the high yet variable set of $\Delta O_2/Ar$ (and NCP) observations at MLDs shallower than 45 m are mainly confined to the mid-latitudes, between 38 – 46°S that encompass the SAZ (Fig 4.2b.d).

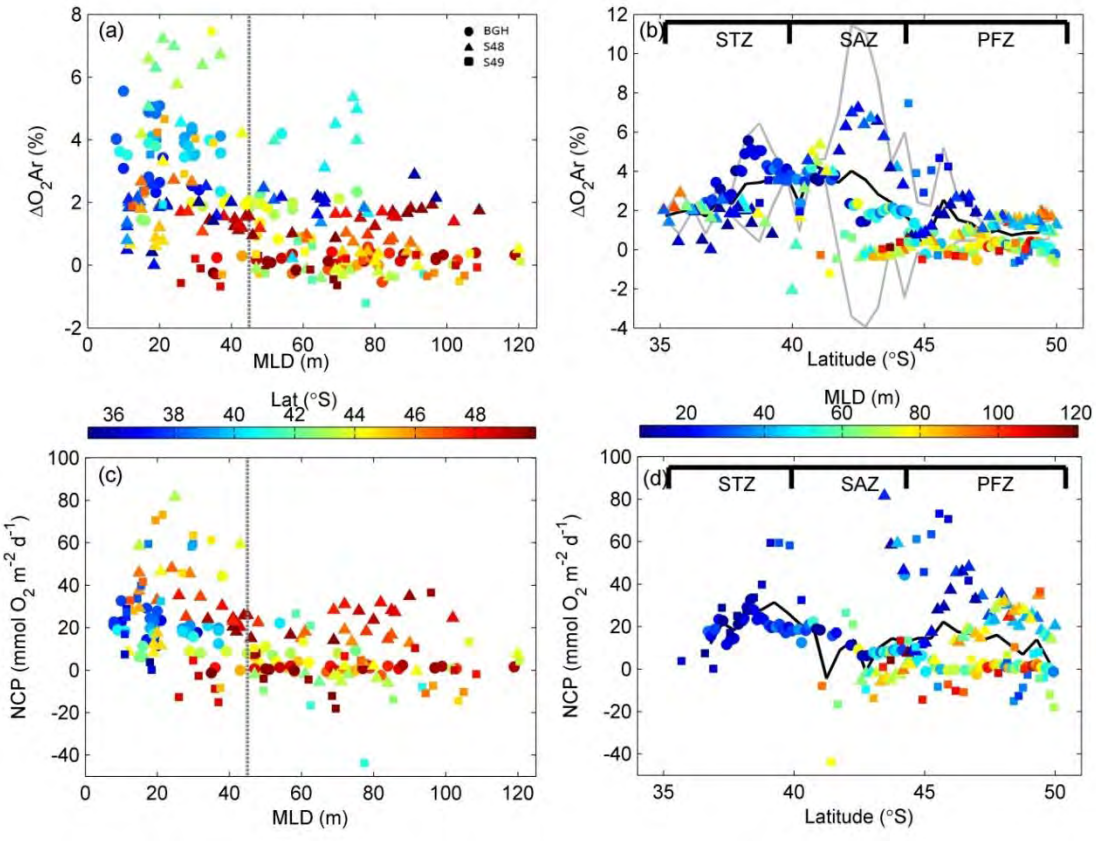

Figure 4.2. a) Relationship of $\Delta O_2/Ar$ ratios with MLD shows two modes of variability: deep mixed layers (> 45m) show diminished biological supersaturation, while shallow mixed layers (< 45m) show increased biological supersaturation with high variability. Colorbar indicates the latitude while circles, triangles and squares represent the three summer cruises, namely Bonus-Good Hope (BGH), SANAE48 (S48) and SANAE49 (S49) respectively. b) Latitudinal $\Delta O_2/Ar$

ratios (%) show the highest variance (grey lines) in the Sub-Antarctic Zone between 38 – 46°S. Variance is calculated from $\Delta O_2/Ar$ data binned in 0.5 degree latitude bands. The colorbar for the panels b and d indicates the corresponding MLD. The mean locations of the frontal zones, as determined using the mean absolute dynamic topography are displayed at the top for all latitudinal figures. c) NCP vs MLD. d) Latitudinal NCP calculated using equation 1.4.

Since mean PAR decreases and mean MLD_{EN3} increases consistently with increasing latitude from 35°S – 50°S (Fig. 4.3a,b), their latitudinal gradients alone cannot account for the observed mid-latitude (38 – 46°S) maxima and range in $\Delta O_2/Ar$ ratios (Fig. 4.2b,d). In the STZ, MLD_{EN3} are shallow (average ~ 25m) and characterised by low variability (σ ± 4.2 m), whereas in the PFZ, MLD_{EN3} are deep and more variable (~ 70 m ± 20.4 m). In the SAZ (38 – 46°S), MLD_{EN3} variable around the 45m threshold where the maximum $\Delta O_2/Ar$ ratios are observed (Fig. 4.3b).

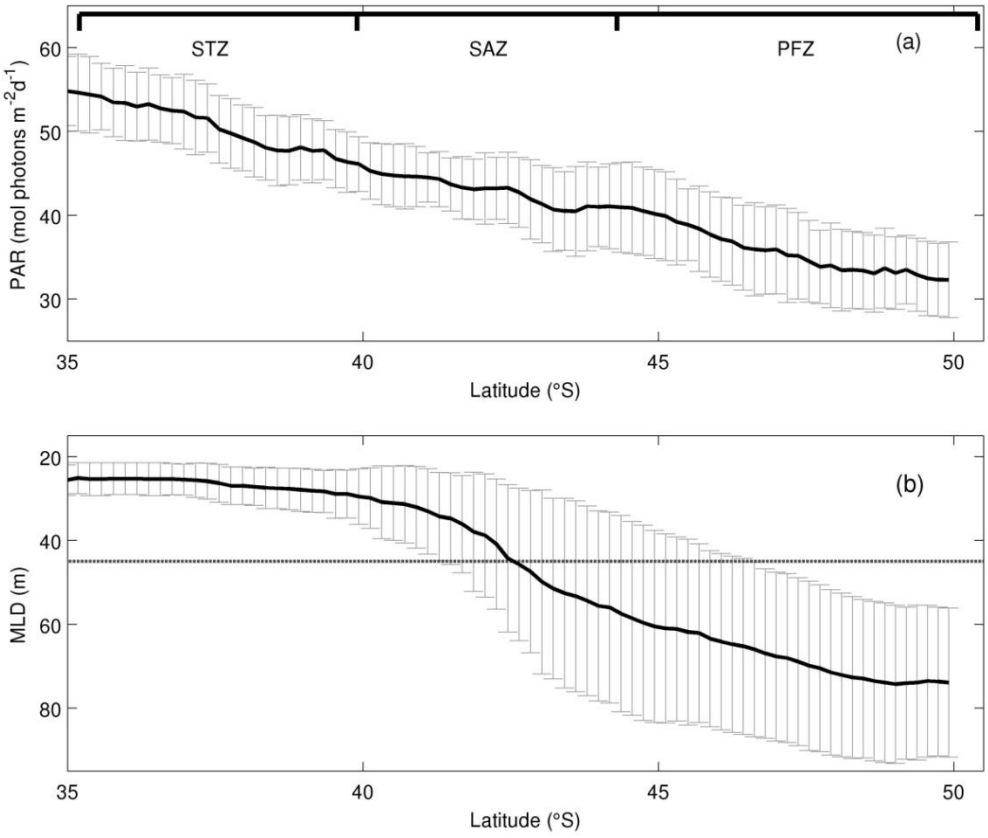

Figure 4.3. a) MODIS surface PAR climatology (2002 – 2012) for summer months (Dec to Feb) in units of mol photons m-2 d-1 along the cruise track. b) MLDEN3 summer climatologicy (period 2002 – 2012) and associated standard deviation. A steep gradient is observed in the SAZ separating the shallow, low variability MLD to the north and the deep, highly variable MLD to the south.

4.3.2 Intra-seasonal Fe supply and demand in the euphotic zone

Supply mechanisms of dFe into the euphotic zone include convective overturning, diapycnal diffusion (*Tagliabue et al*., 2014) and lateral advection downstream of landmass (*Blain et al.,* 2007). Lateral advection of surface water plays an important role in water column stability as well as iron supply in Southern Ocean regions downstream of islands and continents. Together with MLD driven light availability through water column stability, NCP may also be responding to variations in the supply of iron that is driven by synoptic scale variations in mixing. Regional dFe concentration data (from the literature and summarised in *Tagliabue et al*., 2012) are limited to relatively few profiles (*Chever et al.*, 2010; *Klunder et al*., 2011). These selected profiles (from the SAZ) were collected in Feb – Apr 2008 during the Bonus Goodhope cruise campaign (*Chever et al.*, 2010) and the ANT XXIV/3 expedition (*Klunder et al*., 2011) along the same transect as this current study. Data from the SAZ shows an increase from 0.20 nmol L^{-1} at depths shallower than 45 m to 0.26 nmol L^{-1} at depths deeper than 45 m (Fig. 4.4). Based on the limited *in-situ* observations a gradient of dFe was approximated and then used in Equation 4.1 to calculate the potential entrainment of dFe into the layer 0 – 45 m.

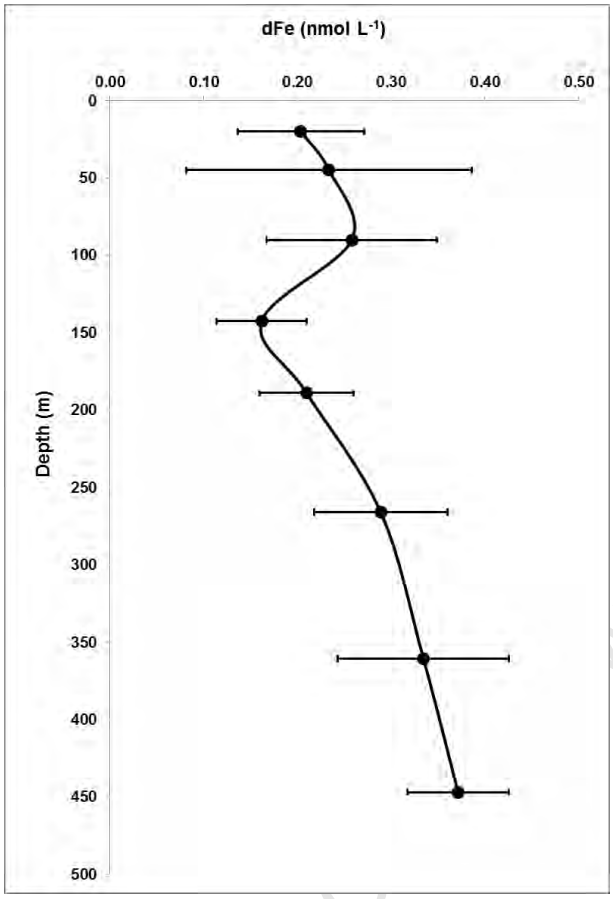

Figure 4.4. dFe for the upper 500 m of the water column within the SAZ region modified from data published in (*Tagliabue et al*., 2012).

To assess the potential entrainment flux of dFe from below the euphotic layer, daily synoptic mixed layer entrainment rates of dFe ($F_{Fe\text{-}syn}$ in units of nmolFe m^{-2} d^{-1}) were estimated using a range of the number of positive daily MLD change events (i.e. deepening of MLD to below 45m) taken from daily glider MLD data in the SAZ between September 2012 and February 2013 (*Swart et al*., 2014) and the available dFe profiles along the transect (data from Chever et al. 2010, Klunder et al., 2011).

$$F_{Fe-syn} = N / n \int_0^{MLD} (([dFe]_{subMLD} - [dFe]_{euphotic}) \times \frac{\Delta MLD_{45}}{MLD_t}).dz \qquad (4.1)$$

Where $[dFe]_{subMLD}$ and $[dFe]_{euphotic}$ are the dFe concentrations from below the mixed layer and the 0 – 45 m ('compensation') zone respectively, MLD_t is the depth of the

mixed layer after a daily deepening event, ΔMLD_{45} the difference between the observed MLD_t and a depth of 45 m (the depth identified for elevated NCP and hypothesised to represent the compensation depth), and *N* is the number of events of entrainment over the month, and *n* the number of days in per month. In equation 4.1 the post entrainment concentration of dFe is scaled to the deepening of the MLD and the flux is derived by integration to the depth of the mean summer MLD. This correction for 'detrainment' is important as this part of the entrained dFe is lost and no longer available to primary production when the MLD shoals following a deepening event. When mixed layers remained > 45 m for several consecutive days, the average MLD was used to calculate daily entrainment rates. Equation 4.1 assumes a constant gradient between the dFe < 45 m and dFe in the 0 – 45 m layer, calculated from the data used in Figure 4.4. Furthermore, the compensation depth is approximated to 45 m, whereby the MLD fluctuates above and below this light requirement for increased NCP, is assumed to be constant throughtout the study region. Finally, this model assumes MLD entrainment events calculated from the number of deepening and shoaling events occurring per month using glider MLD data from the SAZ over several months (*Swart et al.,* 2014). To derive a mean daily dFe flux, all synoptic MLD deepening events to below 45m were summed for each month and divided by the number of days per month. To test the sensitivy of the model in Equation 4.1 to the iron gradient, dFe concentration in the euphotic zone was varied between 0 nmol L^{-1}, reflecting complete consumption of dFe in the euphotic zone and 0.15 nmol L^{-1}, reflecting partial consumption of dFe concentrations, and a subsurface concentration of 0.25 nmol L^{-1}, taken from the profile data of *Chever et al*., (2010) and *Klunder et al*., (2011).

Glider data suggests the number of synoptic events would likely range between 2 and 5 per month and the mixed layer gradient perturbation would be between 1 – 35 m deeper

than the 45m threshold. Within this range, $F_{Fe\text{-}syn}$ is between 10 – 600 nmolFe m^{-2} d^{-1}, depending on the surface and subsurface dFe concentrations, as well as the depth and frequency of the MLD deepening events (Fig. 4.5). Unsurprisingly, the largest $F_{Fe\text{-}syn}$ rates are found when the depth and frequency of deepening events in the glider data are the largest. In addition, $F_{Fe\text{-}syn}$ is enhanced markedly by assuming complete consumption of the euphotic zone dFe reservoir (compare Fig. 4.5b with 4.5a). Nevertheless, even the lowest rates of $F_{Fe\text{-}syn}$ estimated here (98 nmolFe m^{-2} d^{-1}) are similar to or larger in magnitude than those associated with diapycnal diffusion (*Boyd et al*., 2005, *Frants et al*., 2013, *Tagliabue et al*., 2014).

4.4 Discussion

4.4.1 The role of MLD variability in driving NCP variability in the SAZ

Based on the observations of ΔO_2/Ar ratios, NCP and MLD, we consider a mechanism where intraseasonal synoptic scale MLD deepening entrains essential nutrients from below the euphotic zone, followed by rapid buoyancy driven shoaling of the MLD. In the STZ, nutrient limitation through persistently shallow MLDs is known to limit primary production (*Pollard et al*., 2002; *Joubert et al*., 2011) preventing high values of NCP. Here buoyancy forced stratification in the summer dominates over wind stress mixing (*Swart et al*., 2014). In the PFZ, wind stress mixing dominates over buoyancy forcing resulting in persistent deep MLDs, low mean PAR and low Fe concentrations (*Chever et al*., 2010; *Klunder et al*., 2011) that constrains NCP to a low range (13.1 ±18 mmol m^{-2} d^{-1}). The SAZ lies between these two zonal modes and is characterised by a rapid meridional change in the mean MLD depth as well as MLD excursions above and below the 45 m light requirement (Fig. 4.3b, and Fig. 4.5) for positive NCP. These sub-

seasonal MLD excursions around ~ 45 m are linked to a combination of intraseasonal high-wind-stress events (*Swart et al.*, 2014) and restratification. These are driven by mesoscale activity associated with fronts, mesoscale instabilities and eddies generated from interactions of the Antarctic Circumpolar Current (ACC) with topography and downstream advection (*Swart and Speich*, 2010).

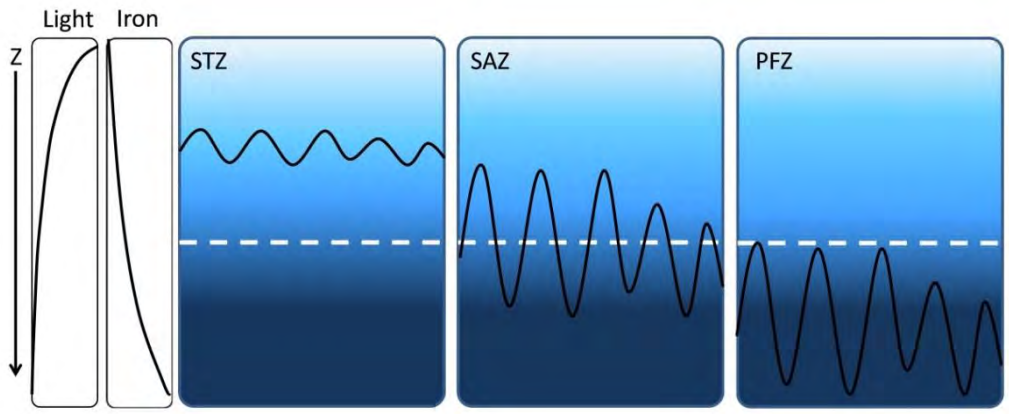

Figure 4.5. Conceptual model shows MLD variability (black line) in the STZ, SAZ and PFZ, in relation to a water column irradiance depth threshold (dotted white line). This model proposes that the SAZ is the only region where the MLD deepening, driven by short term storm events, followed by shoaling during quiescent periods drives short term variability in phytoplankton production.

It is possible that elevated and highly variable $\Delta O_2/Ar$ ratios in the SAZ is due to MLD variability around a community compensation depth requirement of ~ 45 m at intra-seasonal timescales. For example, *Mahadevan et al*. (2012) show that, in the North Atlantic, eddies increase water column stratification through eddy slumping when lateral (horizontal) density gradients destabilise the water column by transporting light

water over dense water over weekly timescales. Such mechanisms rapidly reduce the depth of mixing, leading to increased light exposure and phytoplankton growth (*Mahadevan et al*., 2012). Similarly, *Taylor and Ferrari* (2011) showed that frontal instabilities can rapidly re-stratify the upper ocean (suppressing vertical mixing), even in the presence of strong surface cooling and destabilizing winds enhancing mean light exposure and stimulating elevated primary production in low light conditions.

It is possible that intraseasonal high-wind-stress events characteristic of the SAZ (*Braun*, 2008; *Swart et al*., 2014) drive MLD deepening and nutrient entrainment, while increased buoyancy associated with high mesoscale activity that creates density gradients necessary to drive rapid re-stratification of MLD to a depth > 45 m, favouring mean light conditions for elevated NCP (Fig. 4.5). Repetition of this pattern on intraseasonal timescales reconciles both the observed highly variable NCP (up to 80 $mmolO_2\ m^{-1}\ d^{-1}$) in this study with sustained summer blooms characteristic of the SAZ (*Thomalla et al*., 2011; *Swart et al.*, 2014). In this way, biomass can amass through production cycles driven by intra-seasonal re-supply of Fe (MLD > 45 m) and light (MLD < 45 m) at appropriate timescales for phytoplankton growth. This hypothesis rests on the presence of both intraseasonal storm events deepening the mixed layer, which entrain limiting nutrients (primarily Fe) from below the euphotic zone, and subsequent stratification at depth shallower than the compensation NCP depth, which alleviates light limitation and hence stimulates phytoplankton growth (depicted in Fig. 4.5).

4.4.2 Early versus late summer sampling

It can be argued that the $\Delta O_2/Ar$ (NCP) variability observed in shallow mixed layers potentially reflect interannual changes in productivity between 2008 and 2010. It is unlikely that interannual variability is responsible for the observed $\Delta O_2/Ar$ variability in

shallow mixed layers since all cruises, indicated by different symbols show the non-linear relationship of $\Delta O_2/Ar$ with MLD (Fig. 4.6a,b) regardless of the early (Dec) or late (Feb) summer sampling.

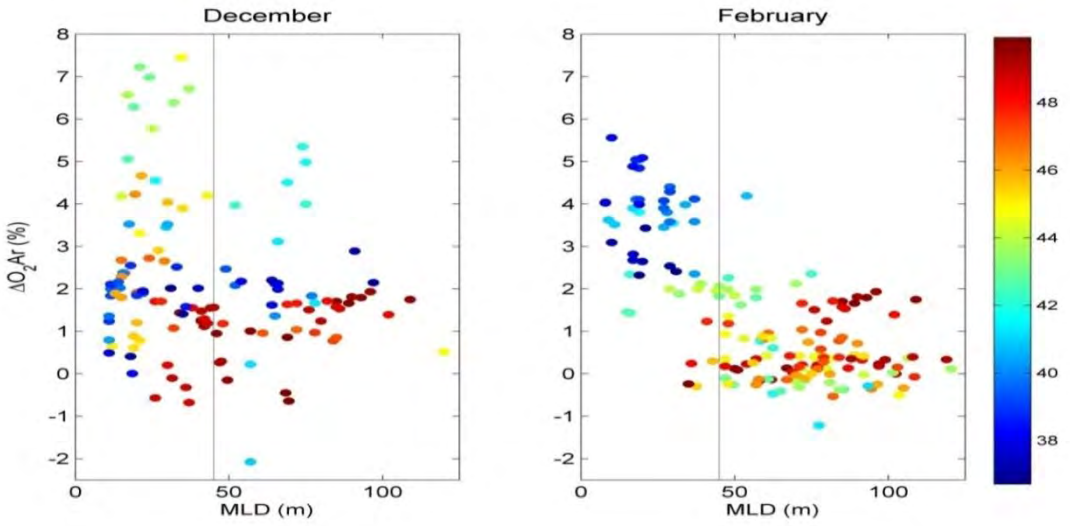

Figure 4.6. Comparison between early (December) and late summer (February) $\Delta O_2/Ar$ ratios shows robust relationship of elevated and variable productivity in shallow MLDs.

4.4.3 Synoptic input of dissolved iron during summer

The role of synoptic inputs of iron to the euphotic zone in driving the variability of summer phytoplankton production has received little attention. *Tagliabue et al*. (2014) set out a seasonal paradigm of a wintertime dFe pulse from entrainment followed by little addition dFe supply from diapycnal diffusion that required high rates of dFe recycling to sustain primary production. In this context, the synoptic Fe fluxes estimated here can potentially provide a significant additional source of Fe. For example, the maximum summertime NCP is 80 mmol O_2 m^{-2} d^{-1}, which, assuming a photosynthetic quotient of 1.4 (*Laws et al*., 1991), is ~ 57 mmol C m^{-2} d^{-1}. This equates to an iron requirement of ~ 50 to 500 nmol Fe m^{-2} d^{-1} using Fe:C ratios from typical

Southern Ocean phytoplankton (0.8 – 8.6 μmol Fe/mol C (*Strzepek et al*., 2011)). The $F_{Fe\text{-}syn}$ presented here (10 – 600 nmolFe.m^{-2}.d^{-1}) are comparable with the lower end of diapycnal diffusion estimates (Table 5.1), and exceeds the maximum iron utilization rates (up to 145 nmolFe.m^{-2}.d^{-1}) estimated in the region (*Boyd et al.*, 2012). The observational evidence however suggests that much of the phytoplankton iron demand is met by recycled iron (*Bowie et al*., 2009; *Sarthou et al*., 2008; *Strzepek et al*., 2005). *f*e-ratio estimates range from 0.1 to 0.5 for low to high iron waters, which would imply a 'new' iron requirement of ~5 to 250 nmol Fe m^{-2} d^{-1}. Overall, summertime dFe supply must therefore provide 5 to 500 nmol Fe m^{-2} d^{-1}, assuming a low to high reliance on 'new' Fe input. Diapycnal fluxes from the Atlantic SAZ of 2 – 15 nmol Fe m^{-2} d^{-1} (*Tagliabue et al*., 2014) are too low to support all but the lowest of our estimated Fe demand.

Several studies have indicated rapid recycling of dFe in the surface waters (*Boyd et al*., 2005; *Sarthou et al.*, 2008; *Strzepek et al.*, 2005), which potentially contribute to the subsurface source of dFe presented here. The uptake of 'new iron' relative to total iron ('new + regenerated iron') termed the "*fe*-ratio" are small (0.17) (*Boyd et al.*, 2005) with regeneration rates of ~17 – 20 pmol Fe L^{-1} d^{-1} (*Strzepek et al*., 2005) highlight the small contribution of 'new' iron into the eupthotic zone. Regeneration rates of 20 pmol Fe L^{-1} d^{-1} (*Strzepek et al.*, 2005), integrated through a 45m water column equates to roughly ~900 nmol Fe m^{-2} d^{-1}, which exceeds the maximum of relative entrainment fluxes calculated here.

Table 4.1: Flux rates of iron entrainment, diapycnal diffusion and Fe utilization from literature.

Reference	Rate	Process	Area

	nmol Fe m^{-2} d^{-1}		
This study	10 - 600	ML entrainment	Atlantic SO
Frants et al., 2013	64	diapycnal diffusion	Drake Passage
Frants et al., 2013	5 - 25	ML entrainment	Drake Passage
Bowie et al., 2009	15	ML entrainment	SAZ Tasmania
Tagliabue et al., *2014*	1 - 15	diapycnal diffusion	Southern Ocean
	Utilization		
Boyd et al., 2012	145*	utilization	Atlantic SO
Strzepek et al., 2005	900^{+}	remineralization	Southern Ocean
Sarthou et al., 2008	63 - 162	remineralization	Kerguelen

*calculated from annual rates assuming 365 days.

$^{+}$rates calculated assuming a 45m surface mixed layer.

The relative entrainment flux of dFe presented here are high, and the origin of the subsurface source of iron are likely rapid regeneration of the dFe pool (*Strzepek et al*., 2005; *Tagliabue et al*., 2014) in line with regeneration of dFe. Lateral advection along isopycnals is also a potential source, while vertical mixing from below the ferricline is unlikely due to the deep ferricline in this region (200 – 500m) (*Tagliabue et al*., 2012; 2014). Furthermore, the supply of an iron source below the ferricline would contribute to the 'new iron' pool, reflected in the small '*fe*-ratio' (*Boyd et al*., 2005). Iron supply dynamics remain difficult to assess with the current available data, and this work highlights the need for a better understanding of how dissolved Fe reservoirs are coupled to ML dynamics on intra-seasonal scales in the SAZ to better appraise this mechanism.

In contrast, the synoptic dFe inputs of 10 - 600 nmol Fe m^{-2} d^{-1} more closely match demand estimates, suggesting that such supply mechanisms may be of importance in regions that experience strong variability in MLD dynamics over summer. In addition to the frequency and magnitude of the synoptic events themselves, the highest rates of

synoptic dFe input require exhaustion of the surface dFe reservoir (Fig. 4.7). The overall goal was to test the sensitivity of the synoptic dFe entrainment flux to a weak and strong gradient in dFe, the extent of the MLD deepening and the number of events per month. Unfortunately, currently available dFe observations in the Southern Ocean rarely constrain the seasonal minima in dFe (*Tagliabue et al*., 2012).

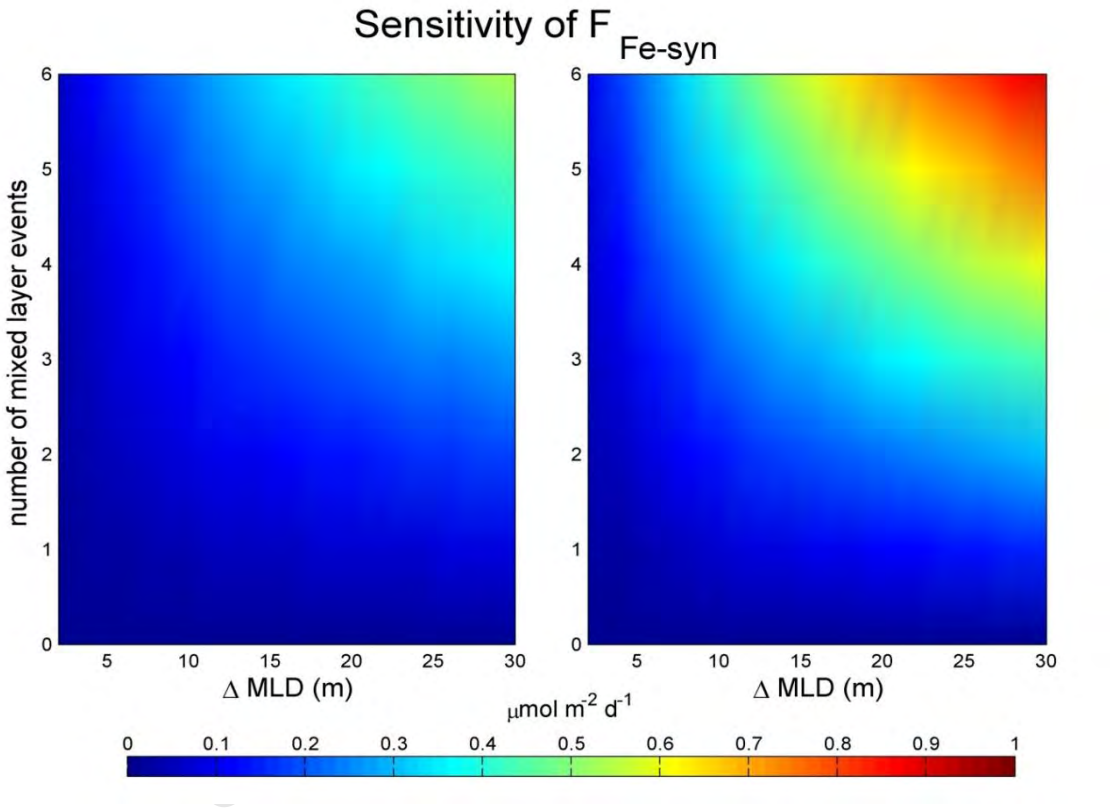

Figure 4.7. Sensitivity of synoptic dFe flux rates to number of deepening events and change in the MLD. The left and right panels represent a surface dFe concentration of 0.15 nM (conservative estimate) and 0 nM (assuming complete surface consumption of iron) respectively.

This additional flux of 'new' dFe from synoptic events might also account for potential intraseasonal losses of dFe associated with detrainment from shoaling subsequent following storm-driven deep mixing of phytoplankton biomass (*Behrenfeld et al*., 2013). This detrainment of biomass is exported from the mixed layer and lost from the

euphotic zone as it is sequestered below the thermocline. Mixed layer deepening events then entrain new iron from a reservoir below the mixed layer on short timescales as described above, which replenish the Fe lost due to detrainment. Since this mechanism of entrainment/detrainment cycles has not been considered before, the implication is that low *f*e-ratios potentially underestimate the contribution of new Fe in the iron budget and new production.

The assumptions that underpin these calculated constraints to short-term event scale variability of productivity in the euphotic zone require a more vigorous test to assess synoptic entrainment fluxes. For instance, we find a strong sensitivity of synoptic input to the assumed surface dFe concentration which needs to be better constrained in the future (*Tagliabue et al*., 2012). In addition, our estimates of NCP were collected during the summer seasons of 2008 - 2010, dFe profiles were collected in summer 2008 (*Chever et al*., 2010; *Klunder et al*., 2011), while glider data were collected during summer 2012/13, and so do not necessarily reflect the conditions during the NCP observations. However, the iron and glider datasets were used to estimate the potential role of synoptic iron input rather than a precise value for a given year. Finally, top down processes (such as grazing) were not considered which may also influence phytoplankton biomass during deepening and shoaling of the mixed layer (*Behrenfeld et al*., 2013). In the future, a comprehensive process study, similar to the FeCycle III experiment (*Boyd et al*., 2012), that accurately constrains Fe demand and its relation to mixed layer dynamics at the appropriate timescales is required.

4.5 In Summary

In this study, a quasi non-linear relationship between NCP and MLD is presented, which is proposed to be modulated by intraseasonal modes of variability in the Atlantic sector of the Southern Ocean, north of the Polar Front. The highest and most variable NCP were observed only when the MLD was < below 45 m in the SAZ. The SAZ thus represents a dynamic transition zone between oligotrophic, shallow (< 45 m) and buoyancy-dominated stratified mixed layers to the north (STZ), and deep (z > 45 m) light-limited mixed layers to the south (PFZ) at high higher latitudes. It is proposed that elevated and highly variable and sustained primary net community production in the SAZ results from intraseasonal scale storm events, alternating between deepening of the mixed layer, that entrains Fe, followed by rapid shoaling that favours growth in a transient iron replete, high light environment. Rates of synoptic dFe entrainment fluxes were estimated to range between 100 – 600 nmol Fe m^{-2} d^{-1}, which are in the same order of magnitude as the Fe requirements for the observed elevated NCP. This dynamic helps explain the seasonal persistence of primary production and biomass observed during summer in the SAZ (*Swart et al*., 2014). If this is correct, it highlights another potentially important climate sensitivity in respect of mid latitude ecosystems and the role of the SAZ in the biological carbon pump. A more rigorous test of this hypothesis is required using NCP, MLD and iron flux data at the same meso- submesoscale resolution in order to elucidate the impact of MLD variability on primary productivity.

Chapter 5

The sensitivity of Net Community Production to light availability within the mixed layer

Preface

In the previous chapter, two patterns of NCP variability emerged, namely, elevated and variable NCP in shallow mixed layers (MLD < 45 m) and a clear latitudinal gradient in NCP with highest NCP in the SAZ (Fig. 4.2). To consider chl-a and MLD as drivers of primary productivity, NCP is normalised to chl-a and MLD. The objective here is to empirically examine the dependence of NCP on chl-a and water column irradiance using a very simple approach with some process-level information.

5.1 Introduction

Iron and light both have an important influence on primary productivity in the Southern Ocean (*Boyd et al*., 2001). The previous chapter highlighted the important role of intraseasonal dynamics of the surface mixed layer in modulating the light and iron conditions that influence NCP. Light within the mixed layer is not only important for providing the energy requirements to drive photosynthesis but is also thought to modulate the response of phytoplankton to iron supply (*Boyd et al*., 2001). This is because iron demand has been shown to increases under low light conditions (*Sunda and Hunstman*, 1997), when more iron is required for photon harvesting pigment

synthesis (*Van Leeuwe*, 1998). In addition to supplying the required energy essential for photosynthesis and influencing the cellular Fe requirements, light also provides the heat flux required to stabilise the surface mixed layer. It has long been recognised that shallow mixed layers are required for elevated productivity, particularly in the development of seasonal phytoplankton blooms (*Sverdrup*, 1953). Furthermore, iron enrichment experiments assert that iron limits primary productivity (e.g. *Boyd et al.*, 2007) while the interaction between iron and light limitation remains important (*Boyd*, 2002; *Sunda and Huntsman*, 1997), but not well understood.

The critical depth hypothesis (*Sverdrup*, 1953) relates the primary productivity to the available light in the water column, under nutrient replete conditions. It is defined as the depth where integrated rates of photosynthesis and respiration are in balance. When the MLD is deeper than the critical depth (Z_{cr}), light required for net positive production is insufficient. Shoaling of the mixed layer (shallower than Z_{cr}) increases the average light within the mixed layer, such that production rates can increase above respiration rates and allow net positive production (*Sverdrup*, 1953). Light availability within the mixed layer is a function of PAR at the surface and the diffuse light attenuation coefficient integrated over the MLD (Morel, 1988). Sverdrup's model assumes that phytoplankton are homogenously mixed throughout the upper mixed layer, that specific losses are constant with depth and that specific growth rates are proportional to the amount of light in the water column. This means that as light increases with seasonal increases in PAR, the critical depth may deepen below the MLD favouring positive NCP. The opposite is true for when losses increase, for example increased grazing following a bloom will cause the critical depth to shoal. Under low light conditions (when nutrients are replete) the rate of photosynthesis increases with increasing irradiance, until photosynthetic capabilities are saturated. At low irradiance,

photoacclimation has been shown to occur when phytoplankton cells adjust their photosynthetic pigment concentration (chl-a) in response to variable incident irradiance (*Falkowski and La Roche,* 1991; *Behrenfeld et al.,* 2008). At high irradiance, photosynthesis remains constant even if light increases (see *PvsE* curve in Fig. 1.5) until the point where photoinhibition occurs. Since the initial light-dependent slope of the *PvsE* curve (α) provides a measure of the quantum efficiency of phytosynthesis, a decrease in α values may reflect iron limitation. When iron stress is relieved however, such as *in situ* iron fertilisation experiments conducted in the Pacific Southern Ocean, light dependent phytoplankton growth rates, and α have been shown to effectively double (*Hiscock et al.*, 2008).

Positive NCP can occur in the mixed layer when water column integrated photosynthetic rates are greater than loss rates from auto- and heterotrophic respiration and other loss terms (e.g. bacteria, grazing, sinking, viral infection, parasitism, physical flushing, dilution and mixing) (*Behrenfeld,* 2010; *Siegel et al.*, 2002; *Smetacek and Passow*, 1990; *Sverdrup,* 1953). NCP has been shown to be consistently low when mixed layers are deep (in other words under low light conditions) regardless of iron sufficiency (*Cassar et al.*, 2011), which highlights the importance of irradiance for phytoplankton growth. The opposite has been shown to be true under Fe limiting conditions, despite sufficient light photosynthetic rates remain low (*Moore et al.*, 2006). These findings demonstrate the importance of both irradiance and Fe for net phytoplankton community growth. In this section, we use high resolution observations of NCP, chl-a and mixed layer PAR to examine the influence of light availability in the Atlantic Southern Ocean.

5.2 Methodological Context

Five crossings of a cruise transect in the Atlantic Southern Ocean were conducted between 2008 and 2010 as described in the Chapter 2 (Fig 2.1).

NCP (in units of mmol O_2 m^{-2} d^{-1}) was calculated from the $\Delta O_2/Ar$ ratios, the saturation concentration of dissolved oxygen and the gas transfer velocity as described previously (see Chapter 2). In order to investigate the influence of irradiance on production, NCP was normalized to chl-a concentration and mixed layer depth. The resulting normalized rate term has units of mmolO_2 mg chl^{-1} d^{-1}, and we refer to it as "normalized NCP" (NCP*). This rate was compared with the average irradiance in the mixed layer ($\bar{I}_{MLD}$), computed by averaging the light profile within the mixed layer, calculated from sea surface PAR and the diffuse attenuation coefficient (K_d). K_d is assumed to be constant throughout the mixed layer and is estimated from surface satellite PAR and surface *in situ* chl-a using the empirical relationship of *Morel*, (1988):

$$K_d = 0.121 \text{ x } [\text{chl-a}]^{0.428} \qquad (5.1)$$

Mean water column irradiance in the mixed layer ($\bar{I}_{MLD}$) is calculated as:

$$\bar{I}_{MLD} = \frac{1}{MLD} \int_0^z I_o \, e^{-Kd.z} . dz \qquad (5.2)$$

Where MLD is the *in situ* mixed layer depth (in meters), I_o is the surface irradiance and z is the depth level in meters. To calculate $\bar{I}_{MLD,}$ PAR was taken from the standard monthly MODIS climatology product for summer months (Dec – Feb) in units of mol photons m^{-2} d^{-1} (http://oceancolor.gsfc.nasa.gov/cgi/l3), for the years coinciding with each cruise.

5.3 Results

Surface temperatures remain in excess of 16^{o}C in the STZ northwards of the SAF, decreasing to between 6 – 10^{o}C in the SAZ (Fig 5.1). In surface waters of the PFZ, temperatures ranged between 2 and 6^{o}C, while remaining below 2^{o}C poleward of the PF. Shallow mixed layers depths (mean MLD = 26.6 m ± 4.4 m) were observed in the STZ, mainly driven by elevated surface temperatures in this region. Intermediate MLDs (mean MLD = 44.5 m ±16.8 m) were observed in the SAZ, while MLDs were deep (mean MLD = 69.1 m ± 19.8 m) in the PFZ, and reached values of ±100 m south of the PF. In the seasonal ice zone south of the Sbdy, MLDs were similar to the values reported in the STZ, a consequence of melting sea-ice.

NCP data were highly variable along the transect without any clear latitudinal pattern (Fig. 5.1). Positive NCP indicate efflux of O_2 to the atmosphere. In Feb 2008, a latitudinal decrease in NCP was observed from ~ 15 mmol O_2 m^{-2} d^{-1} in the STZ to near zero poleward of 45^{o}S. This latitudinal pattern was absent in subsequent cruises. Highest NCP (up to 100 mmol O_2 m^{-2} d^{-1}) were recorded during December 2008 and December 2009 in all regions, due to higher $\Delta O_2/Ar$ ratios in early (December) compared to late summer (February) highlighting seasonal differences. Lowest NCP were observed during Februay 2008. NCP reached up to 90 mmol O_2 m^{-2} d^{-1} in the MIZ during December 2009 compared to other years. Negative NCP values indicating either net heterotrophic conditions or upwelling of undersaturated water were observed near the Sbdy (55 – 60^{o}S) in almost all instances. Some data are missing in the SAZ in Dec 2009, and the STZ in December, Febuary 2009 and 2010, due to instrument malfunction and sporadic satellite wind speed data.

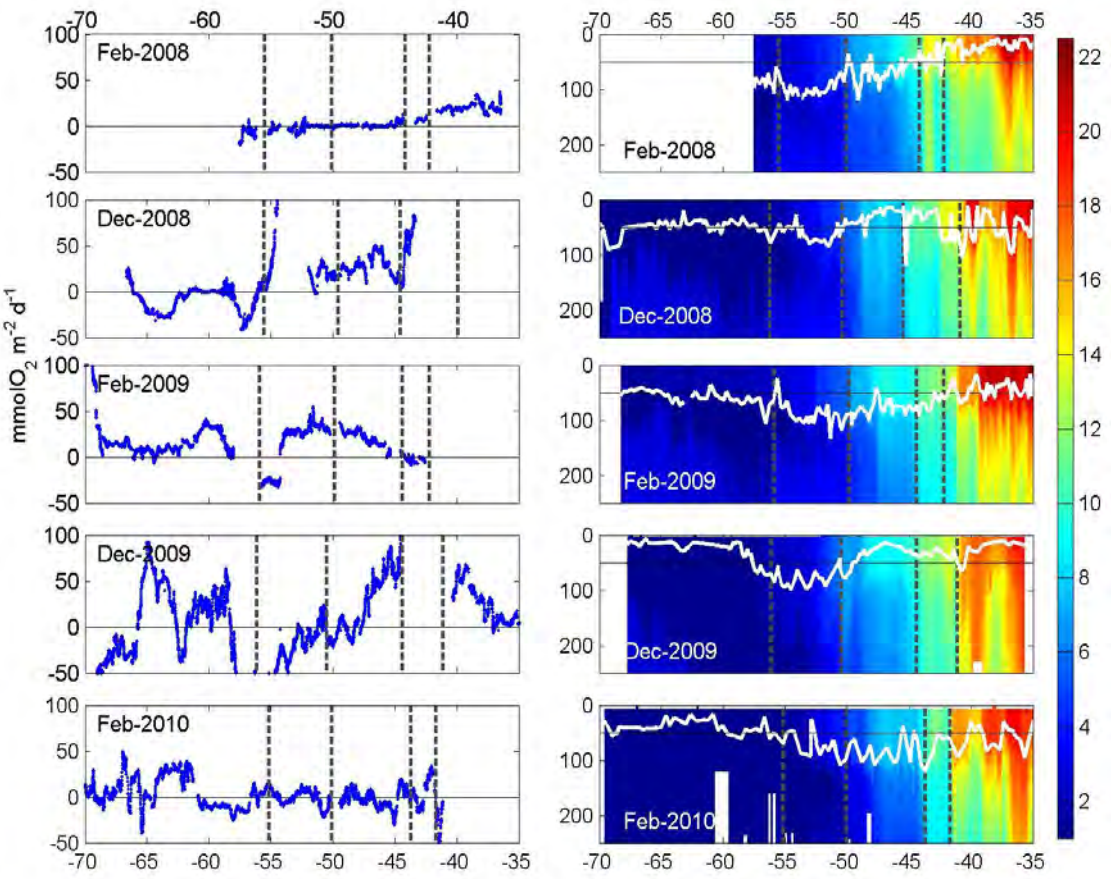

Figure 5.1. High resolution NCP (left side panels), temperature (right side panels) and MLD between 2008 and 2010. Positive NCP indicate efflux of O_2 to the atmosphere. MLDs (white line) are superimposed on the temperature profile in the right hand side panels. Vertical grey lines delineate the frontal positions from north to south indicating the STF, SAF, PF and the Sbdy of the ACC.

Meridional chl-a biomass distribution from both MODIS and *in-situ* observations show three peaks associated with the frontal regions suggesting a significant spatial separation between areas of elevated productivity and areas of high biomass (Fig. 4.2c; Fig. 5.2). Frontal advection of high biomass is widely observed downstream of ACC interactions with topography where upwelling of nutrients favours productivity (*Blain et al.,* 2007; *Pollard et al.*, 2002; *Tremblay et al.*, 2002). Similarly, highest chl-a concentrations (up

to 1.5 mg m^{-3}) were observed near the continental and MIZ while lowest values of chl-a were observed in the oligotrophic STZ (0.1 – 0.2 mg m^{-3}).

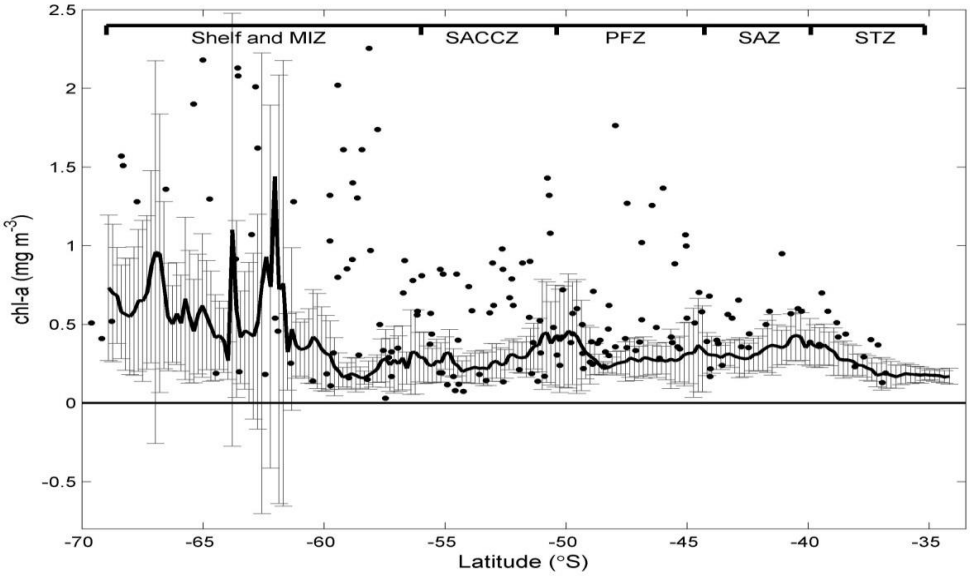

Figure. 5.2. *In situ* surface chl-a data (dots) from the upper 10 m of the water column overlain on the mean MODIS weekly chl-a (line and errorbars) for the cruises during 2008 – 2010 along the cruise track. Errorbars indicate the standard deviation calculated using the weekly MODIS chl-a product. Weekly MODIS data corresponding to the cruise dates are presented. Frontal positions and zones are also indicated.

Surface PAR showed a typical decrease with increasing latitude from ~ 58 mol photons m^{-2} d^{-1} in the STZ to ~35 mol photons m^{-2} d^{-1} (Fig. 5.3a) poleward of ~ 50°S. Diffuse attenuation coefficient (K_d) tracked chl-a, which is expected given that chl-a was used to determine K_d (Fig. 5.3b). $\bar{I}_{MLD}$ exceeded 20 mol photons m^{-2} d^{-1} north of the STF, decreasing to between 10 – 20 mol photons m^{-2} d^{-1} in the SAZ, and values of less than 10 mol photons m^{-2} d^{-1} at the PF (thought to be driven primarily by deep MLDs) followed by a slight increase to between 10 - 15 mol photons m^{-2} d^{-1} from the PF to the Antarctic continent (Fig. 5.3d) resulting from weaker surface PAR further south (Fig. 5.4a).

In situ chl-a derived $\bar{I}_{MLD}$ values compared well with $\bar{I}_{MLD}$ derived from satellite chl-a (Fig. 5.3d) north of the 50°S whereas polewards of the PF *in situ* estimates tend to be lower than satellite estimates, particularly in the SACCF and the MIZ where they are closer to ~ 5 – 10 mol photons m^{-2} d^{-1} (compared to ~15 mol photons m^{-2} d^{-1} for satellite derived). Lower *in situ* chl-a derived $\bar{I}_{MLD}$ values observed in these regions are likely due to satellite retrieval of chl-a whose standard algorithms typically underestimate chl-a in the Southern Ocean by 2 – 3 times compared to *in situ* measurements (*Kahru and Mitchell*, 2010). Underestimation of chl-a concentrations will influence K_d values, which are used to calculate the light profile and can therefore result in higher $\bar{I}_{MLD}$. In spite of this possible bias, the $\bar{I}_{MLD}$ presented here compares well with data from *Venables and Moore.*, (2010).

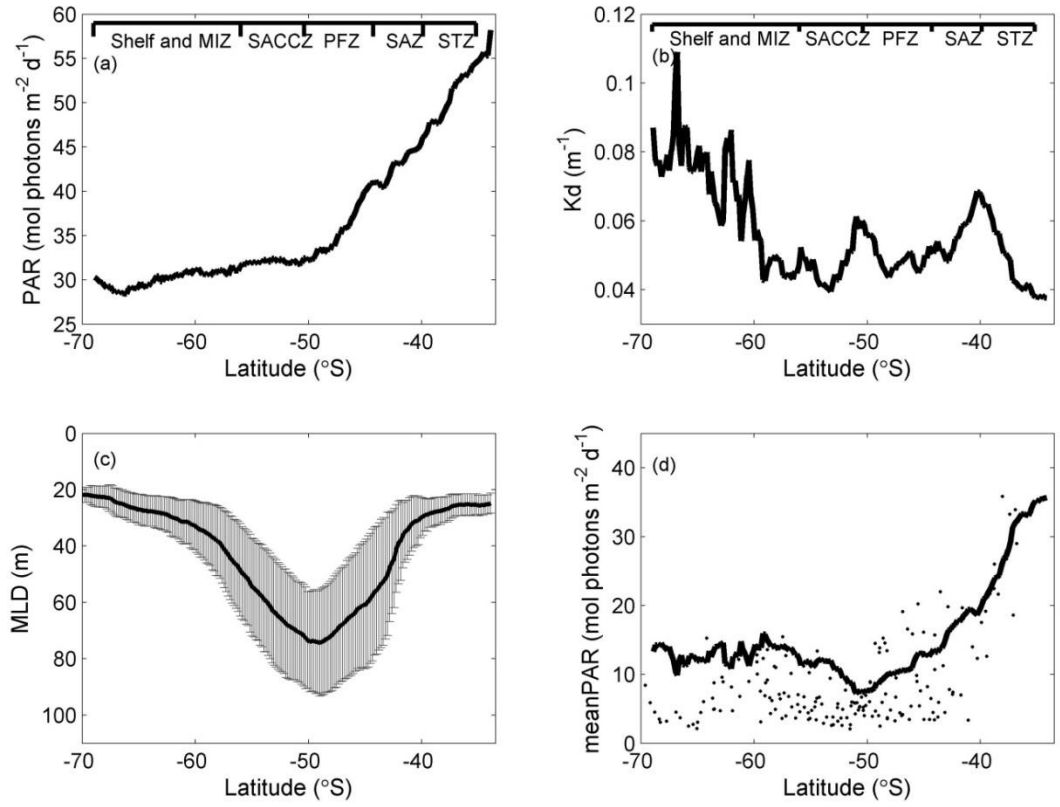

Figure 5.3. a) MODIS summer (DJF) climatology of surface PAR; (b) diffuse attenuation coefficient (K_d); c) Climatological MLD (EN3 monthly dataset); and d) MODIS climatological $\bar{I}_{MLD}$ (line) and *in situ* $\bar{I}_{MLD}$ (dots) along the Goodhope Transect.

A significant positive relationship (r^2 = 0.3, p<0.001) is observed between NCP* and $\bar{I}_{MLD}$ (Fig. 5.4a) when using an exponential fit and negative NCP* data are removed. Negative NCP indicate net heterotrophic conditions and were excluded from the regression analysis but shown in Fig. 5.4b. Samples with low $\bar{I}_{MLD}$ (< 10 mol photons m^{-2} d^{-1}) are typically associated with latitudes greater than the PF (> 50°S), where low seasonal PAR drives the lowest NCP* (< 2 mmolO_2 mg $chla^{-1}$ d^{-1}). Similarly regions associated with $\bar{I}_{MLD}$ from deep MLDs (> 60 m) at (~ 50 - 55°S) show low NCP*. On the other hand, regions (latitudes < 50°S) with shallower mixed layers (< 45 m) and higher $\bar{I}_{MLD}$ (> 10 mol photons m^{-2} d^{-1}) were associated with high NCP* (up to 14 mmol O_2 mg $chla^{-1}$ d^{-1}).

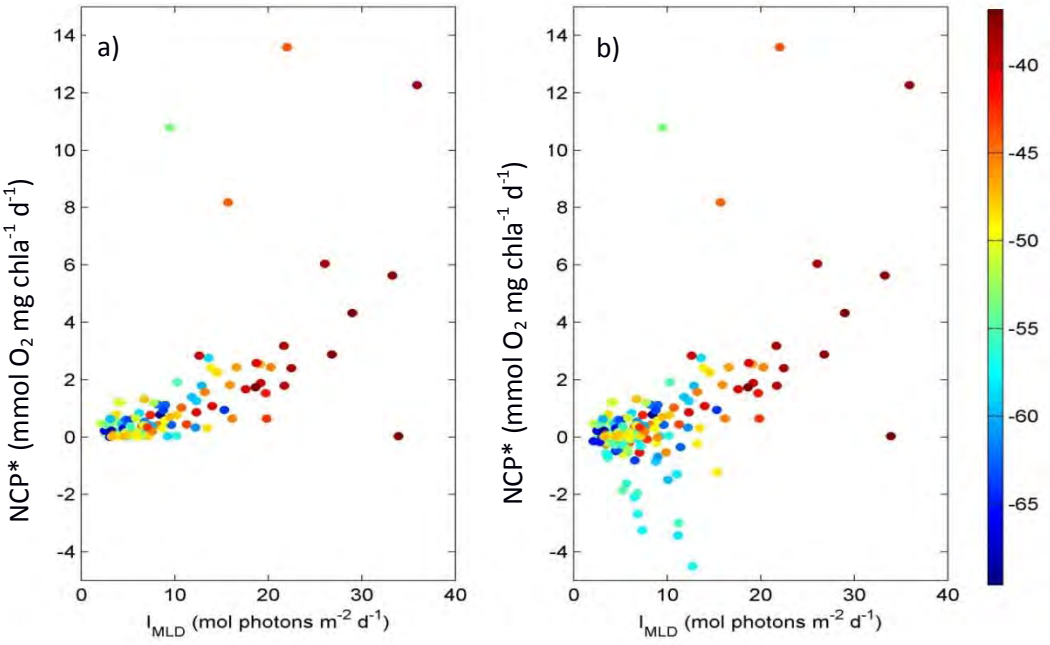

Figure 5.4. Scatterplot of NCP* vs $\bar{I}_{MLD}$ (all data included on the right side panel, while negative data are excluded on left side panel to determine r^2). Latitude (°S) is indicated by the colorbar. It shows a marked increase in NCP* with increased $\bar{I}_{MLD}$. In particular, lower latitude regions typically have higher $\bar{I}_{MLD}$ (> 10 mol photons m^{-2} d^{-1}) and higher NCP* exceeding 2 mmol O_2 mg Chl-a d^{-1}.

5.4 Discussion

To investigate the sensitivity of NCP to light availability within the mixed layer, NCP is normalised to chl and MLD and then plotted against $\bar{I}_{MLD}$ (Fig 5.4). Normalisation removes the sensitivity of NCP to these parameters such that any relationships between normalised NCP* and $\bar{I}_{MLD}$ will be driven by mean light availability in the MLD rather than chl-a or the MLD per se. This interpretation of the NCP* vs $\bar{I}_{MLD}$ relationship however excludes other factors that are known to influence parameters of *PvsE* curves such as light history, physiology, species composition, temperature, CO_2 concentration, season, region, vertical mixing and ultraviolet radiation (*Yoder and Bishop*, 1985; *Dower and Lucas,* 1993; *Macedo et al*., 2001; *Villafane et al*., 2003)

Plotting NCP* versus $\bar{I}_{MLD}$ provides a similar tool for assessing light dependent responses of photosynthesis as *PvsE* curves. Here it reveals a significantly positive relationship (r^2 = 0.3; p<0.001; Fig. 5.4a). It might be surprising that $\bar{I}_{MLD}$ alone can explain as much as 30% of the variability in NCP* given the attention that is usually placed on Fe-mediated regulation of productivity in the Southern Ocean (*Aumont and Bopp,* 2006; *Boyd,* 2002; *Boyd et al.*, 2007). The reason for this is most likely that the role of iron is implicit in our approach since an increase in iron in the Southern Ocean, where iron is generally limiting, would be expected to result in higher primary production. Since NPP can account for nearly 40% of the variance in mixed layer NCP in the Southern Ocean (*Reuer et al.*, 2007), one would therefore expect that increased concentrations of Fe would result in both increased NPP and NCP*.

What is also noteworthy is that low NCP* (< 2 mmol O_2 mg chl^{-1} d^{-1}) always coincides with low $\bar{I}_{MLD}$ (< 10 mol photons m^{-2} d^{-1}) found in regions of deep MLD's (> 60 m) where phytoplankton are mixed in a low light environment as well as at high latitudes (> 55^{o}S) where low seasonal PAR diminishes $\bar{I}_{MLD}$. This emphasises the important role

of water column irradiance in driving elevated productivity previously discussed (Chapter 4). In other words, in low light conditions, productivity will be curtailed even if nutrient replete conditions prevail. When light is sufficient to stimulate productivity (shallow MLD's) however, low NCP* indicate potentially Fe limiting conditions.

Since NCP* continues to rise with increasing $\bar{I}_{MLD}$ in Fig. 5.4 (and never reaches light saturating conditions) one can infer that NCP* remains in the light dependent portion of the *PvsE* curve, where light harvesting capacity is optimised through photosynthetic efficiency (*Falkowski and LaRoche*, 1991; *MacIntyre et al.,* 2002), described by the initial slope (α). This inference is supported by *Hiscock et al.*, (2008)'s results during the SOFeX programme, which report a maximum saturation irradiance (I_k) of ~ 8.6 mol photons m^{-2} d^{-1} in the Pacific Sector of the Southern Ocean. In the present study, along the entire transect roughly 63% of $\bar{I}_{MLD}$ observations reported here falls below this saturated irradiance level of ~ 8.6 mol photons m^{-2} d^{-1} (Fig 5.3.d). *Hiscock et al.* (2008) found that the initial slope (α) of the *PvsE* curve is highly dependent on iron availability through regulating the light harvesting proteins and reduced electron transport efficiency which leads to a reduction in chl-a concentration within phytoplankton cells. Their incubation experiments in the Pacific Southern Ocean showed that Fe addition in light limiting conditions could effectively double the initial slope of the *PvsE* curve. It is proposed here that when light is sufficient to stimulate productivity (high $\bar{I}_{MLD}$) low NCP* indicate potentially Fe limiting conditions. As such, the variability observed in the positive relationship between NCP* and $\bar{I}_{MLD}$ (Fig 5.4) particularly at high irradiances ($\bar{I}_{MLD}$ > 10 mol photons m^{-2} d^{-1}) is thought to be driven by the availability of iron affecting photosynthetic efficiency of the community under light dependent conditions.

High $\bar{I}_{MLD}$ were confined to regions equatorward of the 50°S where MLD's are particularly shallow (< 30m). Although shallow MLD's promote a high light environment, the drawback is that shallow MLD's have a smaller Fe reservoir that can quickly be utilised by phytoplankton production to become limiting and thus driving low NCP*. NCP* in this region ranged between 0 – 12 mmol O_2 mg $chla^{-1}$ d^{-1}. Iron limitation here is thought to suppresses NCP* to the low end of the range, while higher NCP* indicates iron stress relief.

The previous chapter highlighted the role of variable mixed layers in alleviating both iron and light limitation at the appropriate timescales for stimulating productivity. This mechanism potentially contributes to the observed scatter in the NCP* vs $\bar{I}_{MLD}$ particularly in the mid to low latitudes. Between 45 – 55°S, NCP* had a narrow range (0 – 3 mmol O_2 mg $chla^{-1}$ d^{-1}), with $\bar{I}_{MLD}$ ranging from 0 – 20 mol photons m^{-2} d^{-1}. Here deep mixed layers (up to 100 m at the PF), drive low $\bar{I}_{MLD}$ and effectively low NCP*, while iron limitation drive low NCP* when high $\bar{I}_{MLD}$ conditions prevail.

5.5 Summary

Metabolic and biophysical processes that regulate photosynthesis are reflected in *PvsE* curve experiments (*Platt and Jassby,* 1991; *Falkowski and Raven,* 1997). This chapter highlights the importance of availability of changing irradiance within the surface mixed layer in stimulating NCP*. A compact exponential relationship between NCP and $\bar{I}_{MLD}$ was observed, with the dependence reflecting basic understanding about controls on photosynthesis. It showed an increase in NCP* with increasing $\bar{I}_{MLD}$ indicating the dependence of NCP on irradiance. However, at higher $\bar{I}_{MLD}$ both low and high NCP* were observed reflecting a mechanistic response of NCP* due to potential

iron limitation. Similarly, NCP* vs $\bar{I}_{\mathrm{MLD}}$ was shown to remain in the light dependent portion of the *PvsE* curve, such that the slope was likely being controlled by the availability of iron, modulating the community carbon uptake efficiency. This highlights the ecological importance of light depended photosynthesis, which is not considered in VGPM models (*Behrenfeld and Falkowski*, 1997) where the latter mainly utilise light saturated photosynthetic parameters (P^b_{max} or P^b_{opt}) to calculate productivity in the euphotic zone.

Chapter 6

Synthesis and Implications

This study has examined three aspects of the scale sensitivity and dynamics of the Southern Ocean paradox: the High-Nutrient Low-Chlorophyll (HNLC) character of its primary production (*Chisholm and Morel,* 1991). 1) New production in relation to nutrient supply, 2) Variability of NCP in relation to vertical iron supply at intraseasonal timesales and 3) the influence of light availability on NCP rates in the mixed layer.

The principal drivers of the HNLC characteristics of the Southern Ocean are known to be light and nutrient limitation (*Boyd*, 2002; *Mitchell et al*., 1991), which have varying bottom-up roles over the growing season (*Boyd,* 2002; *Swart et al.*, 2014), as well as the top-down contribution from zooplankton grazing (*Behrenfeld,* 2010). The mean spatial distribution of surface chl-a blooms in the Southern Ocean in summer is thought to be consistent with a Fe limited regime, and this argument has been well documented (*De Baar et al*., 1995; *Boyd et al.*, 2000; *Blain et al*., 2007; *Pollard et al.*, 2009). However, what is less well understood are the physical control mechanisms responsible for supplying surface waters with Fe and modulating light that are ultimately responsible for controlling variability in the phytoplankton seasonal cycle and its spatial distribution. It has been recently adcanced that the iron stock required to sustain chl-a biomass during summer, is predominantly resupplied through winter convective mixing (*Tagliabue et al.,* 2014). However, recent work has implicated an additional role for sub-seasonal atmospheric forcing modes in modulating the Fe and light supply in summer and thus contributing to the seasonal characteristics of primary production in

the SAZ south of Africa (*Thomalla et al.*, 2011; *Fauchereau et al*., 2011; *Swart et al.,* 2012; 2014). In this context, a better understanding of the spatial and temporal characteristics of the surface mixed layer are crucial as they modulate the light and nutrient conditions that drive productivity.

The research undertaken commenced with an investigation of the meridional characteristics of primary productivity in the Atlantic Southern Ocean during summer. A north-south gradient in elevated surface macronutrient concentrations (Fig. 1.3) is known to exist in the Southern Ocean, which is inconsistent with the observed chl-a biomass since maximum chl-a concentrations are found at mid-latitudes (Fig. 1.1). The study set out to initially characterize the variability of nitrogen-based new production along a meridional transect in the Atlantic Southern Ocean in the context of the drivers (iron and light limitation) of the HNLC characteristics of the region. Therefore it was hypothesised that regions of elevated summer biomass would result from relief of iron and light limitation which would be expected to be linked to elevated *f*-ratios since these limiting factors are thought to control primary productivity in the Southern Ocean. To address this hypothesis, new and export productivity rates were measured using isotopically labelled nitrogen uptake experiments conducted in late summer 2008. It showed meridionally distinct regions of new and regenerated uptake, with low *f*-ratios (f = 0.2) in the STZ dominated by picophytoplankton (< 0.2 μm). High ambient regenerated nutrient concentrations (NH_4 and urea) in surface waters were indicative of active regeneration processes throughout the transect and ascribed to the late summer season (February/March 2008) sampling. New production rates were shown to be elevated in the SAZ relative to adjacent regions, where highest *f*-ratios (f = 0.49) ascribed to increased input of iron associated with an anticyclonic eddy observed in this region. It was considered surprising that such high *f*-ratios (potentially contributing up

to 50% of productivity) were observed in the SAZ region, particularly in the context of it being conducted during the in late summer (February - March), when a seasonal supply of iron was expected to be depleted. High *f*-ratios measured in the SAZ were thought to be indicative of a potential source of an intraseasonal replenishment of iron supporting new production in this region in late summer when seasonal surface iron are considered to be depleted. Furthermore, it also highlighted the previously underestimated role of mesoscale eddy activity as a potential supply mechanism of new iron into the euphotic zone. This meridional *f*-ratio gradient study highlighted the gap in the understanding of the role of fine space and temporal scale dynamics as drivers as of variability in iron and light availability and responses of primary productivity as well as its potentially important climate sensitivities in the SAZ.

The important role of sub-seasonal temporal scales, and meso- to submeso- spatial scales on characterising the seasonal cycle of upper ocean physics and biogeochemistry was highlighted in a number of recent studies in the Southern Ocean (*Thomalla et al*., 2011; *Fauchereau et al*., 2011; *Swart et al*., 2014). These scale sensitivities of primary productivity in the SAZ south of Africa were investigated using high resolution *in situ* estimates of NCP and MLD. It set out to test the hypothesis that sub-seasonal dynamics in the summer MLD are central to explaining the persistence of phytoplankton biomass throughout the summer. A quasi-non-linear relationship was observed between NCP and MLD consistent with elevated and more variable NCP when MLD are shallow (MLD < 45 m) and reduced NCP when MLDs are deeper (MLD > 45 m). This elevated and variable NCP in shallow MLDs (MLD < 45 m) was confined mainly to the SAZ, as well as the edges of its adjacent regions. The STZ to the north showed lower productivity relative to the SAZ, associated with shallow and more stable MLD (mean MLD ~ 25 m ± 4.2 m) which maintained oligotrophic surface conditions. On the other

hand, the low NCP to the south in the PFZ were considered to be maintained by unfavourable light conditions through highly variable but deep MLD (~ 70 m ± 20.4 m). It is proposed that the elevated and highly variable NCP observed during summer in the SAZ results from intraseasonal scale storm events. These drive an alternating dynamic between deepening of the mixed layer, that entrains Fe from below the euphotic zone, followed by rapid shoaling that favours phytoplankton growth as well as detrainment of phytoplankton biomass and associated Fe. This hypothesis rests on the presence of both intraseasonal storm events deepening the mixed layer, which entrain dFe from below the euphotic zone, and subsequent stabilisation shallower than the light depth required to alleviate light limitation that stimulates phytoplankton growth (depicted in Fig. 4.5). Rates of synoptic inputs of dissolved iron to the euphotic zone estimated from mixed layer entrainment events and subsurface dFe concentrations (Fig. 4.4) were comparable with the iron demand for the NCP observations. This dynamic helps explain the seasonal persistence primary production and biomass observed during late summer in the SAZ (*Thomalla et al.,* 2011; *Swart et al.*, 2014), in addition to the larger dFe supply during winter through convective overturning (*Tagliabue et. al*., 2014).

These results highligth the concurrent influence of iron and light alleviation on phytoplankton growth parameters previously reported (*Behrenfeld et al.,* 2004; *Boyd et al*., 2001; *Fauchereau et al.,* 2011 *Sunda and Huntsman,* 1997; *Van Leeuwe and Steffels*, 1998). Co-limitation is not surprising considering that the influence of iron and light on phytoplankton photosynthesis is inextricably linked, as growth irradiance also controls cellular iron demand (*Sunda and Huntsman*, 1997). The crux of the iron-light co-limitation discussion is that under light-limiting conditions (irradiances below the light saturation level), light-dependent modulation of cellular chl-a content optimises phytoplankton growth under varying light conditions (*McIntyre et al.*, 2002; *Behrenfeld*

et al., 2008; *Hasley et al.*, 2010). Iron alleviation has been shown to effectively double photosynthetic rates under light limiting conditions reflected through an increase in the initial slope (α) of the *PvsE* curve (*Hiscock et al.,* 2008). In chapter 5, this idea is extended and examined through *in situ* observations of NCP and mean water column irradiance. When comparing chl-a normalized NCP (NCP*) with the average irradiance in the mixed layer ($\bar{I}_{MLD}$), a statistically significant positive relationship (r^2 = 0.3, p<0.001) is observed. The slope of the NCP* vs $\bar{I}_{MLD}$ relationship is analogous to the initial slope (α) of the photosynthesis-irradiance (*PvsE*) curve (*Platt and Jassby*, 1976). Results from this study show that $\bar{I}_{MLD}$ alone can explain 30% of the variance in NCP* which is somewhat unexpected given the attention that is usually placed on Fe-mediated regulation of productivity in the Southern Ocean (*Boyd* 2002; *Boyd et al.*, 2007; *Tagliabue et al*., 2014). The results presented here show that NCP* lies in the 'light-dependent' part of the NCP*-$\bar{I}_{MLD}$ curve (i.e. NCP never plateaus to light saturating conditions). Since this part of the curve which defines the initial slope (α) is highly dependent on iron availability (*Hiscock et al.* 2008), one might argue that the role of iron is embedded in the NCP*-$\bar{I}_{MLD}$ relationship. It is then proposed that natural Fe availability drives the observed scatter about the relationship adjusting the slope of the NCP*- $\bar{I}_{MLD}$ curve (Fig. 5.5). This result supports the understanding of the role of iron in affecting light dependent productivity, in showing that NCP* responds to mean water column irradiance, while variable iron concentrations explains the variability observed in this relationship.

The work presented here showed high new production rates in the SAZ in late summer, thought to be driven by inputs of new iron at short timescales. It highlights the important role of sub-seasonal modes of ocean dynamics in modulating the seasonal characterics of primary productivity responses particularly in the Atlantic SAZ.

Ultimately the response of primary productivity to mesoscale dynamics will depend on the changing characterisics of the drivers, particularly iron and light (or both). The extent of deep vertical mixing at short timecales is proposed to influence both the supply of iron into the euphotic zone as well as the light availability through water column stability. This work also revisits the importance of light dependend photosynthesis and showed a mechanistic response of chl-specific NCP under variable light and iron conditions. Physiological drivers such as the slope of the *PvsE* curve are not considered as model inputs in ocean productivity models such as those of *Behrenfeld and Falkowski*, (1997), which rather utilise light-saturated photosynthesis rates to calculate primary productivity. These findings highlight the relevance of including photosynthesis-irradiance parameters when implementing primary production models (*Platt et al.,*1995) and advocate for the development of approaches to estimate these parameters at regional and global scales (*Platt et al.,* 2008; *Huot et al.,* 2013; *Saux Picart et al.,* 2014).

In the coming decades, the Southern Ocean is considered to be particularly vulnerable to uncertain changes in mixed layer characteristics due to differential modifications to warming, freshwater input and eddy activity (*Steinacher et al*., 2010; *Boyd et al*., 2008; *Taucher and Oschlies*, 2011), alongside potential poleward latitudinal migrations and intensification of westerly wind stress (*Russell et al*., 2006; *Visbeck and Hall*, 2004). Understanding the role of these modulators of MLD dynamics is key to projecting the trajectory of Southern Ocean productivity as well as gaining understanding of the climate sensitivity and future trends in large scale carbon cycling. For instance, models predict increased stratification due to increased SST, which could cause a decline in vertical mixing resulting in reduced nutrient (dissolved iron) input required to support primary production (*Bopp et al*., 2001; 2013; *Boyd et al*., 2008). Increased stratification

would alleviate light limitation, and reduce cellular iron requirement (*Sunda and Huntsman*, 1997), however, this may offset by reduced vertical supply of iron (*Bowie et al.*, 2009), as well as potential photoinhibition in shallower MLD (*Alderkamp et al.*, 2010). Furthermore, the role of sub-mesoscale ocean dynamics in affecting the spatial and temporal variability in biogeochemical properties was demonstrated to show a roughly 10 – 20 % decline in global phytoplankton abundance as the resolution is refined (*Levy et al.*, 2012).

Going forward, process studies that measure the biogeochemical dynamics (iron supply) and underlying physics, such as mixed layer variability that drive primary productivity will further improve how these mechanisms are understood in an integrated way. High resolution measurements of primary productivity, along with water column optical properties and biogeochemical parameters such as dissolved iron concentrations all measured at the same temporal and spatial scales (meso and submesoscales) will greatly improve our understanding of the link between these important drivers of the ocean carbon cycle. In particular, the seasonal cycle in physical mechanisms (MLD variability, nutrient supply) and biogeochemical responses (primary productivity) provides a great opportunity to further investigate the impact of fine scale variability (meso and sub-mesoscale) on the seasonal carbon cycle dynamics such as such the proposed Southen Ocean Seasonal Cycle Experiment III (*Swart et al*., 2014).

Bibliography

Arhan, M., Speich, S., Messager, C., Dencausse, G., Fine, R., & Boye, M. (2011). Anticyclonic and cyclonic eddies of subtropical origin in the subantarctic zone south of Africa. *Journal of Geophysical Research*, 116(C11), C11004. doi:10.1029/2011JC007140.

Arrigo, K. R., van Dijken, G. L., & Bushinsky, S. (2008). Primary production in the Southern Ocean, 1997–2006. *Journal of Geophysical Research*, *113*(C8), C08004. doi:10.1029/2007JC004551.

Arrigo, K. R. and G. L. van Dijken. Annual changes in sea ice, chlorophyll a, and primary production in the Ross Sea, Antarctica. *Deep-Sea Reserch* II. 51: 117-138, doi:10.1016/j.dsr2.2003.04.003.

Arrigo, K. R. (2005). Molecular diversity and ecology of microbial plankton. *Nature*, *437*(7057), 343–8. doi:10.1038/nature04158.

Arrigo, K.R., 2005. Marine microorganisms and global nutrient cycles. *Nature*, 437, doi:10.1038/nature04158

Arrigo, K. R., van Dijken, G. L., & Bushinsky, S. (2008). Primary production in the Southern Ocean, 1997–2006. *Journal of Geophysical Research*, 113(C8), C08004. doi:10.1029/2007JC004551.

Aumont, O., & Bopp, L. (2006). Globalizing results from ocean in situ iron fertilization studies. *Global Biogeochemical Cycles*, *20*(2), doi:10.1029/2005GB002591.

Banse, K. (1996). Low seasonality of low concentrations of surface chlorophyll in the Subantarctic water ring: underwater irradiance, iron, or grazing? *Progress in Oceanography*, *37*(3-4), 241–291. doi:10.1016/S0079-6611(96)00006-7.

Banse, K., 1996. Low seasonality of low concentrations of surface chlorophyll in the Subantarctic water ring: underwater irradiance, iron and grazing. *Progress in Oceanography*, 37, 241 – 291.

Bathmann, U. V., Scharek, R., Klaas, C., Dubischar, C. D., & Smetacek, V., (1997), Spring development of phytoplankton biomass and composition in major water masses of the Atlantic sector of the Southern Ocean. *Deep Sea Research Part II*, 44(1-2), 51–67. doi:10.1016/S0967-0645(96)00063-X.

Bathmann, U.V., Scharek, R., Klaas, C., Dubischar, C.D., Smetacek, V., 1997. Spring development of phytoplankton biomass and composition in major water masses of the Atlantic sector of the Southern Ocean. *Deep-Sea Research II* 44 (1-2), 51 – 67.

Behrenfeld, M. J., & Milligan, A. J. (2013). Photophysiological expressions of iron stress in phytoplankton. *Annual Review of Marine Science*, *5*(4.1), 217–46. doi:10.1146/annurev-marine-121211-172356.

Behrenfeld, M. J. (2010). Abandoning Sverdrup's Critical Depth Hypothesis on phytoplankton blooms. *Ecology*, *91*(4), 977–989.

Behrenfeld, M. J., & Falkowski, P. G., (1997), Photosynthetic rates derived from satellite-based chlorophyll concentration. *Limnology and Oceanography*, 42(January), 1 – 20.

Behrenfeld, M. J., Doney, S. C., Lima, I., Boss, E. S., & Siegel, D. a. (2013). Annual cycles of ecological disturbance and recovery underlying the subarctic Atlantic spring plankton bloom. *Global Biogeochemical Cycles*, 27(2), 526–540. doi:10.1002/gbc.20050.

Behrenfeld, M.J., Halsey, K.H., Milligan, A.J., (2008), Evolved physiological responses of phytoplankton to their integrated growth environment. *Philos Trans R Soc Lond B Biol Sci* 363(1504): 2687-2703.

Beker B., Boye, M., Ras, J., Gelay, A., Claustre, H., 2011. Distribution patterns of taxonomy and pigments during the austral summer in the southeastern Atlantic and the Southern Ocean south of South Africa. *Personal Communication*.

Belkin, I. M., & Gordon, A. L., (1996), Southern Ocean Fronts from the Greenwich Meridian to Tasmania. *Journal of Geophysical Research*, 101(C2), 3675 – 3696.

Bender, M., Grande, K., Johnson, K., Marra, J., Williams, P. J. L., Sieburth, J., Pilson, M., Langdon, C., Hitchcock, G., Orchardo, J., Hunt, C., Donaghay, P., Heinemann, K. (1987). A comparison of four methods for determining planktonic community production. *Limnology and Oceanography*, *32*(5), 1085–1098.

Bender, M.L., Ho, D.T., Hendricks, M.B., Mika, R., Bazttle, M.O., Tans, P.P., Conway, T.J., Sturtevant, B., Cassar, N., (2005), Atmospheric O2/N2 changes, 1993 – 2002: Implications for the partitioning of fossil fuel CO2 sequestration, *Global Biogeochemical Cycles*, 19, GB4017.

Berelson, W. M., Anderson, R. F., Dymond, J., Demaster, D., Hammond, D. E., Collier, R., Honjo, S., Leinen, M., McManus, J., Pope, R.., Smith, C., Stephens, M. (1998). Biogenic budgets of particle rain , benthic remineralization and sediment accumulation in the

equatorial Pacific. *Deep Sea Research Part I: Oceanographic Research Papers*, *44*(9), 2251–2282.

Bianchi, M., Feliatra, F., Tréguer, P., Vincendeau, M.-A., & Morvan, J. (1997). Nitrification rates, ammonium and nitrate distribution in upper layers of the water column and in sediments of the Indian sector of the Southern Ocean. *Deep Sea Research Part II: Topical Studies in Oceanography*, *44*(5), 1017–1032. doi:10.1016/S0967-0645(96)00109-9.

Blain, H., Treguer, P., Belviso, S., Bucciarelli, E., Denis, M., Desabre, H., Fiala, M., Martin Jezequel, V., Le Fevre, J., Mayzaud, P., Marty, J-C., Razouls, S. (2001). A biogeochemical study of the island mass effect in the context of the iron hypothesis : Kerguelen Islands , Southern Ocean. *Deep Sea Research Part I: Oceanographic Research Papers*, *48*, 163–187.

Bowie, A. R., Lannuzel, D., Remenyi, T. a., Wagener, T., Lam, P. J., Boyd, P. W., … Trull, T. W. (2009). Biogeochemical iron budgets of the Southern Ocean south of Australia: Decoupling of iron and nutrient cycles in the subantarctic zone by the summertime supply. *Global Biogeochemical Cycles*, 23(4), doi:10.1029/2009GB003500

Boyd, P. W. (2002). Review of environmental factors controlling phytoplankton processes in the Southern Ocean 1. *Journal of Phycology*, *38*(October 2001), 844–861.

Boyd, P.W., Crossley, A.C., DiTullio, G.R., Griffiths, F.B., Hutchins, D.A., Queguiner, B., Sedwick, P.N., Trull, T.N., 2001. Control of phytoplankton growth by iron supply and irradiance in the Subantarctic Ocean: Experimental results from the SAZ Project. *Journal of Geophysical Research* 106, C12, 31573 – 31583.

Boyd, P.W., Jickells, T., Law, C.S., Blain, S., Boyle, E.A., Buesseler, K.O., Coale, K.H., Cullen, J.J., de Baar., H.J.W., Follows, M., Harvey, M., Lancelot, C., Levasseur, M., Owens, N.P.J., Pollard, R., Rivkin, R.B., Sarmiento, J., Schoemann, V., Smetacek, V., Takeda, S., Tsuda, A., Tumer, S., Watson, A.J., 2007. Mesoscale iron enrichment experiments 1993 – 2005: Synthesis and future directions. *Science* 315, 612 – 617, [doi:10.1126/science.1131669].

Boyd, P. W., Law, C. S., Hutchins, D.A., Abraham, E. R., Croot, P. L., Ellwood, M., et. al. (2005). FeCycle: Attempting an iron biogeochemical budget from a mesoscale SF 6 tracer experiment in unperturbed low iron waters. *Global Biogeochemical Cycles*, 19(4). doi:10.1029/2005GB002494.

Boyd, P. W., & Ellwood, M. J. (2010). The biogeochemical cycle of iron in the ocean. *Nature Geoscience*, 3(10), 675–682. doi:10.1038/ngeo964.

Boyd, P.W., Arrigo, K.R., Strzepek, R., Van Dijken, G.L., 2012, Mapping phytoplankton utilization: Insights into Southern Ocean supply mechanisms, *Geophysical Research Letters*, 117, C06009, doi:10.1029/2011JC007726.

Boye, M., Nishioka, J., Croot, P., Laan, P., Timmermans, K. R., Strass, V. H., Takeda, S., and de Baar, H. J. W., (2010) Significant portion of dissolved organic Fe complexes in fact is colloids, *Marine Chemistry*., 122, 20–27.

Boye, M., van den Berg, C.M.G., de Jong, J.T.M., Leach, H., Croot, P., de Baar, H.J.W., 2001. Organic complexation of iron in the Southern Ocean. *Deep-Sea Research I* 48, 1477–1497.

Braun, A. V. 2008. A Comparison of Subtropical Storms in the South Atlantic Basin with Australian East-Coast Cyclones. American Meteorological Society, Conf. *Proc*., 2B.5.

Bronk, D. A., Gilbert, P. M., & Ward, B. B. (1994). Nitrogen uptake, dissolved nitrogen release, and new production. *Science*, *265*(5180), 1843–1846.

Brzezinski, M.A.,(1985), The Si:C:N ratio of marine diatoms: interspecific variability and the effect of some environmental variables. *Journal of Phycology*, 21 (3), 347-357.

Brzezinski, M. a, Dickson, M.-L., Nelson, D. M., & Sambrotto, R. (2003). Ratios of Si, C and N uptake by microplankton in the Southern Ocean. *Deep Sea Research Part II: Topical Studies in Oceanography*, *50*(3-4), 619–633. doi:10.1016/S0967-0645(02)00587-8.

Buesseler, K. O., Ball, L., Andrews, J., Cochran, J. K., Hirschberg, D. J., Bacon, M. P., … Brzezinski, M. (2001). Upper ocean export of particulate organic carbon and biogenic silica in the Southern Ocean along 170°W. *Deep Sea Research Part II: Topical Studies in Oceanography*, *48*(19-20), 4275–4297. doi:10.1016/S0967-0645(01)00089-3

Buesseler, K.O., Cochran, J.K., Bacon, M.P., Livingston, H.D., Casso, S.A., Hirschberg, D., Hartman, M.C., Fleer, A.P., (1992), Determination of thorium isotopes in seawater by non-desctructive and radiochemical procedures, *Deep Sea Research*, 39 (7/8), 1103 – 1104.

Buesseler, K.O., Bacon, M.P., Cochran, J.K., Livingston, H.D., 1992a. Carbon and nitrogen export during the JGOFS North Atlantic Bloom Experiment estimated from 234Th:238U disequilibria. *Deep-Sea Research* I 39, 1115-1137.

Buesseler, K.O., Benitez-Nelson, C.R., Moran, S.B., Burd, A., Charette, M., Cochran, J.K., Coppola, L., Fisher, N.S., Fowler, S.W., Gardner, W.D., Guo, L.D., Gustafsson, O., Lamborg, C., Masque, P., Miquel, J.C., Passow, U., Santschi, P.H., Savoye, N., Stewart, G., Trull, T., 2006. An assessment of particulateorganic carbon to thorium-234 ratios in

the ocean and their impact on the application of 234Th as a POC flux proxy. Marine Chemistry 100 (3-4), 213 - 233.

Caldeira, K., Duffy, P.B., 2000. The role of the Southern Ocean in uptake and storage of anthropogenic carbon dioxide. *Science*, 297, 620 – 622.

Carr, M.-E., Friedrichs, M. a. M., Schmeltz, M., Noguchi Aita, M., Antoine, D., Arrigo, K. R., Asanuma, I., Aumont, O., Barber, R., Behrenfeld, M., Bidagare, R., Buitenhuis, E.T., Campbell, J., Ciotti, A., Dierssen, H., Dowel, Dunne, J., Esaias, W., Gentili, B., Gregg, W., Groom, S., Hoepffner, N., Ishizaka, J., Kameda, T., LeQuere, C., Lohrenz, S., Marra, J., Melen, F., Moore, K., Morel, A., Reddy, T., Ryan, J., Scardi, M., Smyth, T., Turpie, K., Tilstone, G., Waters, K., & Yamanaka, Y. (2006). A comparison of global estimates of marine primary production from ocean color. *Deep Sea Research Part II: Topical Studies in Oceanography*, *53*(5-7), 741–770. doi:10.1016/j.dsr2.2006.01.028

Cassar, N., Barnett, B.A., Bender, M. L., Kaiser, J., Hamme, R. C., & Tilbrook, B. (2009). Continuous high-frequency dissolved O_2/Ar measurements by equilibrator inlet mass spectrometry. *Analytical Chemistry*, *81*(5), 1855–64. doi:10.1021/ac802300u.

Cassar, N., DiFiore, P. J., Barnett, B. A., Bender, M. L., Bowie, a. R., Tilbrook, B., Petrou, K., Westwood, K.J., Wright, S.W., Lefevre, D. (2011). The influence of iron and light on net community production in the Subantarctic and Polar Frontal Zones. *Biogeosciences*, *8*(2), 227–237. doi:10.5194/bg-8-227-2011.

Chan, A.T., 1980, Comparative physiological study of marine diatoms and dinoflagellates in relation to irradiance and cell size II. Relationship between photosynthesis, growth and carbon/chl-a ratio. *Journal of Phycology*, 16, 428 – 432, DOI: 10.1111/j.1529-8817.1980.tb03056.x.

Chever, F., Bucciarelli, E., Sarthou, G., Speich, S., Arhan, M., Penven, P., & Tagliabue, a. (2010). Physical speciation of iron in the Atlantic sector of the Southern Ocean along a transect from the subtropical domain to the Weddell Sea Gyre. *Journal of Geophysical Research*, 115(C10), C10059. doi:10.1029/2009JC005880.

Chisholm, S.W., & Morel, F.M.M., (1991). What controls phytoplankton production in nutrient-rich areas of the open sea? American Society of Limnology and Oceanography Symposium, 22-24 February 1991, San-Marcos, California – Preface *Limnology and Oceanography* 36(8):U1507-U1511, Dec. 1991.

Chisholm, S.W. and F.M.M., Morel, (1991), What controls phytoplankton production in nutrient-rich areas of the open sea? *Limnology and Oceanography*, 36(8):U1507-U1511.

Chiswell, S. M. (2011). Annual cycles and spring blooms in phytoplankton: don't abandon Sverdrup completely. *Marine Ecology Progress Series*, *443*, 39–50. doi:10.3354/meps09453.

Clark, D. R., Rees, A. P., & Joint, I. (2008). Ammonium regeneration and nitrification rates in the oligotrophic Atlantic Ocean: Implications for new production estimates. *Limnology and Oceanography*, *53*(1), 52–62. doi:10.4319/lo.2008.53.1.0052.

Coale, K.H., Bruland, K.W., 1985. 234Th:238Ur disequilibria within the California Current. *Limnology and Oceanography*, 30, 22 – 33.

Cochlan, W.P, 2008. Nitrogen uptake in the Southern Ocean. In: Nitrogen in the Marine Environment. Capone, D. G., Bronk, D. A., Mulholland, M. and Carpenter, E. (eds). Elsevier Press. 561 – 588.

COESA, (1976), U.S. Standard Atmopshere, 1976, Government Printing Office, Washington D.C., p241.

Comiso, J.C., McClain, C.R., Sullivan C.W., Ryan, J.P., Leonard, C.L., 1993. Coastal Zone Color Scanner pigment concentration in the Southern Ocean and relationship to geophysical surface features. *Journal of Geophysical Research*, 98, 2419 – 2451.

Côté, B., & Platt, T., (1984), Utility of the light-saturation curve as an operational model for quantifying the effects of environmental conditions on phytoplankton photosynthesis, *Marine Ecology Press Series*, 18, 57 – 66.

Craig, H. and T. Hayward, (1987), Oxygen supersaturation in the ocean – biological versus physical contributions, *Science*, 235, 199–202.

Croot, P. L., Andersson, K., Öztürk, M., & Turner, D. R. (2004). The distribution and speciation of iron along 6°E in the Southern Ocean. *Deep Sea Research Part II: Topical Studies in Oceanography*, *51*(22-24), 2857–2879. doi:10.1016/j.dsr2.2003.10.012.

Cullen, J.J., (1990), On models of growth and photosynthesis in phytoplankton, *Deep-sea Research*, 37 (4), 667 – 683.

Cullen, J.J., 1990. On models of growth and photosynthesis in phytoplankton. *Deep-Sea Research*, 37 (4), 667 – 683.

Davidson, I.R., (1991), Environmenal effects on algal photosynthesis, *Journal of Phycology*, 27, 1, 2 – 8, doi: 10.1111/j.0022-3646.1991.00002.x.

De Boyer Montégut, C., Madec, G., Fischer, A. S., Lazar, A., Iudicone, D., (2004), Mixed layer depth over the global ocean: An examination of profile data and a profile-based

climatology. *Journal of Geophysical Research*, 109 (C12), C12003. doi:10.1029/2004JC002378.

De Baar, H.J.W., Boyd, P.W., Coale, K.H., Landry, M.R., Atsuhsi, T., Assmy, P., Bakker, D.C.E., Bozec, Y., Barber, R.T., Brzezinski, M.A., Buesseler, K.O., Boyé, M., Croot, P. L., Gervais, F., Gorbunov, M.Y., Harrison, P. J., Hiscock, W.T., Laan, P., Lancelot, C., Law, C., Levasseur, M., Marchetti, A., Millero, F. J., Nishioka, J., Nojiri, Y., Oijen, T. van, Riebesell, U., Rijkenberg, M.J.A., Saito, H., Takeda, S., Timmermans, K.R., Veldhuis, M. J.W., Waite, A., Wong, C.S., 2005. Synthesis of Iron Fertilization Experiments: From the Iron Age in the Age of Enlightenment. In: Orr, J. C., S. Pantoja, and H.-O. Pörtner (eds.) The Oceans in a High-CO2 World. Special Issue of *Journal of Geophysical Research C (Oceans)* 110: 1-24.

Deutsch, C., and Weber, T., (2012). Nutrient ratios as a tracer and driver of Ocean Biogeochemistry, Annual Review of Marine Science, 4,113 – 141.

Dugdale, R. C., & Goering, J. J. (1967). Uptake of New and Regenerated Forms of Nitrogen in Primary Productivity. *Limnology and Oceanography*, *12*(2), 196–206.

Dugdale, RC., Wilkerson, FP., (1986), The use of 15N to measure nitrogen uptake in eutrophic oceans; experimental considerations. *Limnology and Oceanography*, 31(4), 673 – 689.

Dugdale, RC., Wilkerson, FP., 1991. Low specific nitrate uptake rate – a common feature of high-nutrient, low-chlorophyll marine ecosystems. *Limnology and Oceanography* 36, 1678-1688.

Ebuchi, N., Graber, H. C., and Caruso, M. J.: Evaluation of wind vectors observed by QuikSCAT/SeaWinds using ocean buoy data, J. Atmos. Ocean. Tech., 19, 2049–2062, 2002.

Emerson, S., 1987. Seasonal oxygen cycles and biological new production in surface waters of the Sub-Arctic Pacific-Ocean. *Journal of Geophysical Research - Oceans* 92 (C6), 6535–6544.

Emerson, S., Quay, P., and Wheeler, P. A., (1993), Biological productivity determined from oxygen mass-balance and incubation experiments, *Deep-Sea Research* I, 40, 2351–2358.

Eppley, R. W., & Peterson, B. J. (1979). Particulate organic matter flux and planktonic new production in the deep ocean. *Nature*, *282*, 677 – 680.

Eppley, R.W., Stewart, E., Abbott, M. R., and Heyman, U., (1985), Estimating ocean primary production from satellite chlorophyll. Introduction to regional differences and statistics for

the Southern California Bight. *Journal of Planktonic Research,* 7(1), 57 – 70, doi: 10.1093/plankt/7.1.57.

Falkowski, P. G., Barber, R. T., & Smetacek, V. (1998). Biogeochemical Controls and Feedbacks on Ocean Primary Production. *Science*, *281*(5374), 200–206. doi:10.1126/science.281.5374.200.

Falkowski, P.G. and Raven, J.A., (1997) Aquatic photosynthesis. Blackwell Scientific Publishers, Oxford, 375 pp.

Falkowski, P. G., Laws, E.A., Barber, R.T. & Murray, J.W., 2003, Phytoplankton, and their role in primary, new and export production, in: *Ocean Biogeochemistry*, edited by: Fasham, M. J. R., Springer, New York, 109–111.

Fauchereau, N., Tagliabue, A., Bopp, L., & Monteiro, P. M. S. (2011). The response of phytoplankton biomass to transient mixing events in the Southern Ocean. *Geophysical Research Letters*, *38*(17), n/a–n/a. doi:10.1029/2011GL048498

Feely, R. A., Sabine, C. L., & Wanninkhof, R. (2001). Uptake and Storage of Carbon Dioxide in the Ocean : The Global CO_2 Survey. *Oceanography*, *14*(4), 18 – 32.

Feely, R.A., Wanninkhof, R., Milburn, H.B., Cosca, C.E., Stapp, M., Murphy, P., (1998), A new automated underway system for making high precision pCO2 measurements onboard research ships. *Analytica Chimica Acta* 377 (2–3), 185–191.

Fernández I., C., & Raimbault, P. (2007). Nitrogen regeneration in the NE Atlantic Ocean and its impact on seasonal new, regenerated and export production. *Marine Ecology Progress Series*, *337*, 79–92. doi:10.3354/meps337079.

Fiala, M., Kopczynska, E. E., Jeandel, C., Oriol, L., Arago, L., Universite, P., & Curie, M. (1998). Seasonal and interannual variability of size-fractionated phytoplankton biomass and community structure at station Kerfix , off the Kerguelen Islands , Antarctica. *Journal of Plankton Research*, *20*(7), 1341–1356.

Field, C., Behrenfeld, M., Randerson, J., & Falkowski, P. (1998). Primary production of the biosphere: integrating terrestrial and oceanic components. *Science, 281*(5374), 237–40.

Fouilland, E., Gosselin, M., Rivkin, R.B., Vasseur, C., Mostajir, B., 2007. Nitrogen uptake by heterotrophic bacteria and phytoplankton in Arctic surface waters. *Journal of Plankton Research*, 29 (4), 369 – 376.

Franck, V. M., Brzezinski, M. A., Coale, K. H., & Nelson, D. M. (2000). Iron and silicic acid concentrations regulate Si uptake north and south of the Polar Frontal Zone in the Pacifc

Sector of the Southern Ocean. *Deep Sea Research Part II: Topical Studies in Oceanography*, *47*, 3315–3338.

Frants, M., Gille, S. T., Hatta, M., Hiscock, W. T., Kahru, M., Measures, C. I., Mitchell, G.B., & Zhou, M. (2013). Analysis of horizontal and vertical processes contributing to natural iron supply in the mixed layer in southern Drake Passage. *Deep-Sea Research Part II*, 90, 68–76. doi:10.1016/j.dsr2.2012.06.001.

Froneman, P.W., Perissinotto, R., McQuaid, C.D., 1996. Seasonal variation in microzooplankton grazing in the region of the Subtropical Convergence. *Marine Biology*, 126, 433-442.

Frost, B., (1991), The Role of Grazing in Nutrient-Rich Areas of the Open Sea Areas of the Open Sea. *Limnology and Oceanography*, *36*(8), 1616–1630.

Gao, Y., Fan, S., Sarmiento, J.L., 2003. Aeolian iron input to the ocean through precipitation scavenging: A modeling perspective and its implication for natural iron fertilization in the ocean, *Journal of Geophysical Research*, 108, doi:200310.1029/2002JD002420.

Garcia, H. E., & Gordon, L. I. (1992). Oxygen solubility in seawater: Better fitting equations. *Limnology and Oceanography*, *37*(6), 1307 – 1312.

Garside, C. and Garside J.C., (1993), The 'f-ratio' on 20^{o}W during the North Atlantic Bloom Experiment. *Deep-Sea Research II,* 40: 75 – 79.

Geider, R.J., (1987), Light and temperature dependence of the carbon to chl ratio in microalgae and cyanobacteria: implications for physiology and growth in phytoplankton. *New Phytologist*, 106, 1 – 34.

Gladyshev, S., Arhan, M., Sokov, A., & Speich, S., (2008), A hydrographic section from South Africa to the southern limit of the Antarctic Circumpolar Current at the Greenwich meridian, *Deep-Sea Research I*, 55, 1284 – 1303, doi:10.1016/j.dsr.2008.05.009.

Glibert, P.M., Biggs, D.C., McCarthy, 1982. Utilization of ammonium and nitrate during austral summer in the Scotia Sea, *Deep-Sea Research*, 29 (7A), 837 – 850.

Glibert, P.M., Garside. C., 1992. Diel variability in nitrogenous nutrient uptake by phytoplankton in the Chesapeake Bay plume. *Journal of Planktonic Research*, 14, 271-288.

Goeyens, L., Semeneh, M., Baumann, M. E. M., Elskens, M., Shopova, D., & Dehairs, F. (1998). Phytoplanktonic nutrient utilisation and nutrient signature in the Southern Ocean. *Journal of Marine Systems*, *17*(1-4), 143–157. doi:10.1016/S0924-7963(98)00035-9.

Gordon, A. L., (1986), Inter-ocean exchange of thermocline water. *Journal of Geophysical Research*, 91(C4), 5037. doi:10.1029/JC091iC04p05037.

Gordon, A. L., (2001), Bottom water formation. In Columbia University Press, Palisades, NY, USA (pp. 334–340). doi:10.1006/rwos.2001.0006

Gran, H.H., (1931). On the conditions for the production of plankton in the sea. *Conseil Permanent International pour l'Exploration de la Mer* 75, 37 - 46.

Grasshoff, K., Ehrhardt, M., Kremling, K, (1983), Methods of seawater analysis. Verlag Chemi Weinheim, New York.

Greene, R.M., Geider, R.J., Kolber, Z., Falkowski, P.G. (1992). Iron-induced changes in light harvesting and photochemical energy-conversion processes in eukaryotic marine algae. *Plant Physiology,* 100:565–575.

Greenwood, J.E., Feng, M., Waite, A.M., 2007. A one-dimensional simulation of biological production in two contrasting mesoscale eddies in the south eastern Indian Ocean. *Deep-Sea Research II*, 54, 1029 – 1044.

Grotti, M., Francesco, S., Carmela, I., Roberto, F., 2005. Trace metals distributions in coastal sea ice of Terra Nova Bay, Ross Sea, Antarctica. *Science*, 17, 290–300.

Gruber, N., Gloor, M., Mikaloff Fletcher, S.E., Doney, S.C., Dutkiewicz. S., Follows, M.J., Gerber, M., Jacobson, A.R., Joos, F., Lindsay, K., Menemenlis, D., Mouchet, A., Muller, S.A., Sarmiento, J.L., Takahashi, T., (2009), Ocean sources, sinks, and transport of atmospheric CO_2, *Global Biogeochemical Cycles*, 23, GB1005, doi:10.1029/2008GB003349.

Hendricks, M. B., Bender, M. L., Barnett, B. a., Strutton, P., & Chavez, F. P. (2005). Triple oxygen isotope composition of dissolved O 2 in the equatorial Pacific: A tracer of mixing, production, and respiration. *Journal of Geophysical Research*, 110(C12), C12021. doi:10.1029/2004JC002735.

Hendricks, M. B., Bender, M. L., & Barnett, B. A., (2004), Net and gross O2 production in the southern ocean from measurements of biological O2 saturation and its triple isotope composition. *Deep Sea Research Part I*: Oceanographic Research Papers, 51(11), 1541–1561. doi:10.1016/j.dsr.2004.06.006.

Hense, I., Bathmann, U. V, & Timmermann, R. (2000). Plankton dynamics in frontal systems of the Southern Ocean. *Journal of Marine Systems*, *27*(1-3), 235–252. doi:10.1016/S0924-7963(00)00070-1.

Hiscock, M. R., Marra, J., Smith, W. O., Goericke, R., Measures, C., Vink, S., Olson, R.J., Sosik, H.M., Barber, R. T. (2003). Primary productivity and its regulation in the Pacific Sector of the Southern Ocean. *Deep Sea Research Part II: Topical Studies in Oceanography*, *50*(3-4), 533–558. doi:10.1016/S0967-0645(02)00583-0.

Hiscock, M. R., Lance, V. P., Apprill, A. M., Bidigare, R. R., Johnson, Z. I., Mitchell, B. G., Smith, W.O., Barber, R. T. (2008). Photosynthetic maximum quantum yield increases are an essential component of the Southern Ocean phytoplankton response to iron. *Proceedings of the National Academy of Sciences of the United States of America,* 105(12), 4775–80. doi:10.1073/pnas.0705006105

Holm-Hansen, O., El-Sayed, S.Z., Frances-Chini, G.A., and Cuhel, R.L., (1977), Primary production and factors controlling phytoplankton growth in the Southern Ocean, In: Llano, G.A. (Ed.),Adaptations Within Antarctic Ecosystems. *Proceedings of the Third SCAR Symposium on Antarctic Biology*. Gulf Publishing Co.,Houston,TX, pp. 11–50.

Honjo, S. (2004). Particle export and the biological pump in the Southern Ocean. *Antarctic Science*, *16*(4), 501–516. doi:10.1017/S0954102004002287.

Huot, Y., Babin, M., & Bruyant, F., (2013), Photosynthetic parameters in the Beaufort Sea in relation to the phytoplankton community structure. *Biogeosciences,* 10, 3445 – 3453.

Hutchins, D. A., & Bruland, K. W. (1998). Iron-limited diatom growth and Si:N uptake ratios in a coastal upwelling regime. *Nature*, *393*, 65–68.

Ingleby, B., and M. Huddleston, (2007), Quality control of ocean temperature and salinity profiles - historical and real-time data. *Journal of Marine Systems*, 65, 158-175 10.1016/j.jmarsys.2005.11.019.

Jochem, F. J., (1995), Size-fractionated Primary Production in the Open Southern Ocean in Austral Spring. *Polar Biology*, 15, 381–392.

Jones, K.J., and Gowan, R.J., (1990), Influence of stratification and irradiance regime on summer phytoplankton composition in coastal and shelf seas of the British Isles, *Estuarine Coastal and Shelf Science*, 30, 557 – 567.

Jonsson, B.F., Doney., S.C., Dunne, J., Bender. M., (2013), Evaluation of Southern Ocean O_2/Ar-based NCP estimates in a model framework, *Journal of Geophysical Research*, DOI: 10.1002/jgrg.20032.

Joubert, W.R., S.J., Thomalla, H.N.Waldron, M.I.,Lucas, M., Boye, F.A.C., LeMoigne., F., Planchon, and S. Speich., 2011, Nitrogen uptake by phytoplankton in the Atlantic sector of

the Southern Ocean during late austral summer, *Biogeosciences*, 8, 2947–2959, 2011, doi:10.5194/bg-8-2947-2011.

Kahru, M. and Mitchell, B. G., 2010, Blending of ocean colour algorithms applied to the Southern Ocean, *Remote Sensing Letters*, 1, 119– 124.

Karl, D.M., Laws, E.A., Morris, P., LeB.Willams, P.J., Emerson, S., 2003, Metabolic balance of the open sea, *Nature*, 426, p32.

Kirchman, D. L., (2000). Uptake and regeneration of inorganic nutrients by marine heterotrophic bacteria. In Kirchman, D. L. (ed.), Microbial Ecology of the Oceans. John Wiley and Sons, New York, pp. 261–288.

Kirk, J. T. (1984). Solar Altitude Dependence of relationship between inherent and apparent of water on solar altitude optical properties. *Limnology and Oceanography*, *29*(2), 350–356.

Kirk, J.T.O., (1994), Light and Photosynthesis in Aquatic ecosystems, 2nd Edition, Cambridge University Press, ISBN-9780521459662.

Klein, P., & Coste, B. (1984). Effects of winds tress on nutrient transport into the mixed layer. *Deep Sea Research Part I: Oceanographic Research Papers*, *31*(1), 21 – 37.

Klunder, M. B., Laan, P., Middag, R., De Baar, H. J. W., & van Ooijen, J. C. (2011). Dissolved iron in the Southern Ocean (Atlantic sector). *Deep Sea Research Part II*, 58(25-26), 2678–2694, doi:10.1016/j.dsr2.2010.10.042.

Korb, R. E., & Whitehouse, M. (2004). Contrasting primary production regimes around South Georgia, Southern Ocean: large blooms versus high nutrient, low chlorophyll waters. *Deep Sea Research Part I: Oceanographic Research Papers*, *51*(5), 721–738. doi:10.1016/j.dsr.2004.02.006.

Korb, R.E., Whitehouse, M., 2004. Contrasting primary production regimes around South Georgia: large bloom vs high nutrient low chlorophyll waters. *Deep-Sea Research* I, 51, 721 – 738.

Körtzinger, A., Koeve, W., Kähler, P., & Mintrop, L. (2001). C : N ratios in the mixed layer during the productive season in the northeast Atlantic Ocean. *Deep-Sea Research*, *48*, 661 – 688.

Lampitt, R.S., Boorman, B., Brown, L., Lucas, M., Salter, I., Sanders, R., Saw, K., Seeyave, S.; Thomalla, S.J., Turnewitsch, R., (2008), Particle export from the euphotic zone: Estimates using a novel drifting sediment trap, 234Th and new production. *Deep-Sea Research I*, 55 (11). 1484-1502. 10.1016/j.dsr.2008.07.002.

Lane, E. S., D. M. Semeniuk, R. F. Strzepek, J. T. Cullen, and M. T. Maldonado, 2009. Effects of iron limitation on intracellular cadmium of cultured phytoplankton: Implications for surface dissolved cadmium to phosphate ratios. *Marine Chemistry* 115: 155–162, doi:10.1016/j.marchem.2009.07.008.

Lathuiliere, C., Levy, M., & Echevin, V. (2010). Impact of eddy-driven vertical fluxes on phytoplankton abundance in the euphotic layer. Journal of Plankton Research, 33(5), 827–831. doi:10.1093/plankt/fbq131.

Laubscher, R. K., Perissinotto, R., & McQuaid, C. D. (1993). Phytoplankton production and biomass at frontal zones in the Atlantic sector of the Southern Ocean. *Polar Biology*, *13*(7), 471–481. doi:10.1007/BF00233138.

Laws, E. A., Falkowski, P. G., Smith, W. O., Ducklow, H., & Mccarthy, J. J. (2000). Temperature effects on export production in the upper ocean. *Global Biogeochemical Cycles*, *14*(4), 1231 – 1246.

Laws, E.A., 1991, Photosynthetic quotients, new production and net community production in the open ocean, Deep Sea Research, 38, 143 – 167.Martin, H., Gordon, R. M., & Fitzwater, S. E. (1991). Iron limitation? The case for iron. *Limnology and Oceanography*, 36(8), 1793–1802.

Le Moigne F.A.C., Boye, M., Masson, A., Corvaisier, R., Grossteffan, E., Guéneugues, A., Pondaven, P., Nelson, D., 2011. Biogeochemical features of the subtropical southeastern Atlantic and the Southern Ocean south off South Africa during the austral summer of the International Polar Year. *Biogeosciences*, 10, 281-295, 2013.

Le Quéré, C., Bopp, L., Tegen, I., (2002). Antarctic circumpolar wave impact on marine biology: A natural laboratory for climate change study. *Geophysical Research Letters,* 29, doi:10.1029/2001/GL014585.

Lee, J. G., & Francois, M. M. (1995). Replacement of zinc by cadmium in marine phytoplankton. *Marine Ecology Progress Series*, *127*, 305–309.

LeFèvre J., Legendre, L., Rivkin, R.B., 1998. Fluxes of biogenic carbon in the Southern Ocean: Roles of large microphagous zooplankton. *Journal of Marine Systems*, 17, 325 – 345.

Levitus, S., Burgett, R., Boyer, T.P., (1994), World Ocean Atlas 1994 Volume 3: Nutrients, number 3, 1994.

Levitus, S., (1982), Climatological Atlas of the World Ocean, NOAA/ERL GFDL, Professional Paper 13, Princeton, N.J., 173 pp. (NTISPB83-184093),1982.

Levy, M., Bopp, L., Karleskind, P., Resplandy, L., Ethe, C., & Pinsard, F. (2013). Physical pathways for carbon transfers between the surface mixed layer and the ocean interior. *Global Biogeochemical Cycles*, *27*(4), 1001–1012. doi:10.1002/gbc.20092.

Levy, M. (2001). Impact of sub-mesoscale physics on production and subduction of phytoplankton in an oligotrophic regime. *Journal of Marine Research*, 535–565.

Lévy, M., Ferrari, R., Franks, P. J. S., Martin, A. P., & Rivière, P. (2012). Bringing physics to life at the submesoscale. *Geophysical Research Letters*, *39*(14), 1–13. doi:10.1029/2012GL052756.

Lévy, M., Klein, P., & Ben Jelloul, M. (2009). New production stimulated by high-frequency winds in a turbulent mesoscale eddy field. *Geophysical Research Letters*, 36(16), L16603. doi:10.1029/2009GL039490.

Lewis, M. R., Horne, E. P., W., Cullen, J. J., Oakey, N. S., Platt, T., (1984). Turbulent motion may control phytoplankton photosynthesis in the upper ocean. *Nature,* 311: 49-50.

Leynaert, A., Bucciarelli, E., Claquin, P., Dugdale, R.C., Martin-Jézéquel, V. Pondaven, P., Ragueneau, O., 2004. Effect of iron deficiency on diatom cell size and silicic acid uptake kinetics. *Limnology and Oceanography*, 49(4), 1134-1143.

Llido, J., Garcon, V., Lutjeharms, J.R.E., Sudre, J., 2005. Event-scale blooms drive enhanced primary productivity at the Subtropical Convergence. *Geophysical Research Letters* 32, L15611, [doi:10.1029/2005GL022880].

Lucas, M., Seeyave, S., Sanders, R., Mark Moore, C., Williamson, R., & Stinchcombe, M. (2007). Nitrogen uptake responses to a naturally Fe-fertilised phytoplankton bloom during the 2004/2005 CROZEX study. *Deep Sea Research Part II: Topical Studies in Oceanography*, *54*(18-20), 2138–2173. doi:10.1016/j.dsr2.2007.06.017.

Lutjeharms, J. R. E., (1996), The exchange of water between the South Indian and South Atlantic oceans, in The South Atlantic: Present and Past Circulation, edited by G. Wefer et al., Berlin, Heidelberg: Springer-Verlag, 125–162.

Luz, B., Barkan, E., 2000. Assessment of oceanic productivity with the triple-isotope composition of dissolved oxygen. *Science*, 288 (5473), 2028–2031

MacIntyre, H.L., Kana, T.M., Anning, T., Geider, R.J., 2002, Photoacclimation of photosynthesis irradiance response curves and photosynthetic pigments in microalgae and cyanobacteria. *Journal of Phycology*, 38, 17 – 38.

Mahadevan, A., D'Asaro, E., Lee, C., & Perry, M. J. (2012). Eddy-driven stratification initiates North Atlantic spring phytoplankton blooms. *Science*, *337*, 54–58. doi:10.1126/science.1218740

Maldonado, M.T., Price, N.M., 2001. Reduction and transport of organically bound iron by Thalassiosira oceanica (Bacillariophyceae). *Journal of Phycology* 37 (2), 298–309.

Maldonado, M.T., R.F., Strzepek, S. Sander, P.W., Boyd, 2005, Acquisition of iron bound to strong organic complexes, with different Fe binding groups and photochemical reactivities, by plankton communities in Fe-limited subantarctic waters, *Global Biogeochemical Cycles*, 19(4), DOI: 10.1029/2005GB002481.

Marinov, I., Gnanadesikan, A., Toggweiler, J. R., & Sarmiento, J. L., (2006), The Southern Ocean biogeochemical divide. *Nature*, 441(7096), 964–7. doi:10.1038/nature04883

Martin, J. (1990). Glacial-Interglacial CO_2 Change: The Iron Hypothesis. *Paleoceanography*, *5*(1), 1–13.

Martin, J. (1991). Iron, Liebig's Law, and the Greenhouse. *Oceanography*, *4*(2), 52–55. doi:10.5670/oceanog.1991.02.

Martin, H., Gordon, R. M., & Fitzwater, S. E., (1991), Iron limitation? The case for iron. *Limnology and Oceanography*, 36(8), 1793–1802.

Martin-Jézéquel, V., Copernic, P. N., Plouzane, F.-, & Brzezinski, M. A. (2000). Silicon metabolism in diatoms: implications for growth. *Journal of Phycology*, *840*, 821–840.

McGillicuddy, D. J., Anderson, L. a, Bates, N. R., Bibby, T., Buesseler, K. O., Carlson, C. A, Steinberg, D. K. (2007). Eddy/wind interactions stimulate extraordinary mid-ocean plankton blooms. *Science*, 316(5827), 1021–6. doi:10.1126/science.1136256.

Mengesha, S., Dehairs, F., Fiala, M., Elskens, M., Goeyens, L., 1998. Seasonal variation of phytoplankton community structure and nitrogen uptake regime in the Indian Sector of the Southern Ocean. *Polar Biology* 20, 259-272.

Metzl, N., Tilbrook, B., Poisson, A., 1999. The annual fCO2 cycle and the air-sea CO2 flux in the sub-Antarctic Ocean. *Tellus*, 51B, 849 – 861.

Metzl, N., C. Brunet, A.,Jabaud, A., Poisson, B., Schauer, 2006, Summer and winter air-sea CO2 fluxes in the Southern Ocean, *Deep-Sea Research*, 53, 1548 – 1563, doi:10.1016/j.dsr.2006.07.006.

Millero, F. J. and Poisson, A., (1981), International one-atmosphere equation of state of seawater, *Deep Sea Research*, 28, 625–629, 1981.

Mitchell, B. G., Brody, E. A., Holm-Hansen, O., Mcclain, C., & Bishop, J. (1991). Light limitation of phytoplankton biomass and macronutrient utilization in the Southern Ocean. *Limnology and Oceanography*, *36*(8), 1662 – 1677.

Mitchell, B. G., Brody, E. A., Holm-hansen, O., & Mcclain, C. (1991), Light Limitation of Phytoplankton Biomass and Macronutrient Utilization in the Southern Ocean Source: *Limnology and Oceanography*, Vol. 36, No. 8, p1662 - 1677.

Monterey, G., and Levitus, S., (1997), Seasonal variability of mixed layer depth for the world ocean, NOAA Atlas, *NESDIS* 14.

Moore, J. K., & Abbott, M. R. (2000). Phytoplankton chlorophyll distributions and primary production in the Southern Ocean. *Journal of Geophysical Research*, *105*(C12), 28709. doi:10.1029/1999JC000043

Moore, J. K., & Abbott, M. R. (2002). Surface chlorophyll concentrations in relation to the Antarctic Polar Front: seasonal and spatial patterns from satellite observations. *Journal of Marine Systems*, *37*(1-3), 69–86. doi:10.1016/S0924-7963(02)00196-3.

Moore, J.K. and Braucher, O., 2008, Sedimentary and mineral dust sources of dissolved iron to the world oceanm, *Biogeosciences*, 5, 631-656, doi:10.5194/bg-5-631-2008.

Moore, C.M., Mills, M.M.,,Milne, A., Langlois, R., Achterberg, E., Lochte, K., Geider, R.J., LaRoche, J., 2006, Iron limits primary productivity during spring bloom development in the central North Atlantic, *Global Change Biology*, 12, 626–634, doi: 10.1111/j.1365-2486.2006.01122.x.

Morel, F. M. M., Rueter, J. G., & Price, N. M. (1991). Iron nutrition of phytoplankton and its possible importance in the ecology of ocean regions with high nutrient and low biomass. *Oceanography*, *4*(2), 56 – 61.

Morel, F. M. M., Reinfelder, J. R., Roberts, S. B., Chamberlain, C. P., Lee, J. G., Yee, D. (1994). Zinc and carbon colimitation of marine phytoplankton. *Nature*, 369, 740–742.

Morel, A. (1988). Optical modeling of the upper ocean in relation to its biogenous matter content (Case I waters). *Journal of Geophysical Research*, *93*(C9), 10749 – 10768.

Morel, A., (1978). Available, usable, and stored radiant energy in relation to marine photosynthesis. *Deep-Sea Research*. 25: 673-688.

Morel, A. (1991). Light and marine photosynthesis: a spectral model with geochemical and climatological implications. *Progress in Oceanography*, *26*, 263 – 306.

Murphy, J. and Riley, J. P., (1962), A modified single solution method for the determination of phosphorus in natural waters, *Anal. Chim. Acta*, 27, 31–36.

Nelson, D. M., & Smith, W. O. (1991). Sverdrup Revisited: Critical Depths, Maximum Chlorophyll Levels, and the Control of Southern Ocean Productivity by the Irradiance-Mixing Regime. *Limnology and Oceanography*, *36*(8), 1650–1661.

Neori, A., and Holm-Hansen, O., (1982), Effect of temperature on rate of photosynthesisin Antarctic phytoplankton, *Polar Biology,* 1, 33 – 38.

Nodwell, L.M. and N.M.Price, 2001, Direct use of inorganic colloidal iron by marine mixotrophic phytoplankton, *Limnology and Oceanography*, 46(4), 765 – 777.

Orsi, A.H., Whitworth, T., & Nowlin, W.D., (1995), On the meridional extent and fronts of the Antarctic Circumpolar Current Pronounced meridional gradients in surface properties separate waters of the Southern Ocean from the warmer and saltier waters of the subtropical circulations. *Deep Sea Research Part I*, 42(5), 641 – 673.

Orsi, A. H., W. D. Nowlin, and Whitworth, T., (1993), On the circulation and stratification of the Weddell Gyre, *Deep Sea Research Part I*, 40, 169– 203.

Oschlies, A., and Garcon, V., Eddy-induced enhancement of primary production in a model of the North Atlantic Ocean, *Nature*, 1998, 398, p266 – 269.

Park, Y.-H., Charriaud, E., Craneguy, P., (2001), Fronts, transport, and Weddell Gyre at 301oE between Africa and Antarctica. *Journal of Geophysical Research*, 106, 2857–2879.

Peters J., Renz J., van Beusekom J., Boersma, M., Hagen, W., 2006, Trophodynamics and seasonal cycle of the copepod Pseudocalanus acuspes in the Central Baltic Sea (Bornholm Basin): evidence from lipid composition. *Marine Biology*, 149, 1417-1429. doi:10.1007/s00227-006-0290-8.

Planchon F., Cavagna A.J., Cardinal, D., Dehairs F., 2013. Late summer particulate organic carbon export and twilight zone remineralisation in the Atlantic sector of the Southern Ocean. *Biogeosciences,* 10, 803-820.

Platt, T., & Jassby, A. D. (1976). Relationship between photosynthesis and light for natural assemblages of coastal marine phytoplankton. *Journal of Phycology*, *12*, 421 – 430.

Platt, T., Gallegos, C.L., Harrison, W.G., (1980), Photoinhibition of photosynthesis in natural assemblages of marine phytoplankton, *Journal of Marine Research*, 38, 687 – 701.

Platt, T., & Sathyendranath, S., (1993), Estimators of primary production for interpretation of remotely sensed dataon ocean colour. *Journal of Geophysical Research,* 98, 14561 – 14576.

Platt, T., & Sathyendranath, S., (1995), Modelling primary production, *Bedford Institute of Oceanography*, Box 1006, Darmouth, N.S., Canada, B2Y 4A2.

Platt, T., Sathyendranath, S., Forget, M.-H.,White, G.N., III, Caverhill, C., Bouman, H., (2008), Operational estimation of primary production at large geographical scales. Remote sensing of the environment, 112, 3427 – 3448.

Pollard, R. T., Venables, H. J., Read, J. F., & Allen, J. T. (2007). Large-scale circulation around the Crozet Plateau controls an annual phytoplankton bloom in the Crozet Basin. *Deep Sea Research Part II: Topical Studies in Oceanography*, *54*(18-20), 1915–1929. doi:10.1016/j.dsr2.2007.06.012.

Pollard, R. T., Lucas, M. I., & Read, J. F. (2002). Physical controls on biogeochemical zonation in the Southern Ocean. *Deep Sea Research Part II: Topical Studies in Oceanography*, *49*(2002), 3289–3305.

Pollard, R., Sanders, R., Lucas, M., & Statham, P., (2007), The Crozet Natural Iron Bloom and Export Experiment (CROZEX). *Deep Sea Research Part II*: Topical Studies in Oceanography, 54(18-20), 1905–1914. doi:10.1016/j.dsr2.2007.07.023.

Pondaven, P., Druon, J. N., Fravalo, C., & Treguer, P. (1999). Factors controlling silicon and nitrogen biogeochemical cycles in high nutrient, low chlorophyll systems (the Southern Ocean and the North Pacific): Comparison with a mesotrophic system (the North Atlantic). *Deep Sea Research Part I: Oceanographic Research Papers*, *46*, 1923 – 1968.

Price, N. M., Ahner, B. A., & Morel, F. M. M. (1991). The Equatorial Pacific Ocean : Grazer-Controlled Phytoplankton Populations in an Iron-Limited Ecosystem. *Limnology and Oceanography*, *39*(3), 520–534.

Price, N.M., Ahner, B.A., Morel, F.M.M., 1994. The equatorial Pacific Ocean: Grazer-controlled phytoplankton in an iron-limited ecosystem. *Limnology and Oceanography*, 39(3), 520 – 534.

Priddle, J., Smetacek, V., Bathmann, U., (1992), Antarctic marine primary production, biogeochemical cycles, and climate. *Philosophical Transactions of the Royal Society*, London, B, 338, 289 – 297.

Probyn, T. A., & Painting, S. J. (1985). Nitrogen Uptake by Size-Fractionated Phytoplankton Populations in Antarctic Surface Waters. *Limnology and Oceanography*, 30(6), 1327–1332.

Raven, J.A., and Geider, R.T., (1988), Temperature and algal growth, *New Phytologist*, 110 (4), 441 – 461, DOI: 10.1111/j.1469-8137.1988.tb00282.x.

Raven, J.A., 1986. Physicological consequences of extremely small size for autotrophic organisms in the sea. *Can. Bull. Fish. Aquat. Sci*, 214, 1 – 70.

Raven, J.A., 1988. The iron and molybdenum use efficiencies of plant growth with different energy, carbon and nitrogen sources. *New Phytologist* 109, 279 – 288.

Redfield, A. C., Ketchum, B.H., Richards, F.A., (1963), The influence of orfanisms on the composition of seawater, in *The Sea*, vol 2, M. N. Hill ed, 26 – 77, Wiley Interscience, New York.

Reuer, M. K., Barnett, B. a., Bender, M. L., Falkowski, P. G., & Hendricks, M. B. (2007). New estimates of Southern Ocean biological production rates from O_2/Ar ratios and the triple isotope composition of O_2. *Deep Sea Research Part I*: Oceanographic Research Papers, 54(6), 951–974. doi:10.1016/j.dsr.2007.02.007.

Roy, B. T., Rayner, P., Matear, R., Francey, R., & Cooperative, A. (2003). Southern hemisphere ocean CO_2 uptake: reconciling atmospheric and ocean estimates, *Tellus*, 55B, 701–710.

Rubin, S.I., (2003), Carbon and nutrient cycling in the upper water column across the Polar Frontal Zone and Antarctic Circumpolar Current along 170°W, *Global Biogeochemical Cycles,* 17 (3), DOI: 10.1029/2002GB001900.

Ruiz, J., Echevarría, F., Font, J., Ruiz, S., García, E., Blanco, J.M., Jiménez-Gómez, F., Prieto, L., González-Alaminos, A., García, C.M., Cipollini, P., Snaith, H., Bartual, A., Reul, A., Rodríguez, V., (2001), Surface distribution of chlorophyll, particles and gelbstoff in the Atlantic jet of the Alborán Sea: from submesoscale to subinertial scales of variability, *Journal of Marine Systems,* 29 (1-4), 277 – 292.

Ryther, J. H., & Yentsch, C. S. (1957). Production in the Ocean from The Estimation of Phytoplankton and Light Data , Chlorophyll. *Limnology and Oceanography*, *2*(3), 281–286.

Sabine, C. L., Feely, R. a, Gruber, N., Key, R. M., Lee, K., Bullister, J. L., Wanninkhof, R., Wong, C.S., Wallace, D.W.R., Tilbrook, B., Millero, F.J., Peng, T-H, Kozyr, A., Ono, T., Rios, A. F. (2004). The oceanic sink for anthropogenic CO_2. *Science 305*(5682), 367–71. doi:10.1126/science.1097403

Sakshaug, E., Bricaud, A., Dandonneau, Y., Falkowski, P. G., Kiefer, D. A., Legendre, L., Morel, A., Parslow, J. and Takahashi, M. (1997) Parameters of photosynthesis: definitions, theory and interpretation results. *J. Plankton Res*., 19(1), 1637–1670.

Sakshaug, E., D., Slagstad, 1991, Light and productivity of phytoplankton in polar marine ecosystems: a physiological view. in Sakshaug. E.. Hopkins. C. C. E. & Britsland. N. A. (eds.): Proceedings of the Pro Mare Symposium on Polar Marine Ecology. Trondheim. 12-16 May 1990. *Polar Research* 10 pp. 6S-85.

Sakshaug. E.L, and O. Holm-Hansen, (1986), Photoadaptation in Antarctic phytoplankton: Variations in growth rate, chemical composition and P vs I curves. *J. Planktonic Res*. 8. 459 -473.

Sambrotto, R. N., & Mace, B. J. (2000). Coupling of biological and physical regimes across the Antarctic Polar Front as reflected by nitrogen production and recycling. *Deep Sea Research Part II: Topical Studies in Oceanography*, *47*, 3339–3367.

Sanders, R., Morris, P.J., Stinchcombe, M., Seeyave, S., Venables, H., Lucas, M., (2007), New production and the f ratio around the Crozet Plateau in austral summer 2004–2005 diagnosed from seasonal changes in inorganic nutrient levels. *Deep-Sea Research II,* 54, (18-20), 2191 – 2207.

Sarmiento, J.L., and Gruber, N., (2004), Ocean Biogeochemical Dynamics, *Princeton University Press*, ISBN: 9780691017075.

Sarmiento, J. L., Gruber, N., Brzezinski, M. A., & Dunne, J. P., (2004), High-latitude controls of thermocline nutrients and low latitude biological productivity, *Nature*, 427, 1–5. doi:10.1038/nature02204.1.

Sarthou, G., Vincent, D., Christaki, U., Obernosterer, I., Timmermans, K. R., & Brussaard, C. P. D. (2008). The fate of biogenic iron during a phytoplankton bloom induced by natural fertilisation: Impact of copepod grazing. *Deep Sea Research Part II*: Topical Studies in Oceanography, 55(5-7), 734–751. doi:10.1016/j.dsr2.2007.12.033.

Saux Picart, S., Sathyendranath, S., Dowell, M., Moore, T., Platt, T., (2014), Remote sensing assimilation number for marine phytoplankton. *Remote Sensing of the Environment,* 146, 87 – 96.

Savoye, N., Dehairs, F., Elskens, M., Cardinal, D., Kopczynska, E. E., Trull, T. W., Wright, S., Baeyens, W., Griffiths, F. B. (2004). Regional variation of spring N-uptake and new production in the Southern Ocean. *Geophysical Research Letters*, *31*(3), L03301. doi:10.1029/2003GL018946.

Schlitzer, R. (2002). Carbon export fluxes in the Southern Ocean: results from inverse modeling and comparison with satellite-based estimates. *Deep Sea Research Part II*: Topical Studies in Oceanography, 49(9-10), 1623–1644. doi:10.1016/S0967-0645(02)00004-8.

Sedwick, P.N., DiTullio, G.R., (1997). Regulation of algal blooms in Antarctic shelf waters by the release of iron from melting sea ice. *Geophysical Research Letters* 24, 2515–2518.

Seeyave, S., Lucas, M., Moore, C.M., Poulton, A.J., 2007. Phytoplankton productivity and community structure in the vicinity of Crozet Plateau during austral summer 2004/2005. *Deep-Sea Research II*, 54, 2020 – 2044.

Shaked, Y., Kustka, A.B., Morel, F.M.M., 2005, A genetic model for iron acquisition by eukaryotic phytoplankton, *Limnologyy and Oceanography*, 50(3), 872 – 882.

Siegel, D.A., Doney, S. C., & Yoder, J.A., (2002). The North Atlantic spring phytoplankton bloom and Sverdrup's critical depth hypothesis. *Science*, *296*(5568), 730–3. doi:10.1126/science.1069174.

Siegel, D. a, Doney, S. C., & Yoder, J. A. (2002). The North Atlantic spring phytoplankton bloom and Sverdrup's critical depth hypothesis. Science (New York, N.Y.), 296(5568), 730–3. doi:10.1126/science.1069174

Sigman, D. M., & Boyle, E. A. (2000). Glacial/Interglacial variations in atmospheric CO2. *Nature*, *407*(October), 859–869.

Slawyk, G., & Raimbault, P. (1995). Simple procedure for simultaneous recovery of dissolved inorganic and organic nitrogen in 15N-tracer experiments and improving the isotopic mass balance. *Marine Ecology Progress Series*, *124*, 289–299. doi:10.3354/meps124289.

Slawyk,G., Collos.Y., Auclair,J.C., 1977. The use of the I3C and I5N isotopes for the simultaneousmeasurements of carbon and nitrogen turnover rates in marine phytoplankton. *Limnology and Oceanography*, 22, 925-932.

Smayda, T.J., 1997, Harmful algal blooms: Their ecophysiology and general relevance to phytoplankton blooms in the sea. *Limnol. Oceanogr*., 42(5), 1137 – 1153.

Smetacek, V., Assmy, P., & Henjes, J. (2004). The role of grazing in structuring Southern Ocean pelagic ecosystems and biogeochemical cycles. *Antarctic Science*, *16*(4), 541–558. doi:10.1017/S0954102004002317.

Smetacek, V., & Passow, U. (1990). Spring bloom initiation and Sverdrup ' s critical-depth model. *Limnology and Oceanography*, *35*(l), 228–234.

Smetacek, V., de Baar, H.J.W., Bathmann, U.V., Lochte, K., Van Der Loeff, M.M.R., 1997. Ecology and Biogeochemistry of the Antarctic Circumpolar Current during austral spring: a summary of Southern Ocean JGOFS cruise ANT X/6 of R.V.Polarstern. *Deep-Sea Research II* 44, 1 – 21.

Smith, K., Jr., B. Robison, J. Helly, R. Kaufmann, H. Ruhl, T. Shaw, B. Twining, and M. Vernet (2007), Free-drifting icebergs: Hot spots of chemical and biological enrichment in the Weddell Sea, *Science,* 317(5837), 478–482, doi:10.1126/science.1142834

Smith, W. O., & Comiso, J. C. (2008). Influence of sea ice on primary production in the Southern Ocean: A satellite perspective. *Journal of Geophysical Research*, *113*(C5), C05S93. doi:10.1029/2007JC004251.

Smith,W.O. & Sakshaug. E., (1990), Polar phytoplankton. Pp.477-525 In Smith. W.O.: *Polar Oceanography:* PartB Chemistry, Biology and Geology. Academic Press. New York

Smith, W.O., Jr. and Nelson, D.M., 1986. Importance of ice edge phytoplankton production in the Southern Ocean, *BioScience*, 36, 251– 257.

Sokolov, S., & Rintoul, S. R. (2007). On the relationship between fronts of the Antarctic Circumpolar Current and surface chlorophyll concentrations in the Southern Ocean. *Journal of Geophysical Research*, *112*(C7), C07030. doi:10.1029/2006JC004072.

Sokolov, S., & Rintoul, S. R. (2007). Multiple Jets of the Antarctic Circumpolar Current South of Australia. *Journal of Physical Oceanography*, 37(5), 1394–1412. doi:10.1175/JPO3111.1

Speich, S., Blanke, B., and Cai, W., (2007), Atlantic meridional overturning and the Southern Hemisphere supergyre, *Geophysical Research Letters*, 34, L23614, DOI: 10.1029/2007GL031583.

Speich, S., Arhan, M., Fine, R.A., 2011. Water masses and ocean dynamics along the BONUS-GoodHope transect. Ocean Sciences.

Strass, V.H., Garabato, A.C.N., Pollard, R.T., Fischer, H.I., Hense, I., Allen, J.T., Read, J.F., Leach, H, Smetacek, V., 2002. Mesoscale frontal dynamics: shaping the environment of primary production in the Antarctic Circumpolar Current. *Deep-Sea Research II* 49, 3735 – 3769.

Strickland, J. D. H. and Parsons, T. R., (1971), A practical handbook of seawater analysis, *Fisheries Research Board of Canada, 2nd Edition*.

Strzepek, R. F., Maldonado, M. T., Higgins, J. L., Hall, J., Safi, K., Wilhelm, S. W., & Boyd, P. W. (2005). Spinning the "Ferrous Wheel": The importance of the microbial community in

an iron budget during the FeCycle experiment. *Global Biogeochemical Cycles*, 19(4), doi:10.1029/2005GB002490.

Strzepek, R. F., Maldonado, M. T., Hunter, K. a., Frew, R. D., & Boyd, P. W. (2011). Adaptive strategies by Southern Ocean phytoplankton to lessen iron limitation: Uptake of organically complexed iron and reduced cellular iron requirements. *Limnology and Oceanography*, 56(6), 1983–2002. doi:10.4319/lo.2011.56.6.1983.

Suggett, D. J., Moore, C. M., Hickman, A. E., & Geider, R. J. (2009). Interpretation of fast repetition rate (FRR) fluorescence: signatures of phytoplankton community structure versus physiological state. *Marine Ecology Progress Series*, *376*, 1–19. doi:10.3354/meps07830.

Sullivan, C.W., McClainJ., C.R., Comiso, C., Smith Jr. W. O., (1988), Phytoplankton standing crops within an Antarctic ice edge assessed by satellite remote sensing. *Journal of Geophysical Research*, 93, C10, 12487 – 12498.

Sunda, W. G., & Huntsman, S. A. (1997). Interrelated influence of iron, light and cell size on marine phytoplankton growth. *Nature*, *2051*(1977), 389–392.

Sunda, W.G., 2001, Bioavailability and Bioaccumulation of Iron in the Sea, in "The Biogeochemistry of Iron in Seawater", edited by D.R. Turner, K.Hunter, Wiley, Chinester, UK.

Sverdrup, H. U. (1953), On conditions for the vernal blooming of phytoplankton, *J. Cons. Cons. Int. Explor. Mer*., 18, 287–295.

Swart, S., & Speich, S., (2010), An altimetry-based gravest empirical mode south of Africa: 2. Dynamic nature of the Antarctic Circumpolar Current fronts. *Journal of Geophysical Research*, 115(C3), C03003. doi:10.1029/2009JC005300.

Swart, S., Speich, S., Ansorge, I. J., Goni, G. J., Gladyshev, S., & Lutjeharms, J. R. E. (2008). Transport and variability of the Antarctic Circumpolar Current south of Africa. *Journal of Geophysical Research*, 113(C9), C09014. doi:10.1029/2007JC004223.

Swart, S., Thomalla, S.J., & Monteiro., P.M.S., (2014), The seasonal cycle of mixed layer dynamics and phytoplankton biomass in the Sub-Antarctic Zone: a high resolution glider experiment, *Journal of Marine System*, doi:10.1016/j.jmarsys.2014.06.002

Sweeney, C., Smith, W. O., Hales, B., Bidigare, R. R., Carlson, C. A., Codispoti, L. A., Gordon, L.I., Hansell, D.A., Millero, F.J., Park, Mi-OK., Takahashi, T. (2000). Nutrient and carbon removal ratios and fluxes in the Ross Sea, Antarctica. *Deep Sea Research Part II: Topical Studies in Oceanography*, *47*, 3395–3421.

Tagliabue, A., Bopp, L., Dutay, J.-C., Bowie, A. R., Chever, F., Jean-Baptiste, P., Bucciarelli, E., Lannuzel, D., Remenyi, T., Sarthou, G., Aumont, O., Gehlen, M., and Jeandel, C., 2010. Hydrothermal contribution to the oceanic dissolved iron inventory, *Nature Geosciences*, 3, 252–256.

Tagliabue, a., Mtshali, T., Aumont, O., Bowie, a. R., Klunder, M. B., Roychoudhury, A. N., & Swart, S. (2012). A global compilation of dissolved iron measurements: focus on distributions and processes in the Southern Ocean. *Biogeosciences*, *9*(6), 2333–2349. doi:10.5194/bg-9-2333-2012.

Tagliabue, A., Mtshali, T., Aumont, O., Bowie, a. R., Klunder, M. B., Roychoudhury, a. N., & Swart, S. (2012). A global compilation of dissolved iron measurements: focus on distributions and processes in the Southern Ocean. *Biogeosciences*, 9(6), 2333–2349. doi:10.5194/bg-9-2333-2012.

Tagliabue A., Sallée, J-B., Bowie, A.R., Lévy, M., Swart, S., & Boyd, P.W., (2014), Towards Reconciling Seasonal Iron Supply and Utilisation in the Southern Ocean, *Nature Geoscience*, 7, 314–320 (2014) doi:10.1038/ngeo2101.

Takahashi, T., Sutherland, S. C., Sweeney, C., Poisson, A., Metzl, N., Tilbrook, B., Bates, N., Wanninkhof, R., Feely, R.A., Sabine, C., Olafsson, J., & Nojiri, Y. (2002). Global sea–air CO2 flux based on climatological surface ocean pCO_2, and seasonal biological and temperature effects. *Deep Sea Research Part II: Topical Studies in Oceanography*, *49*(9-10), 1601–1622. doi:10.1016/S0967-0645(02)00003-6.

Takahashi, T., Sweeney, C., Hales, B., Chipman, D. W., Newberger, T., & Goddard, J. G. (2012). The Changing Carbon Cycle in the Southern Ocean. *Oceanography*, *25*(3), 26 – 37.

Takahashi, T., Olafsson, J., Goddard, J.G., Chipman, D.W., Sutherland, S.C., (1993), Seasonal-variation of CO_2 and nutrients in the high-latitude surface oceans: a comparative study. *Global Biogeochemical Cycles*, 7 (4), 843–878.

Takeda, S. (1998). Influence of iron availability on nutrient consumption ratio of diatoms in oceanic waters. *Nature*, *393*, 774 – 777.

Taylor, J. R., & Ferrari, R. (2011). Shutdown of turbulent convection as a new criterion for the onset of spring phytoplankton blooms. *Limnology and Oceanography*, *56*(6), 2293–2307. doi:10.4319/lo.2011.56.6.2293.

Taylor, J. R., & Ferrari, R. (2011). Ocean fronts trigger high latitude phytoplankton blooms. *Geophysical Research Letters*, 38(23), doi:10.1029/2011GL049312.

Taylor, A.H., Joint, J., 1990, Steady-state analysis of the 'microbial loop' in stratified systems. *Marine Ecological Progress Series*, 59, 1-17.

Thomalla, S. J., Fauchereau, N., Swart, S., & Monteiro, P. M. S. (2011). Regional scale characteristics of the seasonal cycle of chlorophyll in the Southern Ocean. *Biogeosciences*, *8*(10), 2849–2866. doi:10.5194/bg-8-2849-2011.

Thomalla, S.J., Waldron, H.N., Lucas, M.I., Read, J.F., Ansorge, I.J., Pakhomov, E., 2011. Phytoplankton distribution and nitrogen dynamics in the Southwest Indian Subtropical gyre and Southern Ocean waters. *Ocean Sciences*, 7, 113 – 127, doi: 10.5194/os-7-113-2011.

Timmermans, K., van Leeuwe, M., de Jong, J., McKay, R., Nolting, R., Witte, H., van Ooyen, J., Swagerman, M.J.W.,Kloosterhuis, H., de Baar, H. (1998). Iron stress in the Pacific region of the Southern Ocean:evidence from enrichment bioassays. *Marine Ecology Progress Series*, *166*, 27–41. doi:10.3354/meps166027.

Treguer, P., Jacques, G., 1992. Dynamics of nutrients and phytoplankton, and fluxes of carbon, nitrogen and silicon in the Antarctic Ocean. *Polar Biology* 12, 149 – 162.

Treguer, P., LeCorre, P., 1975. Manuel d'analyse des sels nitritifs dans l'eau de mer (utilisation de l'Autoanalyser 2. Technicon), 2nd ed. Univ. Bretagne Occidentale. 110p.

Tremblay, J. E., Lucas, M. I., Kattner, G., Pollard, R., Strass, V. H., Bathmann, U., & Bracher, A., (2002). Significance of the Polar Frontal Zone for large-sized diatoms and new production during summer in the Atlantic sector of the Southern Ocean. *Deep Sea Research Part II: Topical Studies in Oceanography*, *49*(18), 3793–3811. doi:10.1016/S0967-0645(02)00111-X

Tremblay, J.E., Legendre, L., Klein, B., Therriault, J.C., 2000. Size-differential uptake of nitrogen and carbon in a marginal sea (Gulf of St. Lawrence, Canada): significance of diel periodicity and urea uptake. *Deep-Sea Research* II, 47, 489 - 518.

Tremblay, J.E., Lucas, M.I., Kattner, G., Pollard, R., Strass, V.H., Bathmann, U., Bracher, A., 2002. Significance of the Polar Front Zone for large-sized diatoms and new production during summer in the Atlantic sector of the Southern Ocean. *Deep-Sea Research II* 49, 3793 – 3811.

Trenberth, K.E., W.G., Large, J.G., Olson, (1990), The mean annual cycle in global ocean wind stress. *Journal of Physical Oceanography*, 20:1742- 1760.

Van de Poll, W. H. Alderkamp, A. C., Janknegt, P. J., Roggeveld, J., Buma, A. G. J., 2006. Photoacclimation modulates excessive photosynthetically active and

ultraviolet radiation effects in a temperate and an Antarctic marine diatom. *Limnol. Oceanogr.* 51: 1239–1248.

van Leeuwe, M. A., (1998), A Barren Ocean, iron and light interactions with phytoplankton growth in the Southern Ocean, Ph.D. thesis, 189 pp., Univ. of Groningen, Groningen, Holland.

Venables, H., & Moore, C. M. (2010). Phytoplankton and light limitation in the Southern Ocean: Learning from high-nutrient, high-chlorophyll areas. *Journal of Geophysical Research*, *115*(C2), C02015. doi:10.1029/2009JC005361.

Visbeck M, Hall A (2004) Interannual Southern Hemisphere Atmospheric Variability in the NCEP reanalysis between 1980 and 2002. *Journal Climate*, 17: 2255-2258

Waldron, H.N., Attwood,.C.G., Probyn, T.A., Lucas, M.L., (1995). Nitrogen dynamics in the Bellinghausen Sea during the Austral spring of 1992. *Deep-Sea Research* II, 42 (4 – 5), 1253 – 1276.

Wanninkhof, R., Thoning, K., (1993), Measurement of fugacity of CO2 in surface water using continuous and discrete sampling methods. *Marine Chemistry*, 44 (2–4), 189–204.

Weeks, S.J., & Shillington, F.A., (1996), Phytoplankton pigment distribution and frontal structure in the subtropical convergence region south of Africa. *Deep Sea Research Part I: Oceanographic Research Papers*, 43(5), 739–768. doi:10.1016/0967-0637(96)00016-7.

Weiss, R.F., 1970, The solubility of nitrogen, oxygen and argon in water and seawater, *Deep Sea Research*, 17, 721 – 735.

Weiss RF, & Price, B.A., (1980), Nitrous oxide solubility in water and seawater. *Marine Chemistry*, 8:347-359.

Whitehouse, M.J., Korb, R.E., Atkinson, A., Thorpe, S.E., Gordon, M., (2008). Formation, transport and decay of an intense phytoplankton bloom within the High-Nutrient low Chlorophyll belt of the Southern Ocean. *Journal of Marine Systems*, 70, 150 – 167.

Whitworth, T., and W. D. Nowlin (1987), Water masses and currents of the Southern Ocean at the Greenwich meridian, *Journal of Geophysical Research*, 92, 6462– 6476.

Williams, LeB. P.J., (1995), Evidence for the seasonal accumulation of carbon-rich dissolved organic matter, its scale in comparison with changes in particulate material and the consequential effect on net C/N assimilation ratios, *Marine Chemistry,* 51, 17 – 29.

Williams, R.G. and M.J. Follows, (2003), Physical transport of nutrients and the maintenance of biological production. In: M. Fasham ed(s). *Ocean Biogeochemistry: The role of the ocean carbon cycle in global change*. Berlin Heidelberg New York, Springer.

Yool, A., Martin, A. P., Fernández, C., & Clark, D. R. (2007). The significance of nitrification for oceanic new production. *Nature*, *447*(7147), 999–1002. doi:10.1038/nature05885.